Rockefeller University
Digital Commons @ RU

Student Theses and Dissertations

2024

Cellular and Circuit Consequences of a Genetic Locus for Attention

Zachary Gershon

Follow this and additional works at: https://digitalcommons.rockefeller.edu/student_theses_and_dissertations

 Part of the Life Sciences Commons

Cellular and Circuit Consequences of a Genetic Locus for Attention

A Thesis Presented to the Faculty of

The Rockefeller University

in Partial Fulfillment of the Requirements for

the degree of Doctor of Philosophy

by

Zachary Gershon

April 2024

© Copyright by Zachary Gershon 2024

Cellular and Circuit Consequences of a Genetic Locus for Attention

Zachary Gershon

The Rockefeller University 2024

Animals are constantly bombarded by any number of sensory inputs but have a limited capacity with which to process them. A mechanism for filtering, prioritizing, and directing mental assets is required to prevent sensory overload, enable meaningful comprehension, and allow for further action. Attention is the process of directing cognitive resources toward specific stimuli, which can be dispensed in a top-down manner to carry out higher-order cognitive functions. However, despite extensive and careful study at the molecular, cellular, and, circuit scales, unifying principles have been challenging to elicit. In this thesis, I aimed to provide a new perspective by taking a forward genetics approach to identify genes with prominent contributions to attentional performance. We studied 200 mice from a highly genetically diverse, multiparent mouse population on measures of pre-attentive processing and through genetic mapping identified a small locus on chromosome 13 (95%CI: 92.22-94.09 Mb) driving substantial variation (19%) in this trait. After identifying the parental genomic contributions driving this variation, we validated that the locus also drove variation in attention, but not other related cognitive processes, using similarly diverse mice homozygous for the appropriate founder haplotypes. Further characterization of the locus revealed *Homer1*, encoding a synaptic protein, as the causative gene. Further analysis determined that down-regulation in the prefrontal cortex (PFC) only during a developmental critical period of two short, activity-dependent isoforms *Homer1a* and *Ania3* led to significant improvements in multiple measures of attentional performance in the adult. Subsequent single-cell RNA seq experiments revealed that prefrontal *Homer1* downregulation in excitatory neurons is associated with GABAergic receptor upregulation in those same cells. Moreover, physiological studies demonstrated that this increase in GABAergic receptors corresponded to strong inhibitory tone in PFC. This enhanced inhibitory influence, together with dynamic neuromodulatory coupling, led to strikingly low PFC activity at baseline periods of an attention task but targeted elevations at cue onset, predicting short-latency correct choices. Notably high-*Homer1*, low-attentional performers, exhibited uniformly elevated prefrontal activity throughout the task. We thus identify a single gene with a large effect on attention – *Homer1* – and find that it improves prefrontal inhibitory tone and signal-to-noise (SNR) to enhance attentional performance. Complementary to older models focused mainly on uniformly amplifying PFC activity, this work provides a new paradigm of attentional control – one in which reduced prefrontal activity can improve SNR.

To the communities that have held me up when times were hard and my mind betrayed me. To the friends who brought laughter and unwavering acceptance. And to my family, I am forever grateful for your boundless love and support – thank you for always encouraging my curiosity.

"It's the encounters with people that make life worth living"

- Guy de Maupassant

ACKNOWLEDGMENTS

I feel incredibly grateful to have spent the better part of a decade studying at The Rockefeller University. I'm appreciative for the funding and institutional support I received from the University during my time here. This caring and collaborative community has made doing science a joy.

First, I want to thank Dr. Priya Rajasethupathy, whose mentorship has meant the world to me. Your compassion, humor, curiosity, and passion for science were an inspiration. You prioritized creating a lab environment that made us excited to come to work every day. I am beyond thankful to have had a mentor who cared about me as a person more than about my science. I will always appreciate your open-door policy and our brainstorming sessions, especially in the early days when I would come to you and say "Do you have five minutes to tell me whether or not this is a crazy idea?". It has been, and will always be, an honor to be your first student. Thank you for taking a chance on me.

I would also like to thank my committee, Dr. Mary Beth Hatten, Dr. Cori Bargmann, and Dr. Bob Darnell. Your guidance and feedback were integral to my completing this project and becoming a better scientist. I am exceedingly grateful for your continued support.

Dr. Alessandra Bonito-Oliva, our fearless lab manager and my project partner, thank you. I am immensely thankful for all of the time and hard work you put into this project to make it a success, I could not have done it without you. I truly appreciate your willingness to always be a sounding board – even when I come to you and work out the answer while asking the question. Your support means so much to everyone in the lab, especially me.

To the current and former members of the Rajasethupathy lab, thank you for being great colleagues and friends. Nakul and Chelsea, thank you for letting me come and talk to you when I needed a break (even if you were a little busy at the time). Josue, Andrea, Florian, Ari, and Milli thank you for reminding me that I need a little fun every once in a while. James, I appreciate being a stop on your walks around the lab when you need a break. Andrew T., thank you for not making me feel bad about being clueless when it comes to sports, and for providing a steady sense of calmness to the lab. Celine, thank you for always bringing a smile, which makes me confident that the fun, caring environment for students that I enjoyed in the lab will continue. Katie, thank you for helping me get started and for never being shy to share your expertise. James and Suraj, I am grateful for helping me understand the basics of systems neuroscience. Andrew L. and Yujin, thank you for always making

yourselves available for questions and brainstorming. Genelle, thank you for always bringing the good vibes and for not minding when I text you after nine at night about our experiments. Leslie, thank you for bringing your infectious excitement and curiosity. Jak, thank you for sharing your expertise at the bench – it's something else – but also thank you for sharing your life-earned wisdom. Sloane and Alejandra, thank you for letting me joke about how old you make me feel. I am so appreciative to have had the pleasure to work with all of you.

Additionally, I would like to thank our collaborators – Praveen, Matt, Brian, and Andrew. Without your help, the science could not have happened.

I want to thank the Dean's Office staff for taking care of all the other stuff so that I could focus on the science. Emily, Andrea, Marta, Cris, Kristen, and Mercedes, I've appreciated all of your help, patience and support, but most of all, I'm grateful for having spent the last seven years knowing that there was an office full of people who had my back.

A special thank you to my ADDA/CHADD/ACO community, especially Melissa, Liz S., Bobby, Kelsey, Kylie C., Patrick, Logan, Mike, Kylie B., Carrie, Lollie, Liz L., Tamara, Brittany, Ari, Sharon, Kate, Suzanne, and Brendan. The work we do helps so many people to simply function in the world. Thank you for making me feel understood, for cheering me on, and for helping me see the impacts of my work from divergent perspectives.

For my friends who have stood by me throughout the years, those who have been by my side for over a decade and become more like family – Jeanie, Lauren B., Geoff, Lauren P., and Jonah – as well as the more recent additions, of whom there are too many to name without forgetting anyone, I am so thankful to be a part of your lives and that you are part of mine.

And finally, to my family – Mom, Dad, Rachel, Matt, Grammy, Aunt Jill, Uncle Peter, Ben, Jonah, Aunt Susan, and Uncle Eli – thank you for your unending encouragement, your unwavering support, and your unconditional love.

Table of Contents

LIST OF FIGURES

LIST OF TABLES

LIST OF ABBREVIATIONS

ABR	Auditory brainstem recording
ACh	Acetylcholine
ADHD	Attention-deficit/hyperactivity disorder
AMPAR	α-amino-3-hydroxy-5-methyl-4-isoxazolepropionic acid receptor
AUC	Area under the curve
B6	C57BL/6J mice
BDNF	Brain-derived neurotrophic factor
BLUP	Best linear unbiased predictor
CC	Collaborative cross
DA	Dopamine
DO	Diversity outbred
EPM	Elevated plus maze
ERP	Event-related potential
GO	Gene ontology
GOI	Gene of interest
GSEA	Gene set enrichment analysis
ITI	Inter-trial interval
LC	Locus coeruleus
LOCO	Leave-one-chromosome-out
LOD	Logarithm of the odds
MAG	Myelin-associated glycoprotein
MD	Mediodorsal thalamus
mEPSC	miniature excitatory postsynaptic current

mGluR	Metabotropic glutamate receptor
MPP	Multiparental population
NE	Norepinephrine
NIDAQ	National Instruments data acquisition
NMDAR	N-Methyl-D-aspartic acid receptor
NORT	Novel object recognition task
OE	Overexpression
OF	Open field
OL	Oligodendrocytes
OPC	Oligodendrocyte precursor cells
PFC	Prefrontal cortex
PPI	Prepulse inhibition
qPCR	Quantitative polymerase chain reaction
QTL	Quantitative trait locus
RNAseq	RNA sequencing
scSeq	Single-cell RNA sequencing
SDT	Signal detection task
shRNA	Short hairpin RNA
SN	Substantia nigra
SNP	Single nucleotide polymorphism
SNR	Signal-to-noise ratio
VTA	Ventral tegmental area

CHAPTER 1. Introduction

In order to experience the world, we must make sense of the multiple streams of sensory input we receive at any given moment. This acquisition of knowledge and its use towards future behavior requires numerous, internal mental processes, together known as cognition (Kandel et al., 2021). To process the incoming streams of information meaningfully, we must direct our cognitive resources toward specific stimuli, a process known as attention (Kahneman, 1973). Given its role in early sensory selection, it is thought to be necessary for many aspects of higher-order cognition, including memory and cognitive flexibility. The topic of attention has received much *attention* over the last century, including work on broad, conceptual ideas of how attention may be carried out as a mental process, which brain regions and activity give rise to it, as well as the cell types, cellular functions, and genes that enable that activity. In this chapter, I will present a framework for how attention functions, from a theoretical, neuropsychological perspective to our current physiological, mechanistic understandings at the cellular and molecular level. Then, I will explore how genes underpinning complex traits, including cognitive processes like attention, have been identified and provide a technical overview of current methods.

1.1 Understanding attention

One of the earliest descriptions of attention came at the end of the 19th century from the psychologist William James in his book *The Principles of Psychology* (James, 1890), where he wrote:

> "Everyone knows what attention is. It is the taking possession by the mind, in clear and vivid form, of one out of what seem several simultaneously possible objects or trains of thought. Focalization, concentration, of consciousness are of its essence. It implies withdrawal from some things in order to deal effectively with others…."

Despite James's claim that "everyone knows what attention is", over a century later a single, operational definition for scientific study remains elusive. In this section, I will review how the notion of attention has been conceptually scaffolded to provide a basis for investigation.

1.1.1 Theories of attention

Attention is generally divided into two major categories – reflexive and voluntary attention. Reflexive attention is a stimulus-driven, bottom-up process, whereas voluntary attention is a top-down process generally associated with goal-directed behavior (Gazzaniga et al., 2014). One of

the key distinctions theorists have made between these two categories of attention comes from the locus of attentional control, i.e. whether attention is being exogenously or endogenously controlled (Pashler et al., 2001; Posner, 1980). While it may be debated whether a bottom-up process is engaged consciously, for the purposes of my work (and therefore the context I present here), we proceeded under the framework that both reflexive and voluntary attention involve conscious detection of target stimuli.

Regardless of the nature of the attention employed, we are constantly and simultaneously bombarded with several channels of sensory input, but the mental resources we have to attend to them are finite. To meet this functional challenge, preliminary processing and filtration of that information must occur. This is known as pre-attentive processing and is defined as the rapid, parallel, and automatic processing of sensory information prior to conscious recognition of stimuli to selectively filter it for conscious use (Atienza et al., 2001; Schneider et al., 1982). Preattive processing was proposed as a filtering mechanism to deal with the perceptual bottlenecks implied by the innate limits on our attentional capacity (Broadbent, 1958). Initial hypotheses regarding pre-attentive processing suggested it occurred early in perception, before meaning being ascribed to any of the inputs (Broadbent, 1958). However, a series of dichotic listening experiments in humans showed that when a participant was focused on one stream of auditory information, competing messages could be perceived and attended to based on meaning. Opposing auditory input with more salient meanings (such as calling a participant's name in the competing channel or content continuity after switching the messages in the attended and competing channels) was better at interfering with conscious registration of the information presented in the attended channel (Moray, 1959; Peters, 1954; Treisman, 1960). These results led to the postulation of two plausible models: 1) that the selective filter occurred late in sensory processing once meaning was prescribed to stimuli (Deutsch & Deutsch, 1963), and 2) that the perceptual filter occurred early in processing but instead of an all-or-nothing filtering system, that information to be filtered out would be attenuated over time so that its signal would be much weaker by the time it reached consciousness. This suggested that if the signal-to-noise ratio (SNR) was high enough, that is if the information was salient enough, an irrelevant stimulus could be consciously recognized and attended to (Treisman & Geffen, 1967; Treisman, 1964). Nevertheless, both models had limitations. The late selection model was inefficient because it implied that all incoming sensory information would receive equal neural resources for processing until the filtering stage, which, with enough inputs could overwhelm the very capacity of the attentional system that a filtering system is meant to conserve. The attenuation model has the opposite problem, where if

presented with multiple stimuli of large salience simultaneously, they would all pass the threshold, resulting in sensory overload. These issues led to an updated model positing a temporally flexible selection filter that balances the demands of the required processing efficiency (i.e. desired response speed) with available attentional capacity via neural modulations of stimulus salience (Johnston & Heinz, 1978; Treisman, 1969).

Given the importance of salience in perceptual filtering, sensory gating is arguably the most critical component of pre-attentive processing. Sensory gating is the regulation of neuronal activity during sensory processing and perception to modulate the salience of stimuli in order to selectively filter sensory inputs used in downstream cognitive processes (Willott et al., 2003). The selection of sensory input is crucial for most, if not all, aspects of cognition – especially attention – to function properly. It is well established that sensory gating is impaired in several psychiatric diseases, many of which are associated with sensory overload, including ADHD (Micoulaud-Franchi et al., 2015), autism spectrum disorder (Perry et al., 2007), schizophrenia (Judd et al., 1992), bipolar disorder (Perry et al., 2001), obsessive-compulsive disorder (Swerdlow et al., 1993), and post-traumatic stress disorder (Neylan et al., 1999). Sensory gating contains both a bottom-up, reflexive, stimulus-driven process, as well as a top-down, voluntary, goal-directed process that can override reflexive responses. These two processes can interact cooperatively or competitively. For instance, when human participants had to report whether a target stimulus appeared in a specific location on a screen following the presentation of a cue that did not predict the target's location, response latencies, a common metric for attention, were significantly increased relative to uncued trials or when there was a large temporal delay (>300ms) between the cue and target (Posner & Cohen, 1984; Posner et al., 1980). However, when cues were predictive of subsequent targets, the response latencies were significantly faster, and the associated event-related potentials (ERPs) at the primary sensory and cognitive pathways were similarly enhanced (Hopfinger & Mangun, 1998, 2001). Thus reflexive attention can be beneficial for performance if the stimulus properties align with top-down objectives, but only in a rapid manner. If the timing or attributes of a stimulus do not align with top-down priorities, it will serve as a distractor and be detrimental to performance.

Top-down, voluntary attention, on the other hand, is often used interchangeably with the terms "selective" or "sustained" attention, the former operating over brief periods, whereas the latter can occur over more prolonged time scales. The most prominent theory of selective attention describes it as a "spotlight" with a central focus, the size of which can vary to an outer limit depending on the available attentional

capacity and the task at hand (Posner et al., 1980). Meanwhile, maintaining attention to report unpredictable events over an extended time period is thought of as a separate, but related process termed vigilance, or sustained attention (Bushnell, 1998). Sustained attention is often confused for arousal because of the outsized impact a suboptimal arousal state can have on sustained attention (Esterman & Rothlein, 2019); but where arousal is a global brain state (Sarter et al., 2001), sustained attention is a discrete process characterized by fluctuations between attention-related networks in the brain (Esterman & Rothlein, 2019). These oscillations are highly impacted by arousal state, motivation, the cognitive resources available, as well as top-down control (Esterman & Rothlein, 2019). Nonetheless, sustained attention makes use of selective attention, which, in turn, makes use of measurable sub-processes such as orienting, the configuring of cognitive resources towards the source of a stimulus or internal semantic assembly (Posner, 1980), detection, the conscious awareness of a stimulus (Posner, 1980), and differentiation, the delineation of one stimulus from another (Bushnell, 1998). Current understandings of the cellular and circuit mechanisms underlying selective and sustained attention will be presented in the next subsection.

1.1.2 Mechanisms of central attentional control

Investigations into the circuits governing attentional control have uncovered that attention is mediated by the interaction of several networks across the brain (Esterman & Rothlein, 2019). Generally, this can be thought of as the brain's frontal cortical regions interfacing with higher-order sensory cortices to exert higher cognitive control, usually through subcortical structures like the thalamus or basal forebrain as intermediaries. Since the majority of attentional research has been done in the visual and auditory systems, in this subsection, I will outline the overlapping circuitry and neural dynamics that are understood to constitute central, cognitive attentional processes.

For vision and audition, perception of sensory information begins with stimulation of the sensory organs, which then transmit that information through thalamic sensory relays such as the lateral geniculate nucleus, in the case of the visual system, or the medial geniculate nucleus, for auditory sensory transduction. The information is then passed to sensory cortices, where it is processed further (Clark et al., 2015; Fritz et al., 2007). However, central attentional systems exert executive control over this processing at multiple stages in those pathways (Figure 1.1). The key brain structure exerting that control is the prefrontal cortex (PFC), aided by its reciprocal connections with the mediodorsal thalamus (MD). In these recurrent thalamocortical loops, MD serves important attentional roles, including improving PFC SNR by amplifying local connectivity to

help it maintain task-relevant representations (Schmitt et al., 2017), aiding in shifting attention based on contextual cues by improving the reliability of PFC neuronal responses by computing expectancy of stimuli presentations (Rikhye et al., 2018), and deal with uncertainty through the amplification or inhibition of distinct populations of PFC interneurons (Mukherjee et al., 2021). Additionally, there is evidence that for both systems inhibitory thalamic nuclei – the thalamic reticular nucleus and pulvinar – modulate the information in sensory thalamic nuclei, under the influence of projections from PFC (Clark et al., 2015; Hockley & Malmierca, 2024).

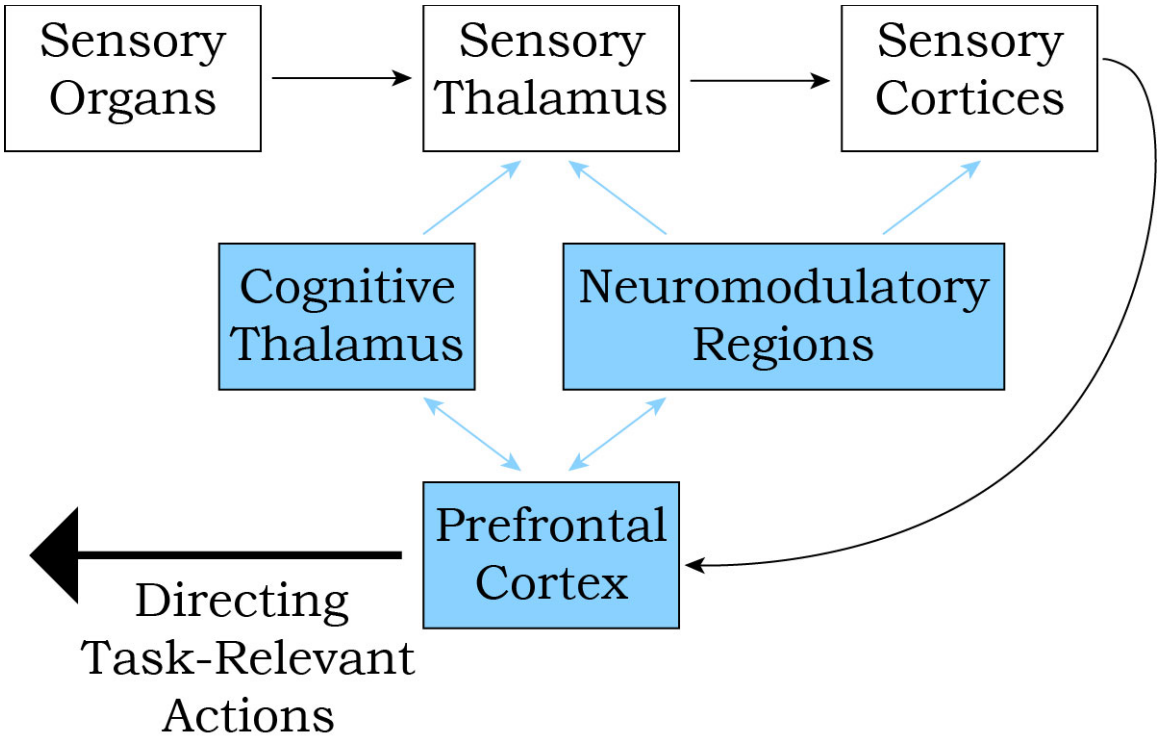

Figure 1.1 PFC exerts top-down attentional control on sensory processing
A schematic representation of how PFC exerts central, attentional control on sensory processing to carry out goal-directed behavior. Blue lines and rectangles indicates the top-down attentional influences.

The neural dynamics of those thalamocortical loops as well as general prefrontal executive attentional control have been shown to be strongly impacted by neuromodulatory influences, most notably acetylcholine, dopamine, and norepinephrine. These neurotransmitters affect attentional performance in a Yerkes-Dodson dose-response (inverted U) relationship (Yerkes & Dodson, 1908), i.e. there is an optimal middle-ground for attentional function and neuromodulatory hypo- or hyperactivity is detrimental to attention (Thiele & Bellgrove, 2018). Interestingly, PFC can tightly control the neuromodulatory inputs it

receives because it is recurrently connected with all of the neuromodulatory regions discussed below (Dembrow & Johnston, 2014). Generally, neuromodulation affects cellular physiology to influence attentional control by increasing postsynaptic cellular excitability or the probability of presynaptic neurotransmitter release. Even though these different neuromodulatory systems have similar net effects on cells, multiple systems may work in attention to provide different handles to cooperatively fine-tune the attentional system based on a variety of factors, including arousal, stimulus salience, and reward value.

Acetylcholine (ACh) originating from the basal forebrain is a crucial neuromodulator involved in top-down attentional control within PFC and MD; particularly, it is thought to mediate attentional orienting (Hasselmo & Sarter, 2011). ACh activates nicotinic receptors on MD projections to PFC, facilitating glutamatergic transmission to increase excitation of PFC neurons (Gioanni et al., 1999; Lambe et al., 2003), thereby improving their responsiveness to incoming sensory information. Furthermore, ACh affects the excitability of deeper-layer PFC cells. Phasic ACh stimulation of muscarinic receptors on layer V PFC pyramidal neurons transiently reduces excitability followed by increases in spiking rates, while tonic activation of the same receptors reduces the resting membrane potential of the layer V cells, making them more excitable (Gulledge et al., 2009). This suggests a mechanism by which ACh enhances thalamic input to PFC regarding task-relevant stimuli and simultaneously augments PFC output activity so that it can exert attentional control on other brain regions.

Dopamine (DA) is provided by inputs from the substantia nigra (SN) and ventral tegmental area (VTA). These two sources of DA appear to have differential attentional effects in PFC based on anatomical and molecular segregation. The SN projects to superficial layers of the PFC where dopaminergic activity is modulated by D1 receptors. Projections from VTA, on the other hand, terminate in deeper layers of PFC and their influence is primarily modulated through D2 receptors (Berger et al., 1991; Soltani et al., 2013). These two streams of dopamine input to PFC are thought to carry different information – the VTA is believed to send motivational, reward-prediction information, while the SN transmits information about stimulus salience (Ott & Nieder, 2019). In rodent studies, chemogenetic activation of VTA increased overall hyperactivity (Boekhoudt et al., 2016), while activation of SN affected response accuracy in an attention task (Boekhoudt et al., 2017). Parallel streams of dopaminergic input can also be fine-tuned locally in PFC through the differential activation of D1 or D2 or both in the various layers and cell types of PFC. For instance, in a visual attention study of non-human primates, firing was suppressed in one population of PFC neurons when treated with DA; yet, another population became not only more excitable

upon DA application, but the variability of their firing was reduced, thus improving SNR (Jacob et al., 2013). Slice physiology experiments have demonstrated that these differential effects are due to differential activation of D1 and D2 receptors – activation of presynaptic D1 receptors reduced glutamatergic transmission in a set of prefrontal neurons (Gao et al., 2001), whereas D2 receptor activation induced burst firing in another subset of PFC cells (Wang & Goldman-Rakic, 2004). Most cortical layers express D1 receptors, whereas D2 receptor expression can be more restricted, thereby allowing for mixed interactions along many areas in PFC (Santana & Artigas, 2017).

Finally, the locus coeruleus (LC) is involved in computations about arousal state conveyed via norepinephrine (NE) release. Historically, LC release of NE has been associated with arousal based on electrophysiological evidence that the frequency of tonic LC activity is modulated in a pattern predictive of sleep-wake cycle transitions (Aston-Jones & Bloom, 1981) and more recent data that optogenetic manipulation of LC neurons could bidirectionally affect wakefulness state (Carter et al., 2010). Across species, it has been demonstrated LC neurons respond to learned, task-relevant stimuli by initiating a pattern of burst firing (Aston-Jones et al., 1997; Bouret & Sara, 2004). The transition between tonic and phasic LC activity is thought to represent lower and higher states of neural gain modulation, respectively, with the latter supporting a focused attentional state (Aston-Jones & Cohen, 2005; Eldar et al., 2013). Similar to DA, the effect of noradrenergic signaling is thought to be dependent on the receptor class that is activated – α_1, α_2, or β. While most PFC cells express all adrenergic receptor classes (Berridge & Spencer, 2016), receptor engagement appears to be determined by NE release rate because α_2 receptors have higher NE affinity than α_1 receptors, with β receptors having the lowest affinity (Arnsten, 2000). Thus, at low concentrations of NE, only α_2 receptors would be engaged and as NE concentration increases, α_1 and β receptors would be activated. NE binding to α_{2A} receptors in PFC inhibits postsynaptic hyperpolarization-activated cyclic nucleotide-gated cation (HCN) channels, improving neuronal tuning to task-relevant stimuli (M. Wang et al., 2007). Stimulation of α_1 receptors, on the other hand, suppress prefrontal neuron firing in a protein kinase C-dependent manner (Birnbaum et al., 2004). Activation of β receptors in PFC increases neuronal excitability, increasing neurons' firing rates. This facilitates a Yerkes-Dodson curve between PFC NE concentration and attention where, in starting conditions with no NE released, attention is suboptimal but as NE concentration increases, α_2 receptors are preferentially activated, increasing PFC activity by making the cells more excitable until the point of greatest attention when the α_2 receptors are at maximum occupancy and α_1 followed by β receptors are engaged,

suppressing prefrontal activity and reducing attention to a suboptimal level once again.

At the single-cell level, the application of attention is reflected in higher neuronal firing rates toward attentionally relevant stimuli. Nonetheless, other observable changes at the population level are indicative of the exertion of attention as well. Action potentials are generated by the summing of postsynaptic potentials, so the efficiency of action potential generation is greatly affected by the timing of synaptic inputs; that is, presynaptic cells firing synchronously onto the same cell have a higher chance of depolarizing the postsynaptic neuron, making the circuit more effective in transmitting information. If this is done repeatedly, those cells end up in rhythmic oscillations of synchronous activity (Sapountzis, 2018). It has been observed in multiple brain regions during periods of attention that local neuronal population activity oscillates in the gamma frequency band (synchronously fire at 30-80 Hz), including the prefrontal cortex (Gregoriou et al., 2009), parietal cortex (Saalmann et al., 2007), as well as visual and auditory cortices (Sokolov et al., 2004). It has been observed that these gamma oscillations can phase lock across brain regions to enhance attention and that the interregional coherence of intraregional gamma synchrony is modulated by the phase of cortical theta (4-8 Hz) rhythms (Doesburg et al., 2008, 2012; Gregoriou et al., 2009). Some have hypothesized that local ensembles synchronize at high-frequency gamma oscillations so they can transmit information rapidly and efficiently, while lower-frequency theta rhythms modulate long-range synchrony because of conduction delays due to those populations' spatial separation (Jensen & Colgin, 2007).

1.2 Forward genetics towards understanding cognition

Although cognition occurs at the circuit level, the many circuits that seem to be involved and the recurrence, redundancy, and complexity of their interaction make it difficult to pinpoint the key nodes in an otherwise complex network. One approach to bring clarity from this complexity is to identify single genes of large effect on attention, which, if they exist, could point to key cellular and circuit nodes. Following this logic, how can we identify genetic contributors to attention? One approach is to pursue reverse genetics, a process of specifically manipulating one gene at a time and testing whether it has an observable effect on the phenotype of interest, i.e. attention. However, this approach can be slow and can be limited in that large, all-or-none deletions can yield non-specific effects, disallowing for the quantification of a true effect size toward the phenotype in question. An alternative, phenotype-based approach, forward genetics, may allow for assessing many genes at once in a more unbiased way, and in some cases with the ability to quantify effect size and prioritize the genes of interest. Typically,

such forward genetics approaches make use of either naturally occurring or induced, random genomic variation to identify organisms differing in a phenotype of interest, then isolate and characterize the gene(s) responsible for driving the observed trait variation (Funato, 2020). Forward genetics is an especially important approach in understanding the genetics underlying non-medelian phenotypes, i.e. phenotypes dependent on the contributions of multiple genes. In this section I will provide a brief summary of the history of forward genetics, especially as it applies to neuroscientific and behavioral discoveries, and then outline current forward genetics methods in mammals, focusing on quantitative trait locus (QTL) analysis.

1.2.1 A historical perspective of forward genetics

As early as the late 19th century, Mendel recorded observations about the segregation of phenotypic inheritance across generations (Mendel, 1866). These observations were then independently confirmed at the turn of the 20th century by Correns, De Vries, and Tschermak (Correns, 1900; de Vries, 1900; Tschermak, 1900). About 10 years later, Thomas Hunt Morgan observed natural variation in the eye color of the fruit fly *Drosophila melanogaster*. He found that a variant eye color trait (white eyes rather than the usual red eyes) was passed to subsequent generations following Mendel's principles of inheritance in a sex-limited manner, thus identifying a physical coupling within a chromosome of different heritable "factors" for two separate phenotypes (Morgan, 1910, 1911b). Around the same time, the term gene was introduced to refer to such physical "factors" of inheritance (Johannsen, 1909). Morgan proposed that the phenotypic linkage was due to the physical distance between genes on a chromosome and their likelihood of separation during chromosomal crossing over:

> "There is good evidence to support the view that during the strepsinema stage homologous chromosomes twist around each other, but when the chromosomes separate (split) the split is in a single plane.... In consequence, the original materials will, for short distances, be more likely to fall on the same side of the split, while remote regions will be as likely to fall on the same side as the last, as on the opposite side. In consequence, we find coupling in certain characters, and little or no evidence at all of coupling in other characters; the difference depending on the linear distance apart of the chromosomal materials that represent the [genes]." (Morgan, 1911a)

Shortly thereafter, Morgan's student Alfred H. Sturtevant used this notion of linkage to create a map of the physical position of six genes

relative to each other on a *Drosophila* sex chromosome (Sturtevant, 1913). This was the first instance of genetic mapping.

One of the earliest examples of the use of forward genetics to link a gene to a behavioral phenotype was also performed in *Drosophila*. However, unlike the eye color variants Morgan observed, this was not a naturally occurring phenotype. The *fruitless* mutation was randomly induced by X-rays and while homozygous females had no anatomical or behavioral differences from wild type females, homozygous males, despite possessing normal genitalia, were behaviorally sterile because they engaged in abnormal courtship behavior (Gill, 1963). During this altered behavior, mutant males would pursue females but would not copulate. Further, males courted other males with as much vigor as they did females, creating "courtship chains", where each male was both a pursuer and the pursued (Gailey & Hall, 1989; Hall, 1978). From the time the *fruitless* mutant was identified, it took over 20 years for the physical, chromosomal region containing the mutation to be identified (Gailey & Hall, 1989) and almost 10 years after that for the *fruitless* gene to be cloned (Ito et al., 1996; Ryner et al., 1996). Soon after the X-ray-induced fruitless mutation was identified, Seymore Benzer pioneered what is now one of the most common strategies of forward genetics – systematized screens for phenotypes of interest following random chemical mutagenesis (Benzer, 1967). This approach was used to characterize multiple *Drosophila* mutants with aberrant circadian rhythm phenotypes, mapping to the same gene called *period* (Konopka & Benzer, 1971). The *period* gene was later characterized and cloned by multiple groups (Bargiello et al., 1984; Bargiello & Young, 1984; Reddy et al., 1984; Zehring et al., 1984). Similar forward genetic screens identified several additional genes regulating circadian rhythm (Allada et al., 1998; Sehgal et al., 1994; Stanewsky et al., 1998), which were subsequently cloned and further explored (Emery et al., 1998; Myers et al., 1995; Rutila et al., 1998). Random chemical mutagenetic screens were also used to identify genes involved in *Drosophila* cognition. After the creation of an olfactory learning paradigm for the flies (Quinn et al., 1974), forward genetic screens identified a number of learning-deficient mutants that allowed the mapping and identification of the causal genes (Dudai et al., 1976; Aceves-Piña & Quinn, 1979; Quinn et al., 1979). Forward genetics is not exclusive to *Drosophila*; in fact, other invertebrate model organisms have used forward genetic screens to identify genes impacting behavior, including the nematode *Caenorhabditis elegans*. In the early 1970s, Sydney Brenner made the case for the utility of *C. elegans*, as a self-fertilizing hermaphrodite, for genetic mapping to understand the molecular basis of behavior (Brenner, 1974). As the *C. elegans* nervous system is made up of 302 neurons (White et al., 1986), its simplicity has been quite advantageous for studying the basic biology of neural function and how that gives rise to behavior. Genetic mapping using both

mutagenesis-based and natural variation-based screens has identified genes for neurotransmitter metabolism (Johnson et al., 1981, 1988), social behavior (de Bono & Bargmann, 1998), and mechanosensation (Chalfie & Au, 1989; Chalfie & Sulston, 1981). Screens of this nature have also been used in mammalian model organisms, most commonly in mice. One of the earliest examples of a genetic mapping study in mice for a behaviorally relevant phenotype used chemical mutagenesis to map and clone the circadian rhythm gene *Clock* (King et al., 1997; Vitaterna et al., 1994).

1.2.2 Modern approaches in forward genetics

Genetic mapping has been incredibly effective at identifying causal genes for phenotypes that are: 1) discrete and 2) have Mendelian patterns of inheritance. Nonetheless, much of the qualitative variation within a population does not meet those criteria. Instead, phenotypes that vary continuously in a population and are impacted by multiple genes to differing degrees are described as quantitative traits, and their inheritance is said to be polygenic (Tanksley, 1993). Accordingly, a discrete genomic locus that significantly contributes to a quantitative trait is called a quantitative trait locus (QTL) (Tanksley, 1993). To identify such loci, a method known as QTL mapping is used, in which statistical methods are used to map the genomic location of QTLs based on their linkage with multiple other genetic markers that differ between individuals of a population. Estimates can then be made regarding the magnitude of the QTL's effect on the phenotype of interest, represented as the percent of phenotypic variance explained by the QTL (Tanksley, 1993). While this idea was first introduced in the 1960s (Thoday, 1961), progress in QTL mapping was slow for the next 20 years until technological advances in molecular biology provided direct molecular markers, i.e. the mapping could use markers in the physical substrate of heredity – DNA. For instance, restriction fragment length polymorphisms, created by genetic variants in naturally occurring restriction enzyme sites, were the earliest genetic markers based in DNA (Botstein et al., 1980), and the first molecular marker covering an entire organism's genome to map QTLs (Paterson et al., 1988). Since then, advances in DNA sequencing allowed for the identification of single nucleotide polymorphisms (SNPs), which are now the standard molecular markers for QTL mapping (Solberg Woods, 2014). Further, at the beginning of the 21st century, the entire genomes of multiple species (Adams et al., 2000; International Chicken Genome Sequencing Consortium, 2004; International Human Genome Sequencing Consortium et al., 2001; Mouse Genome Sequencing Consortium, 2002; The C. elegans Sequencing Consortium*, 1998; Venter et al., 2001) – and subspecies (Lilue et al., 2018) – were sequenced, drastically increasing the number

of molecular markers available for use, thus increasing the efficiency of QTL analyses (Hunter & Crawford, 2008).

As cognition is highly complex, made up of several processes that require coordinated activity of multiple neuronal populations as well as modulation of single neuron function at varying time scales (as discussed above), it is clear that cognitive phenotypes are polygenic. Further, since cognitive processes are internal mental calculations, they must be studied inferentially based on their behavioral manifestations. While some behaviors can be assessed discretely, many behaviors are quantified on a continuous scale. Such behaviors necessitate the use of QTL analysis for genetic study. There has been a good deal of work to apply QTL mapping to behavioral phenotypes. For instance, in *Drosophila*, QTL analysis has identified genes underlying aggressive behavior (Shorter et al., 2015), QTLs have been mapped in *C. elegans* avoidance behavior in response to environmental stimuli (McGrath et al., 2009; Ghosh et al., 2015), and in mice, numerous behavioral QTLs have been elucidated, including those for sensory gating (Joober, 2002; Samocha et al., 2010), anxiogenic behavior (Grazia Turri et al., 2004; Takahashi et al., 2006), learning (Steinberger et al., 2003), memory (Caldarone et al., 1997; Hsiao et al., 2020), and cognitive flexibility (Laughlin et al., 2011).

Early QTL studies in mice often used F2 intercross breeding structures, in which mice from two different inbred strains that are genetically and phenotypically distinct (with only one possessing the phenotype of interest) were mated to produce F1 offspring that were heterozygous for the genomic contributions from each parental strain at every genomic locus; then, F1 siblings were intercrossed with each other to produce F2 progeny that would be assessed for phenotype and genotype and successively subject to QTL analysis (Solberg Woods, 2014). This breeding scheme identified loci that were tens of megabases long, containing hundreds of genes and making it difficult to isolate causal gene(s) (Saul et al., 2019; Solberg Woods, 2014). These large QTL regions are the result of the F2 progeny's large linkage disequilibrium, or association of alleles at differing loci in a non-random manner (Slatkin, 2008), given that only one generation of meiotic recombination occurred. Thus, the linkage of the parental SNP markers is mostly intact across the progeny, making the distances at which markers differ between individuals large. To combat this hurdle, several other breeding schemes have been utilized to improve mapping resolution. One alternate method has been to create congenic strains (Zhang et al., 1994). To do so, the F1 generation is backcrossed to the parental strain not possessing the phenotype of interest for at least 10 generations (Papaioannou & Behringer, 2024). While this can reduce the size of the identified QTL (Shirley et al., 2004), this strategy can be hindered by the presence of

several, tightly linked loci with differing effects on the phenotype leading to the eventual loss of the phenotype of interest (Solberg Woods, 2014). The use of outbred populations has become a common approach for dealing with the drawbacks of their predecessors. Advanced intercross (AI) populations are one such outbred model (Fawcett et al., 2010; Samocha et al., 2010). These populations have similar origins to F2 intercrosses, except the progeny are interbred with each other for several successive generations to allow for many more meiotic recombinations to occur (Solberg Woods, 2014). However, AI populations are limited to finding only QTLs occurring in the two parental populations (Solberg Woods, 2014). Another favored outbred strategy for QTL mapping is the use of heterogeneous stocks (HS). Unlike AI populations, these mice are multiparental, generated using eight inbred founder strains, and are maintained by random mating to non-siblings (Mott et al., 2000). The increased number of parental strains and random mating increases the complexity of the population's genomic architecture since there are more possible haplotypes each mouse can possess and the breeding structure provides higher levels of heterozygosity throughout the population. However, this also increases the complexity of the analysis required, as the relatedness between individuals needs to be accounted for to prevent the detection of false positive QTLs (Solberg Woods, 2014). Each HS mouse is genotypically and phenotypically distinct, so it is impossible to perform replicable studies of functional characterization in the same way one could with an F2 intercross. Moreover, the HS mice were created by only crossing the founder genomes once, so the genetic contributions from each founder are not balanced and there is the possibility of the loss of some alleles (Solberg Woods, 2014). These disadvantages were addressed with the creation of the Collaborative Cross (CC) and Diversity Outbred (DO) mice. Similar to the HS mice, the CC and DO mice were generated using eight founder strains, five of which were classical inbred strains while three were wild-derived, using a multi-funnel breeding scheme, in which the eight founders were intercrossed in different combinations (The Collaborative Cross Consortium, 2012). After three generations of progeny being outbred to the progeny of other intercrosses within a funnel (G0-G2), the CC lines were generated by successive generations of inbreeding to stabilize their genomes as the first multiparental recombinant inbred lines (The Collaborative Cross Consortium, 2012). In the early stages of CC inbreeding, over 100 of the incipient CC lines were randomly outbred across funnels to create the DO population (Svenson et al., 2012). The inclusion of the wild-derived strains in the DO breeding scheme increases the genomic diversity and allows for greater phenotypic variation than the HS (Solberg Woods, 2014). Additionally, the DO population is maintained using a much greater number of breeder mice than the HS (Mott et al., 2000; Svenson et al., 2012). Moreover, even though on its face it would seem that the DO would have the same dilemma regarding the lack of replicable mice

for functional studies as with the HS, in the case of the DO, the CC mice provide a partially outbred intermediate that, due to their shared founder genomes, enable haplotype reconstruction and functional characterization in CCs of QTLs that have been fine-mapped in the DO (Hsiao et al., 2020).

1.3 Summary

In this chapter, I presented a historical overview of the theories for how attention functions, from the earliest stages of pre-attentive processing to attentional control of stimulus selection and behavior over varying timescales. I discussed the nature and necessity of a selective filter, which given our limited cognitive resources, functions to prioritize the multiple streams of sensory information we receive prior to reaching conscious detection and behavioral choice. Additionally, I discussed biological mechanisms of central attentional control at several scales of study. These include the use of PFC-MD thalamocortical loops at the circuit level, neuromodulation at the molecular level, as well as cellular physiology reflecting attention for both individual and populations of neurons.

To understand how the genes underpinning attentional processes could be studied, I provided a brief history of forward genetic methods, which identify genes based on their ability to drive variation in a phenotype of interest. After these methods were first developed in flies, they were expanded to other model organisms. As attention is a complex trait that is perhaps more easily studied in higher-order organisms, I next examined modern methods for identifying QTLs in mice, including mouse resources specifically designed for high-resolution genetic mapping. In the following chapters, I will discuss my efforts to apply genetic mapping in mice, which ultimately led to the identification of a single gene of large effect (*Homer1*) contributing to variation in attention. I subsequently studied the mechanistic basis for this interaction, identifying cellular and circuit consequences of Homer1 enabling improved attentional performance. Collectively, I will describe a genes-to-circuits-to-behavior approach to gain a mechanistic understanding of attention spanning multiple scales.

CHAPTER 2. A genetic locus contributes substantial variability to pre-attentive and attentional processing

2.1 Introduction

Attention is a complex aspect of cognition and, much like other cognitive processes, is a series of internal mental calculations that are often measured using a behavioral readout. To explore the genetic basis of attention in a relatively unbiased manner, we took a QTL mapping approach. In our lab's prior work with genetic mapping, we found that the ability to detect QTL was most successful when using a behavior that was innate, robust to technical replicates, and required minimal experimenter intervention. However, assays of attention generally require substantial training, food or water restriction to incentivize reward associations, and numerous other potential confounds. We thus chose to measure sensory gating as the innate quantitative trait most linked to attention. While many have conceived of attention as a collection of distinct, but related processes (Bushnell, 1998; Dayan et al., 2000; Sarter et al., 2001), sensory gatting, a pre-attentive top-down selective filter for sensory input (Jones et al., 2016; Mease et al., 2014) is an early component thought to be needed for many if not all downstream aspects of attention. Sensory gating can be overridden in a bottom-up manner in instances where a stimulus is salient to the point of externally directing an individual's attention, usually evoking a startle response. This override feature may be an evolutionary feature to allow organisms to recognize threatening aspects of their environments that they are not attending to. The startle response can be inhibited by a weaker stimulus (the prepulse) of any sensory modality in a short time frame preceding the strong stimulus. Inhibition of the startle response by the prepulse is a well-established measure of sensory gating in humans and mice, aptly named prepulse inhibition (PPI) (Braff et al., 2001). Multiple studies have indicated that PPI is a polygenic phenotype (Joober, 2002; Petryshen et al., 2005; Samocha et al., 2010), indicating that it would be a useful candidate phenotype for mapping a QTL related to attentional processing.

QTL mapping relies on the linkage of SNPs, which is due to their physical proximity on a chromosome. QTL mapping is restricted by the number of SNP markers and meiotic recombination rate across subjects' genomes (Gatti et al., 2014). Without sufficient genetic variation, the mapping resolution of identified QTLs is too poor to isolate causal variants (Solberg Woods, 2014); that is a locus could span tens of megabases, containing hundreds or thousands of genes and likely even more regulatory regions (Solberg Woods, 2013). However, in a genetically diverse population with high rates of recombination, QTL mapping is an excellent tool for efficiently isolating genetic variants contributing to

specific components of cognitive behavioral phenotypic variation (Chesler, 2014; Logan et al., 2013). One such mouse recently developed mouse resource, the DO population, has immense genetic diversity and was developed specifically for high-resolution genetic mapping. The DO and their genetic heterogeneity began with the development of the recombinant inbred CC mouse lines. The CC were created by intercrossing eight founder strains (five that are classical inbred strains and three that are wild-derived inbred strains) in a multi-funnel outbreeding strategy for 22 generations followed by subsequent generations of inbreeding (The Collaborative Cross Consortium, 2012). The DO was derived from random crosses of 144 independent CC lines of the F4 to F12 generations and continuously outbred with a unique, pseudorandom breeding strategy to maintain genetic diversity while avoiding drift and bottleneck effects (Figure 2.1A). It is important to note that the DO population maintains an approximately equal allelic representation of the eight founder lines globally, but varies greatly at any given locus. Each individual DO mouse has a unique genomic architecture, each with their own arrangement of the approximately 45 million SNPs independently segregating in the DO population (Svenson et al., 2012). Coupling this massive genetic diversity with the well-documented pedigree of each mouse, QTL mapping at or near sub-megabase resolution is thought to be achievable with a minimum sample size of 200 DO mice (Churchill et al., 2012); and indeed has been achieved in various other studies looking at traits such as atherosclerosis (Smallwood et al., 2014), pain (Recla et al., 2014), anxiety-like behavior (Logan et al., 2013), and memory (Hsiao et al., 2020). Here, I will detail mapping a significant QTL of large effect on chromosome 13 using the DO population, validating the locus effect in CC strains with the founder haplotypes driving the phenotypic variation, and behaviorally confirming that this locus mediates attention.

2.2 Identification of a QTL for pre-attentive processing

Based on our lab's previous work (Hsiao et al., 2020) characterizing the DO founders, and cohorts from the 19th and 25th generations, we determined that successful mapping of genetic loci to behavioral traits would require 1) an automated and robust behavioral assay requiring minimal training, thus narrowing the observed variance to genetic and task-associated features, and 2) approximately 200 mice to detect a quantitative trait locus (QTL) that shifts the trait mean by 1 standard deviation at 95% confidence. Since traditional tests of attention require weeks of training, we selected and optimized a simple and robust assay to test an innate pre-attentive processing behavior, referred to as pre-pulse inhibition (PPI). PPI is the ability to suppress an innate startle response, which reflects a process of filtering irrelevant cues to enhance goal-directed selection. Notably, while the startle response is considered

a bottom-up process (Koch & Schnitzler, 1997), its inhibition is a top-down process (Li et al., 2009) that has been linked to downstream measures of cognition, including selective (Scholes & Martin-Iverson, 2010) and sustained (Scholes & Martin-Iverson, 2009) attention. Although PPI can also be confounded by changes in anxiety and motor response (which we tested post hoc), we chose this task as a fast, high-throughput, sensitive screen for pre-attentive processing, which we could then follow up with more targeted tests for attention.

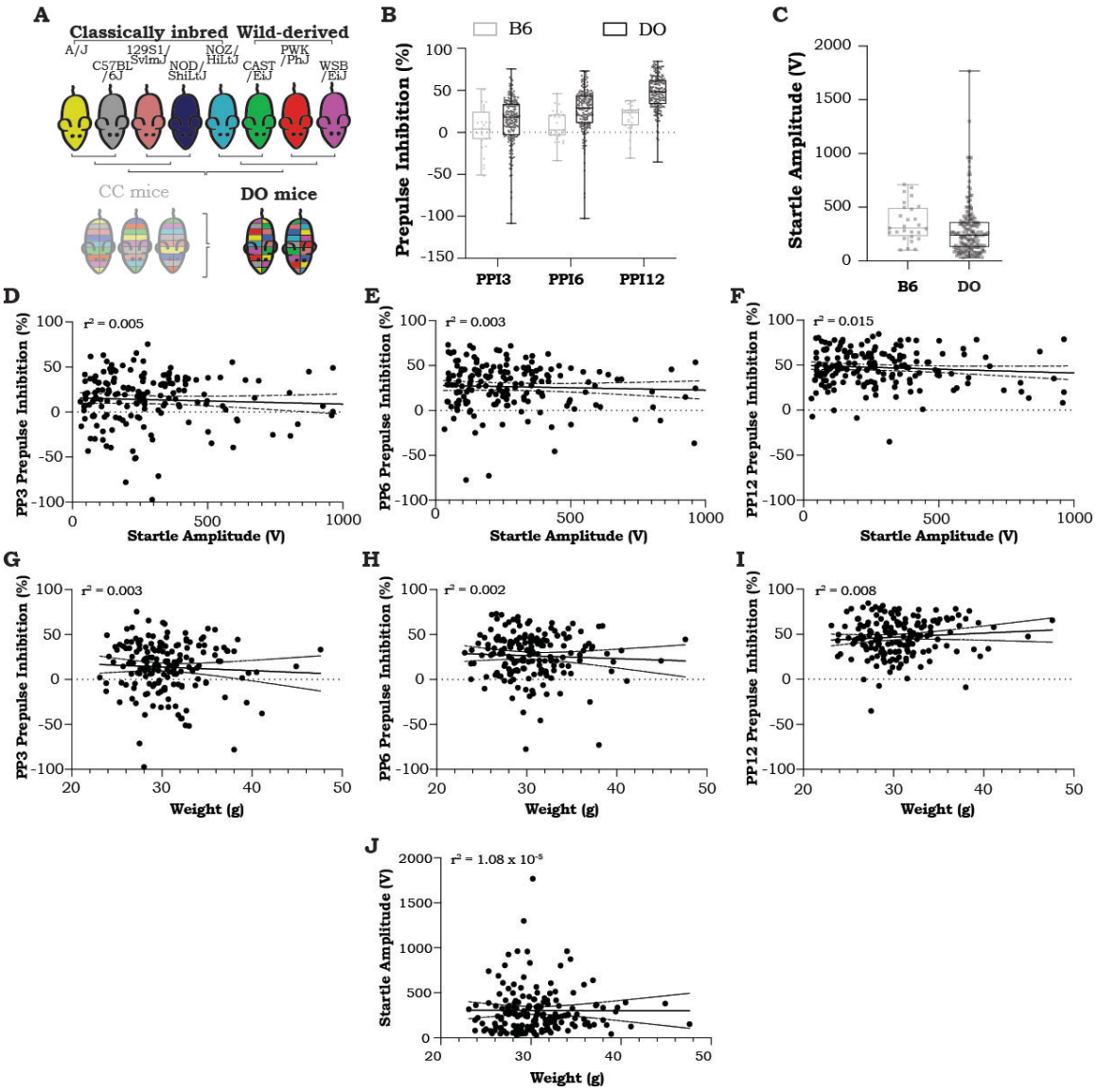

Figure 2.1 PPI and startle response phenotypes in DO mice

(**A**) Outbreeding scheme to generate the DO mice. (**B**) Pre-attentive processing performance (assayed by PPI) in B6 (n=27) and DO (n=176) mice measured as percent of startle response inhibited at 3 different pre-pulse intensities: 3, 6, and 12 dB above background (PPI3, 6, and 12, respectively). Boxes indicate 2nd and 3rd quartiles with median and range. (**C**) Startle response assessed during PPI experiments in B6 (grey, n=27) and DO (black, n=176) mice measured as startle amplitude (V). Boxes indicate 2nd and 3rd quartiles with median and range. (**D-J**) Correlations in DO mice (n=176) between (**D**) startle response, measured as the magnitude of startle amplitude (V), and PPI, measured as percent inhibition, at 3 (PP3, r^2=0.005), (**E**) 6 (PP6, r^2=0.003), and (**F**) 12 (PP12, r^2=0.014) dB above background, (**G**) weight and startle response (r^2=1.084 x 10^{-5}), and (**H-J**) weight and PPI – (**H**) PP3, r^2=0.003; (**I**) PP6, r^2=0.002; (**J**) PP12, r^2=0.008) dB above background.

We tested 191 mice for performance in PPI. Briefly, for each DO mouse, we measured the startle response to a 120 dB tone as well as the percent inhibition of this startle when preceded by a weaker 3, 6, or 12 dB tone (PPI3, PPI6, PPI12). We first confirmed that the phenotypic variability of the DO greatly surpassed that of the C57BL/6J (B6) classical inbred line, as would be expected from the underlying genetic variation (Figure 2.1B). We excluded 15 mice that exhibited greater PPI3 than PPI12, suggesting potential hearing impairment. With the remaining mice, we found no significant correlations between PPI and startle response or body weight (Figures 2.1C-J).

We next genotyped the 176 DO mice using the GigaMUGA platform (114,184 loci had variability in our cohort). Founder haplotype reconstructions were performed with a hidden Markov model (Broman et al., 2019; Hsiao et al., 2020), which showed extensive allelic heterozygosity genome-wide (Figure 2.2A) and we observed approximately equal founder contributions across our cohort suggesting minimal allelic loss. We performed QTL mapping for PPI using R/qtl2[23] and identified a single large effect genetic locus (19% of behavioral variance explained) on chromosome 13 with genome-wide significance of $p \leq 0.01$ (Figure 2.2C; LOD score for PPI6 = 8.22, 95%CI: 92.22- 94.09 Mb). These mapping effects were not due to individual differences in the underlying innate startle response (Figure 2.1E), nor was there any QTL detected when mapping to startle scores (Figure 2.2B). The chromosome 13 QTL for PPI6 was also confirmed to be statistically significant using a second mapping approach, miQTL (Figure 2.2D). QTL mapping of PPI3 and PPI12 did not reveal any loci that surpassed significance thresholds (Figures 2.2E-F), but a suggested peak for PPI3 indeed mapped to the same Chr 13 QTL (Figure 2.2E; LOD score = 5.88, 95%CI: 90.51-94.09 Mb), supporting the functional significance of this locus.

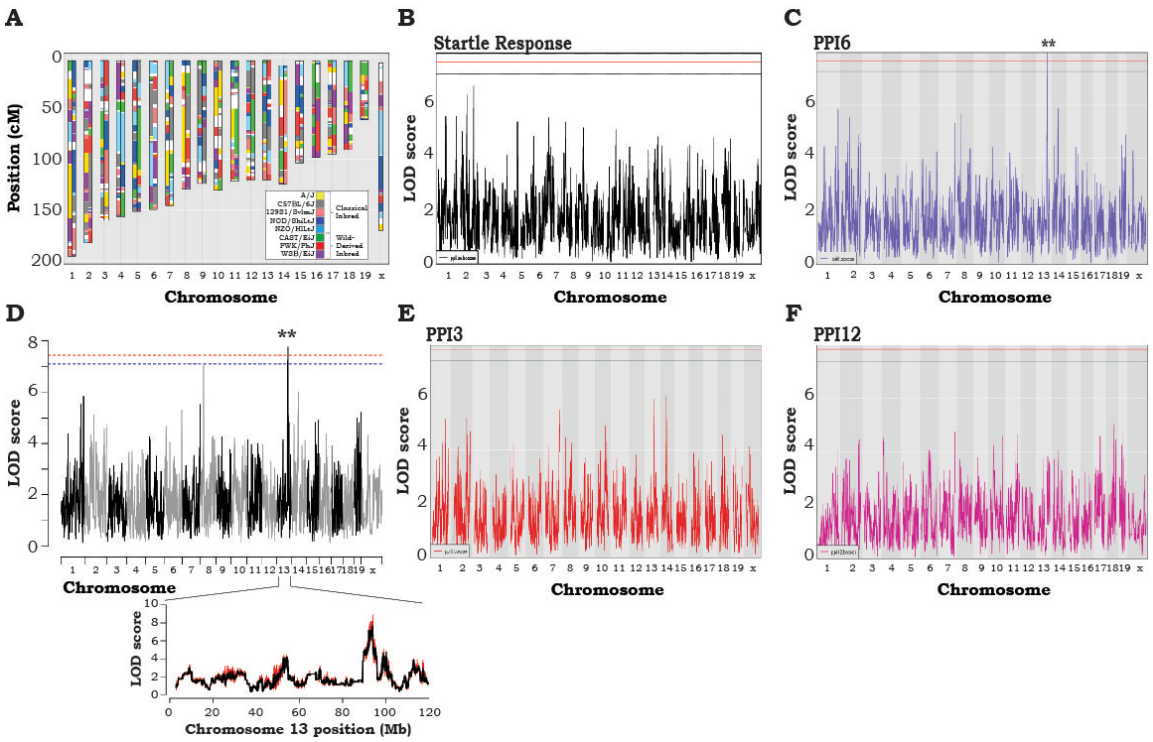

Figure 2.2 QTL mapping in DO mice

(**A**) Haplotype reconstruction of a representative DO mouse from the 25th generation of the population. Colors correspond to the founder lines (shown in legend) for which the genomic contribution is attributed at each depicted locus. (**B**) QTL mapping analysis of startle response (by R/qtl2) shown as a Manhattan plot of startle response. Blue and red lines indicate confidence thresholds, blue: 90%, red: 95%. (**C**) QTL mapping analysis (by R/qtl2), shown as Manhattan plots, of PPI at 6 dB above background (PPI6, purple, genome-wide $p<0.01$). (**D**) Top: QTL analysis (by miQTL) for PPI at 6 dB above background (PPI6) after 50 imputations of genotype. Genome-wide $p<0.01$. Bottom: Mapping analyses performed using R/qtl2 (black) and miQTL (red) revealing minimal fluctuation in LOD score across imputations (overlapping bands). (**E-F**) QTL mapping analysis (by R/qtl2), shown as Manhattan plots, of PPI at (**E**) 3 (PPI3, red) and (**F**) 12 dB (PPI12, magenta) above background. For **B-F**, n=176, blue lines indicate 90% confidence threshold and red lines indicate 95% confidence threshold.

2.3 The Chr13 QTL drives variation in pre-attentive processing

To further increase confidence in this locus we performed an allele effect analysis (Chapter 6 - Methods) and found that the B6 haplotype (henceforth referred to as Chr13QTL^{B6}) was associated with high performance while the WSB/EiJ haplotype (henceforth referred to as Chr13QTL^{WSB}) was associated with low performance (Figures 2.3A-B). We then asked whether specific recombinant inbred Collaborative Cross (CC) lines, which have the same multi-parent origins as the DO (Figure 2.3C) and possess either Chr13QTL^{B6} or Chr13QTL^{WSB} would separate into high- and low-performers, respectively.

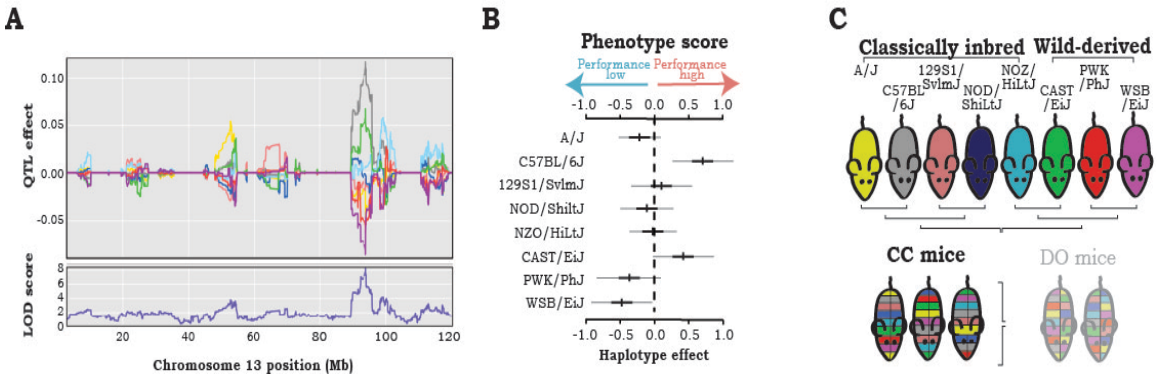

Figure 2.3 Founder haplotype contributions driving PPI phenotypic variance

(**A**) Effect of each founder allele on PPI performance along Chromosome 13, as measured by founder coefficients from the linkage model. Coefficients diverge substantially at peak QTL. Logarithm of odds (LOD) score at each chromosomal position shown. (**B**) Haplotype representation at the Chromosome 13 locus and corresponding *z*-scored phenotypes of each founder strain, quantified as mean ± 95% confidence intervals. (**C**) Outbreeding scheme to generate the CC mice.

We analyzed the genomes of existing CC lines and selected two that were homozygous for our desired Chr13QTL^{B6} (CC083) or Chr13QTL^{WSB} (CC025) haplotypes (Figure 2.4A) while maintaining distinctive mosaic representations of the founder genomes at other loci. We compared PPI performance between CC083 and CC025 mice and found that the CC083 had significantly greater PPI than CC025 (Figure 2.4B). As with the DO, this finding was not explained by differences in peak startle or body weight (Figures 2.4C-J), nor was it due to differences in gross motor activity, motor coordination, or hearing sensitivity (Figures 2.4K-M). These data indicate that genetic variation at the Chr13 locus, specifically the WSB vs B6 genotype, drives significant variation in pre-attentive processing.

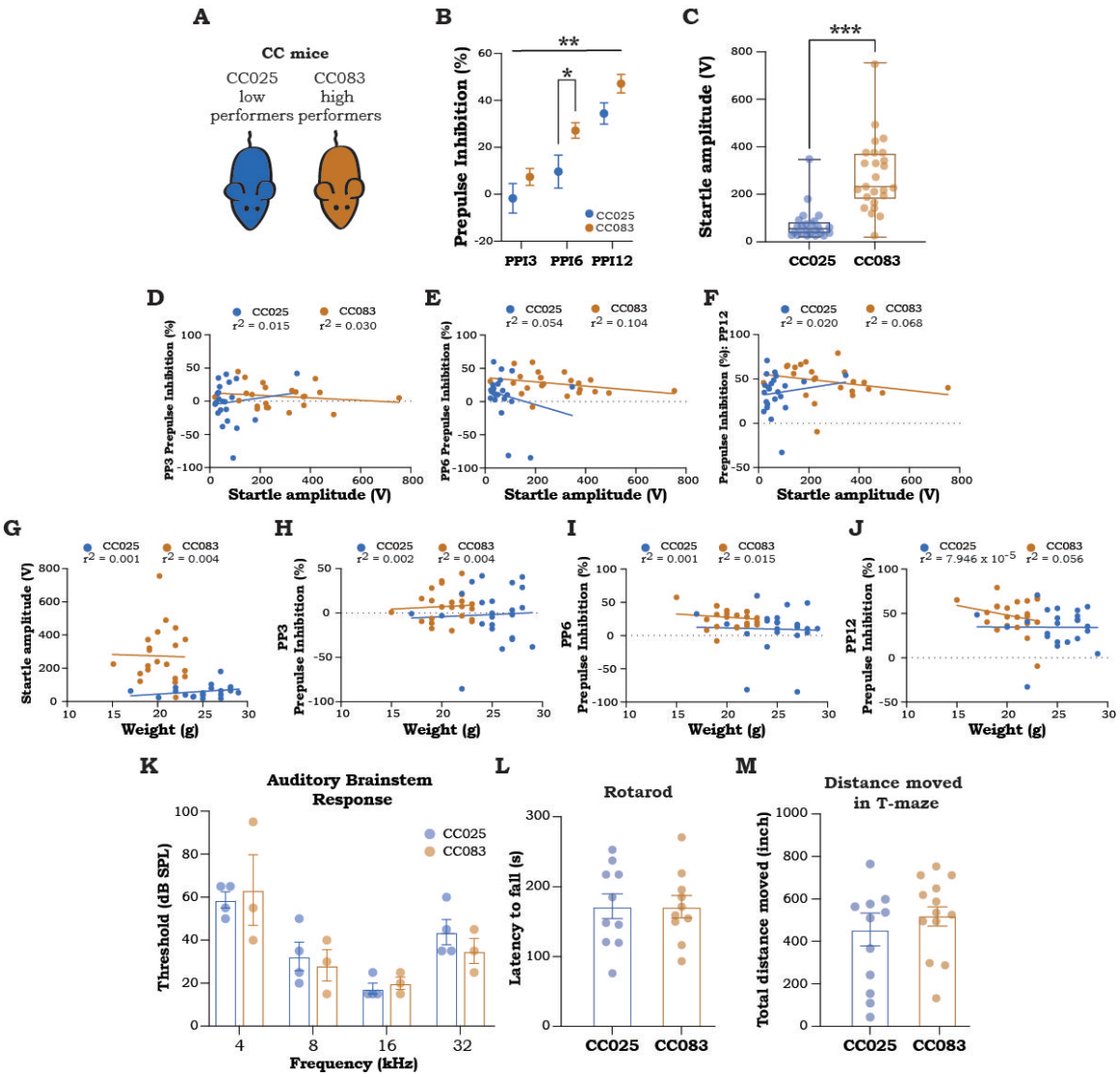

Figure 2.4 PPI and startle response phenotypes in CC mice

(**A**) Cartoon of the CC025 (low-performers, blue) and CC083 (high-performers, tan) used in subsequent experiments. (**B**) PPI3, 6, and 12 values for CC083 (n=27) and CC025 (n=24) mice shown as mean ± SEM. Two-way ANOVA p=0.003 for CC line main effect followed by Holm-Sidak's test for multiple comparison p_{PPI6}=0.05. (**C**) Startle response, measured as the magnitude of the startle amplitude (V) in CC025 (blue, n=24) and CC083 (tan, n=27) mice. Boxes indicate 2nd and 3rd quartiles with median and range. (**D-J**) Correlations in CC025 (n=24) and CC083 (n=27) between startle response and PPI, measured as percent inhibition, at (**D**) 3 (PP3: CC025 r^2=0.015, CC083 r^2=0.030), (**E**) 6 (PP6: CC025 r2=0.054, CC083 r2=0.104), and (**F**) 12 dB (PP12: CC025 r^2=0.020, CC083 r^2=0.068) above background, (**G**) weight and startle response (CC025 r^2=0.001, CC083 r^2=0.004), and (**H-J**) weight and PPI at (**H**) 3 (PP3: CC025 r2=0.002, CC083 r^2=0.004), (**I**) 6 (PP6: CC025 r^2=0.001, CC083 r^2=0.015), (**J**) 12 dB (PP12: CC025 r^2=7.946 x 10-5, CC083 r^2=0.056) above background. (**K**) Auditory brainstem response measured as minimum thresholds in CC025 (n=4) and CC083 (n=3) as sound pressure level (dB) in response to increasing frequencies (4, 8, 16, 32 kHz). (**L**) Gross motor activity measured in CC025 (n=11) and CC083 (n=11) mice as total distance moved (inch) in a T-maze apparatus during a 6-min test. (**M**) Motor coordination measured in CC025 (n=10) and CC083 (n=10) as latency (s) to fall from the rod in the Rotarod test averaged across 4 consecutive trials. Height of bars in **K**-**L** represents mean and error bars indicate SEM.

2.4 The Chr13 QTL mediates attentional variation

To more directly test the role of this Chr 13 QTL in attention, we studied CC083 and CC025 mice in a more targeted assay for attention, an operant signal detection task. Here, mice are trained to nose-poke in response to a 5 second auditory cue within 10 seconds of cue onset to receive a food reward. Once the mice have sufficiently learned the task (Chapter 6 - Methods), their attentional load is then challenged by decreasing the length of the cue to 1 sec and reducing the response window (Figure 2.5A). Similar signal detection tasks have been widely used to assay attention (Bushnell & Strupp, 2009; Callahan & Terry, 2015; Turner et al., 2016). They provide multiple metrics to track attention including accuracy, response latency, and trial omissions. During the initial 5 second cue training, there were no significant differences in learning the task, but CC083 mice were already exhibiting fast latency responses, and after increased attentional load during the 1 second trials, the CC083s significantly outperformed the CC025s in all of the measures of attention including accuracy (percentage of correct responses), proportion of delayed responses, latency to all responses, and, most significantly, latency to correct responses (Figures 2.5B-E).

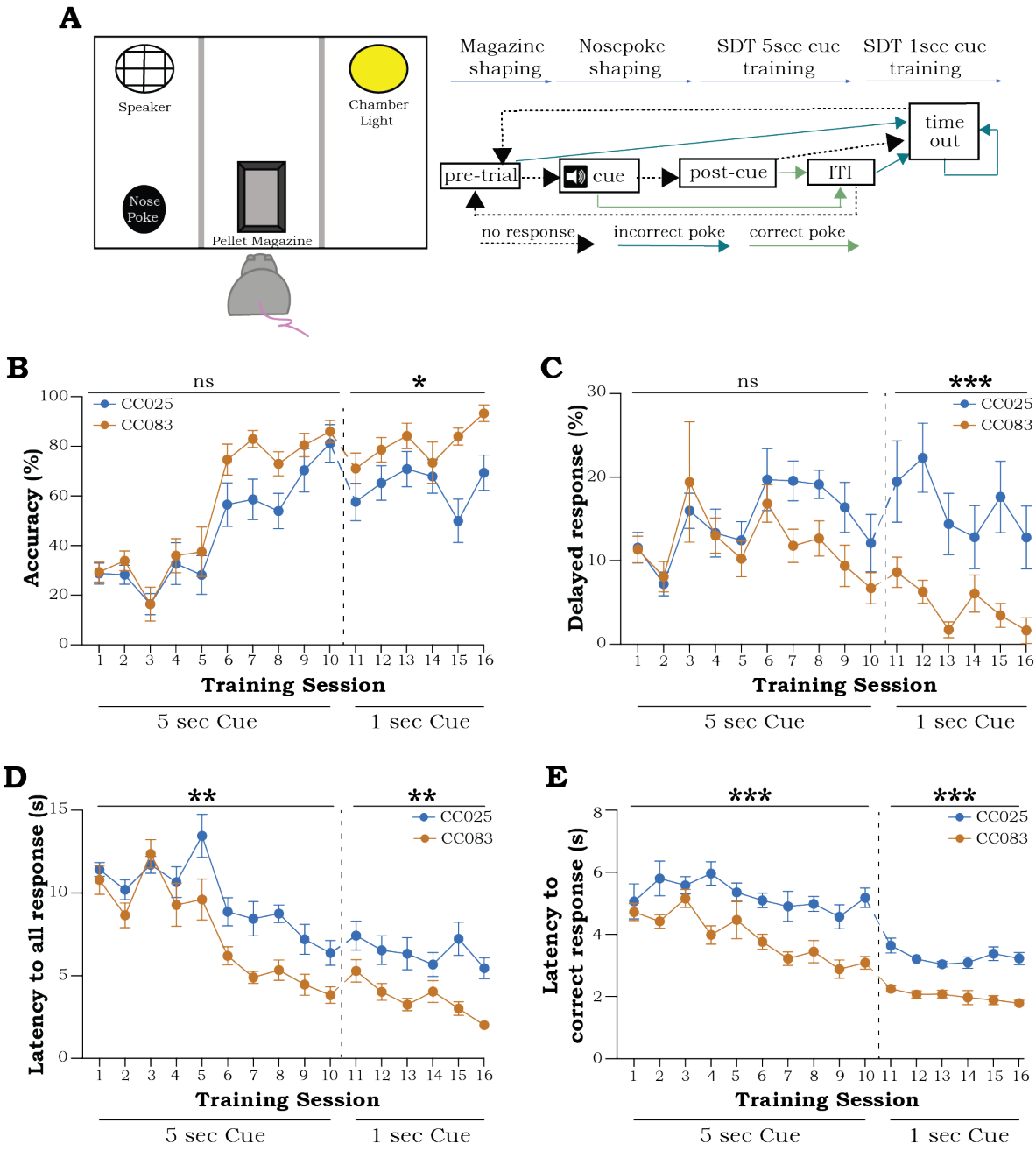

Figure 2.5 Chr13 QTL mediates variation in attentional performance
(**A**) Left: Schematic of operant wall of arena used for signal detection task (SDT). Right: Schematic of SDT protocol. (**B-E**) Performance of CC025 (n=10 for 5 sec cue and n=9 for 1 sec cue) and CC083 (n=10 for 5 sec cue and 1 sec cue) mice during SDT across sessions, showing (**B**) accuracy (correct response) percentage (repeated-measures two-way ANOVA p= 0.02 for CC line main effect in 1 sec cue sessions), (**C**) delayed response percentage (repeated-measures two-way ANOVA p<0.001 for CC line main effect in 1 sec cue sessions), (**D**) mean latency from cue to first response within all trials (repeated-measures two-way ANOVA for p=0.009 and p=0.002 for CC line main effect in 5 sec cue and 1 sec cue sessions, respectively), and (**E**) mean latency from cue to first response within correct trials (repeated-measures two-way ANOVA p<0.001 for CC line main effect in both 5 and 1 sec cue sessions). Data in **B**-**E** shown as mean ± SEM.

Notably, the strains did not differ in other cognitive, or social measures that we tested (Figures 2.6A-C). We did observe differences in measures of anxiety-related behavior (Figure 2.6D-E), which requires further consideration given the important dependencies between anxiety and attention (although of note, in later experiments, when manipulating only the causal gene at this locus, no significant differences in anxiety-like behavior was observed, Figures 3.12F-G).

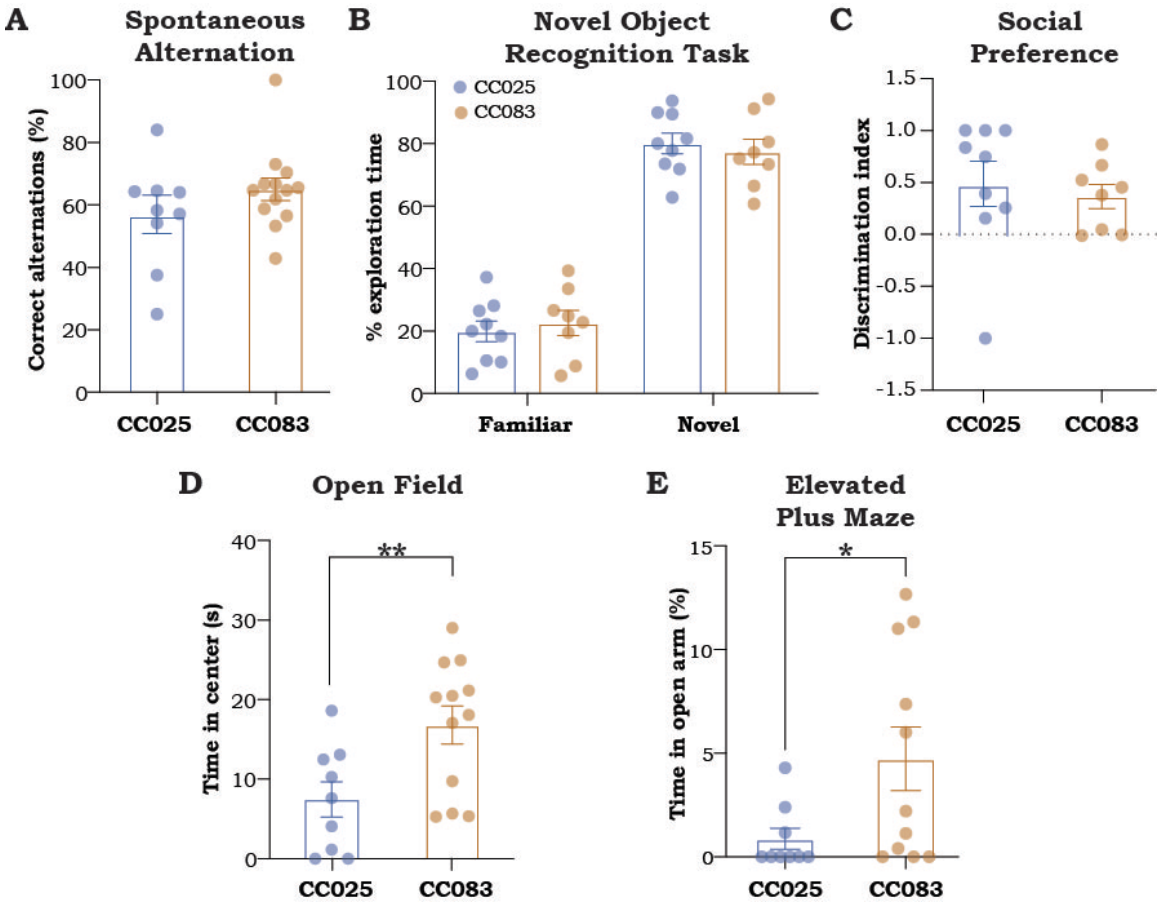

Figure 2.6 Memory, social, & anxiogenic behavioral characterization of CC mice

(**A**) Working memory performance assessed in a T-maze apparatus for CC025 (n=9) and CC083 (n=13) mice, measured as the percent of correct alternations (Methods). (**B**) Short-term memory tested by a novel object recognition test in CC025 (n=9) and CC083 (n=10) mice, measured as time spent exploring the novel object *vs* the familiar one and expressed as percentage of total exploration time during a 5-min test. Two-way ANOVA showed significant main effect for novelty ($p<0.001$), but not for CC line. (**C**) Social behavior for CC025 (n=9) and CC083 (n=8) mice, expressed as discrimination index determined by exploration time in a 3-chamber social interaction test. (**D-E**) Anxiety-like behavior measured as (**D**) time, in seconds, spent in the center of an open field arena during a 5-min test in CC025 (n=9) and CC083 (n=12). Welch-corrected t-test showed a significant difference between CC lines ($p=0.01$) and (**E**) percentage of time spent in the open arm of an elevated plus maze during a 5-min test in CC025 (n=11) and CC083 (n=10) mice. Welch-corrected t-test showed a significant difference between lines ($p=0.03$). For data in **A**-**E**, height of bars represents mean and error bars indicate SEM.

2.5 Summary

In this chapter, I discussed using the highly outbred DO mouse population for genetic mapping to identify a discrete genomic locus on Chromosome 13 for pre-attentive processing. We showed that not only is this locus statistically significant, but explains a large (~19%) proportion of the PPI phenotypic variance. We then validated the locus effect using recombinant inbred CC mouse lines that contain the founder haplotype contributions for high and low PPI performance, as indicated by our DO mapping analysis. Expanding beyond PPI as a pre-attentive measure, we demonstrated that, from all possible downstream cognitive processes linked to PPI, the CC mice only differed in attention (Figures 2.5-2.6). There was also a difference in anxiety-like behavior – a connection that will be further explored in chapters 3 and 6. Together, these data indicate that genetic variation at the Chromosome 13 locus drives differences in attentional performance. We next sought to understand which gene(s) within the locus (Table 2.1) was driving the changes in attentional performance in an unbiased manner.

Table 2.1 Protein-coding genes in the Chr13 QTL

Gene Symbol	Gene Name	Gene Symbol	Gene Name
Msh3	mutS homolog 3 (E. coli)	Cmya5	cardiomyopathy associated 5
Dhfr	dihydrofolate reductase	Papd4	PAP associated domain containing 4
Ankrd34b	ankyrin repeat domain 34B	Homer1	homer scaffolding protein 1
Fam151b	family with sequence similarity 151, member B	Dmgdh	dimethylglycine dehydrogenase precursor
Zfyve16	zinc finger, FYVE domain containing 16	Bhmt	betaine-homocysteine methyltransferase
Spz1	spermatogenic leucine zipper 1	Bhmt2	betaine-homocysteine methyltransferase 2
Serinc5	serine incorporator 5	Mtx3	metaxin 3
Thbs4	thrombospondin 4	Arsb	arylsulfatase B

CHAPTER 3. *Homer1* isoform expression during development modifies attentional performance in adults

3.1 Introduction

Sensory gating circuitry, which has largely been studied in the context of PPI, is thought to be divided amongst two aspects – mediation (bottom-up) and regulation (top-down). Circuit components that directly act on the startle circuitry are considered mediating elements; whereas circuitry that processes the prepulse sensory input and determines its impact on the startle response is regarded as modulatory (L. Li et al., 2009; Rohleder et al., 2016). There is extensive overlap in the circuitry involved in top-down PPI modulation and top-down attention. Both involve PFC-MD recurrent activity (Kim et al., 2021; Schmitt et al., 2017) as well as neuromodulatory input to PFC from regions such as VTA and LC (Alsene et al., 2011; Suzuki et al., 2024; Kabanova et al., 2015; Bari et al., 2020). This overlap suggests that the mechanism of the Ch13 QTL effect on both pre-attentive processing and attention could be the same, acting in the same brain structures. Using these insights, we sought to uncover the causal gene(s) within the QTL. This chapter will delve into our efforts to identify the gene(s) responsible for the Chr13 QTL attentional effect, validate the functional impact, and gain insight into the molecular mechanism. To this end, we carried out bulk RNA sequencing (RNAseq) on overlapping circuit components of pre-attentive and attentional control, *in vivo* shRNA-based gene knockdowns, and single-cell RNA sequencing (scSeq).

3.2 Identification of Chr13 QTL locus gene differentially expressed in mice with high- and low-performance on pre-attentive and attentive behaviors

We performed bulk RNAseq in DO high- and low-performers, focusing on the PFC because of its central role in attentional processing, but also including related, attentionally-relevant brain areas such as MD, and VTA (Figure 3.1A). We found that samples stratified by performance in PFC and MD, but not in VTA (Figure 3.1B), leading us to ask which genes within the Chromosome 13 locus (Table 2.1) were differentially expressed in MD or PFC between high- and low-performers. Of all locus genes, only *Homer1* was significantly differentially expressed, with substantial downregulation in PFC in high-performers (Figure 3.1C, adjusted $p<0.001$). *Homer1* has several transcript variants due to alternative splicing (Figure 3.1D) (Bottai et al., 2002), and thus we assessed whether differential expression was uniform across splice isoforms. Strikingly, only the short, activity-dependent isoforms, *Homer1a* (Brakeman et al., 1997; Kato et al., 1997) and *Ania3* (Bottai et al., 2002), were differentially expressed between DO high- and low-

performers (Figure 3.1E, p(*Homer1a*)=0.003, p(*Ania3*)=0.007, two-way ANOVA with post hoc Holm-Sidak test for multiple comparisons).

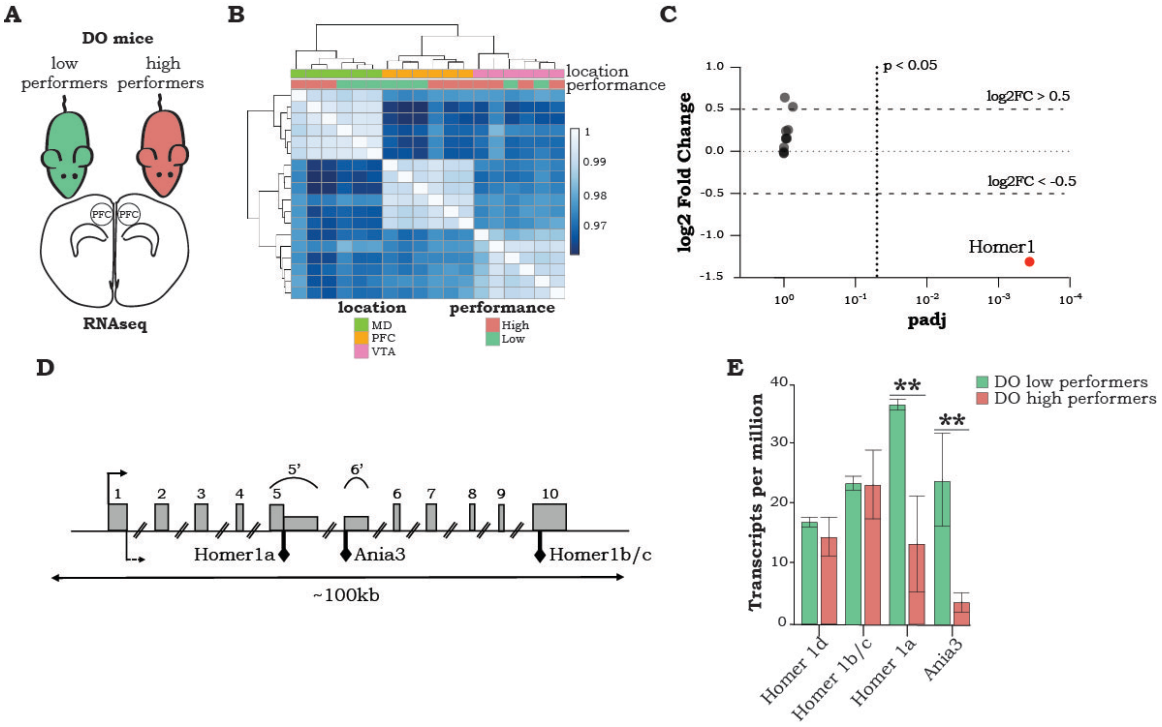

Figure 3.1 Chr13 QTL effect maps to PFC *Homer1* expression in DO mice

(**A**) Schematic of prefrontal cortex (PFC) dissection region for RNAseq in DO high (pink) and low (green) performers. (**B**) Heatmap of hierarchical clustering by Euclidean distance among gene expression profiles in DO high- (pink, n=3) and low- performers (green, n=3) as highlighted in Figure 3A-B and from three brain regions per mouse: mediodorsal thalamus (MD, green), prefrontal cortex (PFC, orange) and ventral tegmental area (VTA, pink). Clustering is visible by brain region and performance in MD and PFC. (**C**) Volcano plots of differential expression between DO high (pink) and low (green) performers for all locus genes (n=3 per group) from bulk PFC RNAseq. Dashed lines indicate significance thresholds (adjusted p=0.05 and log2FC=0.5 or =-0.5). Only *Homer1* crosses both thresholds (red). (**D**) Schematic representation of the *Homer1* genomic exon structure. The bent arrow at the 5' end of exon 1 (solid line, above) indicates the putative transcription start site, while the bent arrow at the 3' end of exon 1 (dashed line, below) represents the translation start site. Black diamonds (below) indicate the translation stop sites of *Homer1a*, *Ania3*, and *Homer1b/c*, respectively. To create *Homer1a*, exon 5 extends into intron 5 to create the *Homer1a*-specific exon (5') through alternative splicing. *Ania3* is generated by alternative splice usage of intron 5 sequence downstream of exon 5' as the *Ania3*-specific exon 6'. (Adapted from Bottai et al. 2002). (**E**) Expression levels of *Homer1* isoforms in PFC from DO high- and low-performers (n=3 per group), significant differential expression of *Homer1a* and *Ania3*, p<0.01 by two-way ANOVA with post hoc Holm-Sidak's test. Height of bars represents mean and error bars indicate SEM.

Furthermore, bulk RNAseq from high (CC083) and low (CC025) performing CC lines also confirmed significant differences in *Homer1* expression (Figures 3.2A-B). As with the DO mice, the differential *Homer1* expression in CC mice (Figure 3.2B) was driven by the

downregulation of *Homer1a* and *Ania3* in the high-performing CC083s (Figure 3.2C, 2-way ANOVA p<0.001, Holm-Sidak test for multiple comparisons p(*Homer1a*)<0.001, p(*Ania3*)<0.001).

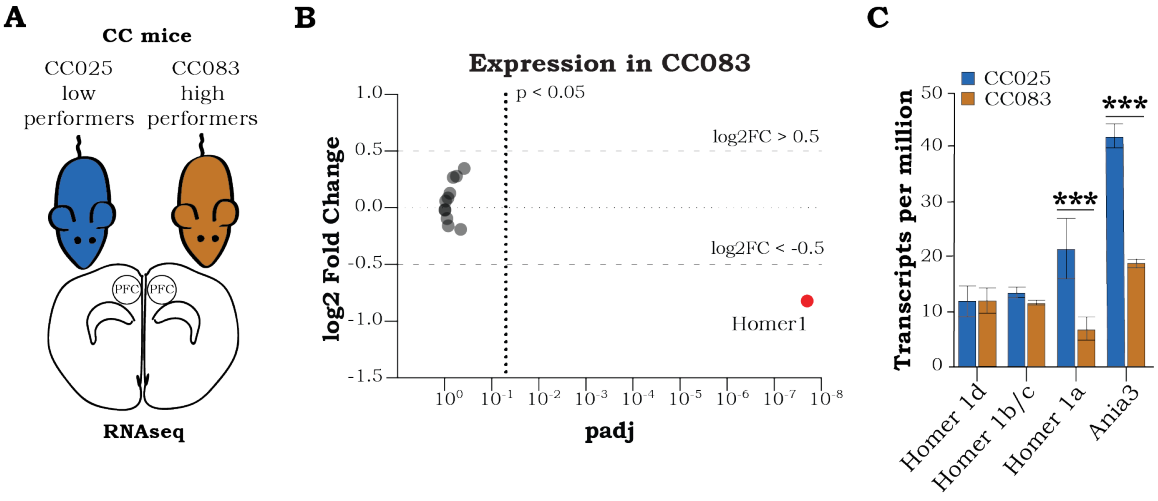

Figure 3.2 *Homer1* is differentially expressed in PFC of CC mice varying in Chr13 QTL composition
(**A**) Schematic of PFC dissection region for RNAseq in CC high (CC083, tan) and low (CC025, blue) performers. (**B**) Volcano plot showing differential expression of Chr13 QTL genes for CC083 (high performers) relative to CC025 (low performers) mice after DESeq2. Dashed lines indicate significance thresholds (adjusted p=0.05 and log2FC=0.5 or =-0.5). Only *Homer1* crosses both thresholds (red). (**C**) Expression levels of *Homer1* isoforms in PFC from CC high- and low-performers (n=3 per group), p<0.001 by two-way ANOVA with post hoc Holm-Sidak's test for multiple comparisons. Height of bars represents mean and error bars indicate SEM.

3.3 *Homer1a* and *Ania3* expression affects attentional performance developmentally

3.3.1 *Homer1a* and *Ania3* do not affect pre-attentive processing when manipulated during adulthood

Since *Homer1a* is better characterized and conserved than *Ania3* (Bottai et al., 2002; Xiao et al., 1998), we next assessed whether *Homer1a* manipulations could drive behavioral changes in attentional performance. To knock down *Homer1a*, we designed and tested AAV-based short-hairpin RNAs (shRNAs) to target the *Homer1a* isoform *in vitro* and selected the most effective shRNA (Figures 3.1A-B) for bilateral PFC injections *in vivo* and behavioral testing. To overexpress *Homer1a,* which has endogenous expression primarily in excitatory pyramidal neurons, we cloned the *Homer1a* coding sequence into an AAV-based CaMKII-eYFP vector (Figure 3.1C) for bilateral PFC injection and behavioral testing.

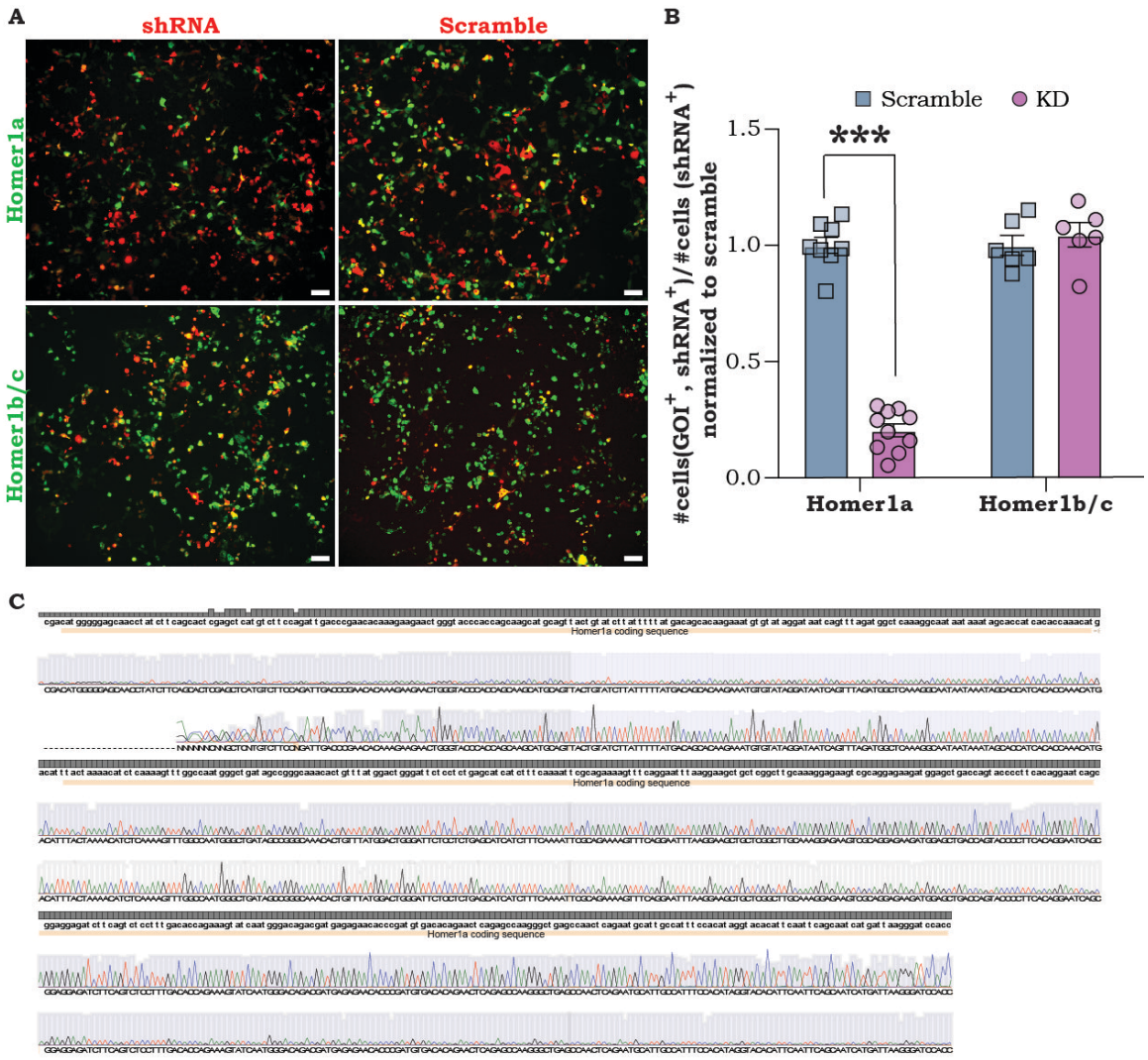

Figure 3.3 *in vitro* validation of *Homer1a* knockdown and overexpression constructs

(**A-B**) *in vitro* validation of *Homer1a* gene knockdown construct. (**A**) Representative images of HEK cells co-transfected with *Homer1a* (left column) or Scramble (right column) shRNA plasmids (red) and *Homer1a* (top row) or *Homer1b/c* (bottom row) expression plasmids (green). Scale bar: 100 µm. (**B**) Quantification of shRNA-mediated gene knockdown, expressed as the fraction of cells co-expressing the gene of interest (GOI; a *Homer1* isoform expression plasmid) and shRNA construct relative to the total number of cells expressing the shRNA plasmid, normalized to the respective scramble control experiments (two-way ANOVA showed significant main effects for *Homer1* isoform expression, $p<0.001$, and shRNA construct, $p<0.001$, as well as a significant interaction between those variables, $p<0.001$; Holm-Sidak's test for multiple comparisons showed a significant difference in *Homer1a* expression between the shRNA (purple, n=10 fields of view across 2 independent experiments) and Scramble (blue, n=8 fields of view across 2 independent experiments) constructs, $p<0.001$). The height of the bars represents mean and error bars indicate SEM. (**C**) Electropherogram AAV-CaMKII(1.3)-*Homer1a*-eYFP overexpression plasmid purified from transformed competent cells aligned to the *Homer1a* coding sequence (tan bar near the top of each line). The height of the grey boxes at the top of each line is proportional to the number of sequencing runs aligned to the reference sequence (maximum # of sequencing runs in image = 2).

To our surprise, despite extensive construct expression (Figures 3.4A-C and 3.4F-H), and validation of substantial decreases or increases respectively in corresponding *Homer1a* RNA levels, we did not observe any significant behavioral effect for either the knockdown or overexpression experiments (Figures 3.4D-E and 3.4I-J).

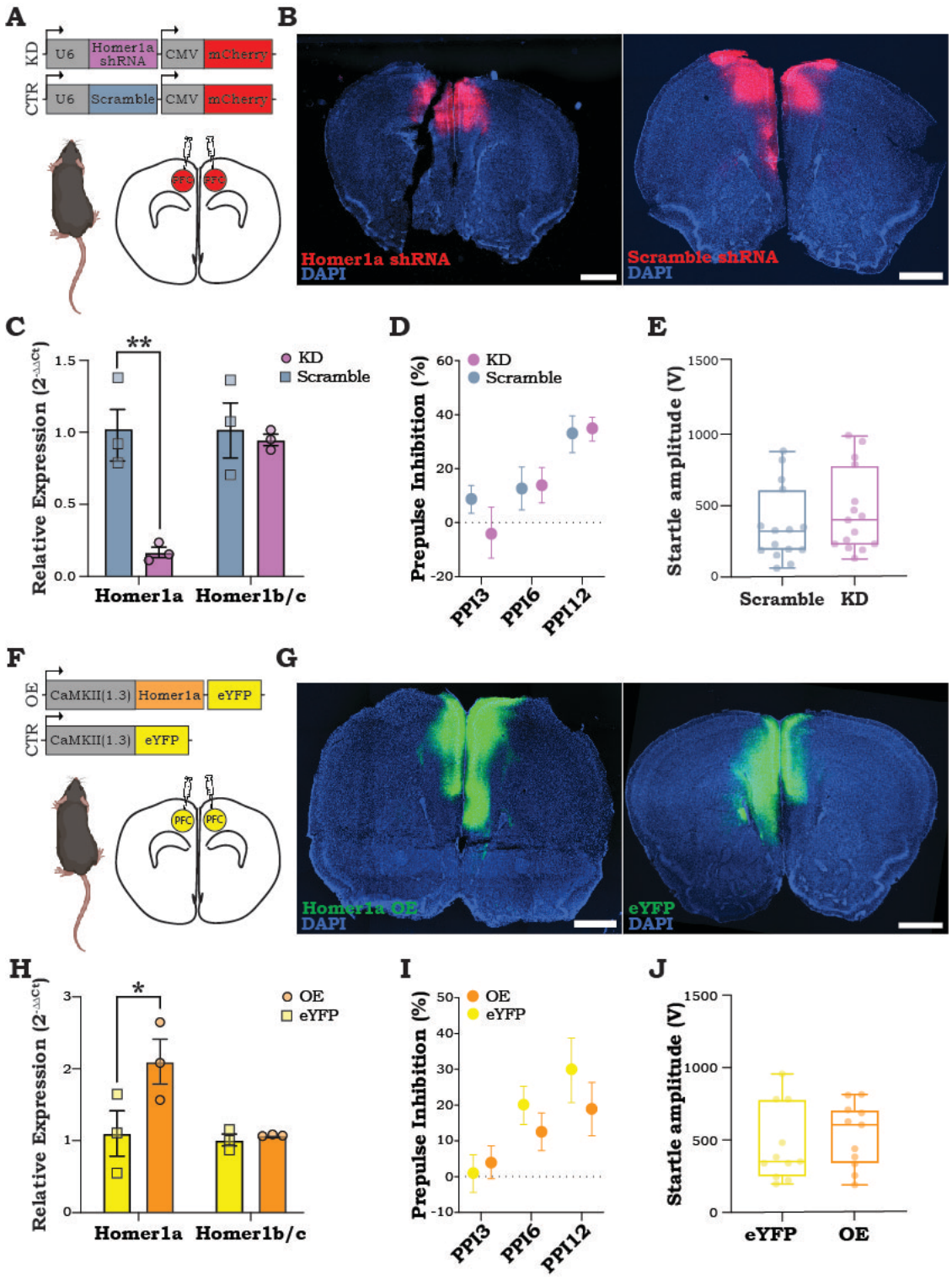

Figure 3.4 *Homer1a* knockdown and overexpression in PFC has no effect *in vivo*

(**A**) Schematic of constructs and injection location (PFC) for knockdown (KD, purple) and control (Scramble, blue) in adult B6 mice. (**B**) Validation histology performed 8 weeks after bilateral injection of AAV-U6-Homer1a shRNA-CMV-mCherry knockdown virus (upper panel) and AAV-U6-Scramble-CMV-mCherry control virus (lower panel) into PFC showing viral transduction in the target area (DAPI, blue; mCherry, red), scale bars: 1000μm.(**C**) *Homer1a* and *Homer1b/c* expression levels (relative to controls) in PFC samples dissected from KD (n=3) and control (n=3) mice measured by qPCR, (two-way ANOVA showed significant main effects for shRNA construct, p=0.007, and *Homer1* isoform expression, p=0.02, as well as a significant interaction between those variables, p=0.02; post hoc Holm-Sidak's test for multiple comparisons shows a significant difference in *Homer1a* expression, p=0.003). (**D**) PPI in KD (n=15) and Scramble (n=15) mice measured as percent inhibition at 3 prepulse intensities: 3, 6, and 12 dB above background (PPI3, 6, and 12, respectively). (**E**) Startle response in Scramble (n=15) and adult KD (n=15) mice. Boxes indicate 2nd and 3rd quartiles with median and range. (**F**) Schematic of constructs and injection location (PFC) for overexpression (OE, orange) and control (eYFP, yellow) in adult B6 mice. (**G**) Validation histology performed 8 weeks after bilateral injection of AAV-CaMKII(1.3)-eYFP overexpression virus (upper panel) and AAV-CaMKII(1.3)-eYFP control virus (lower panel) into PFC, showing viral transduction in the target area (DAPI, blue; eYFP, green), scale bars: 1000μm.(**H**) *Homer1a* and *Homer1b/c* expression levels (relative to controls) in PFC samples dissected from OE (n=3) and control eYFP (n=3) mice measured by qPCR (two-way ANOVA showed significant main effects for expression construct, p=0.04, and *Homer1* isoform expression, p=0.04; post hoc Holm-Sidak's test for multiple comparisons shows a significant difference in *Homer1a* expression, p=0.03). (**I**) PPI in OE (n=11) and control eYFP (n=10) mice measured as percent inhibition at 3 pre-pulse intensities: 3, 6, and 12 dB above background (PPI3, 6, and 12, respectively). (**J**) Startle response in control eYFP (yellow, n=15) and OE (orange, n=15) mice. Boxes indicate 2nd and 3rd quartiles with median and range. Data in **C**, **D**, **H**, and **I** are shown as mean ± SEM.

To account for the potential functional redundancy of *Homer1a* through *Ania3*, after *in vitro* validation (Figures 3.5A-B), we performed bilateral PFC injections of the AAV shRNA targeting *Homer1a* pooled together with an AAV-based shRNA for *Ania3* (Figures 3.5C-D) and also saw no significant behavioral effect (Figures 3.5E-F).

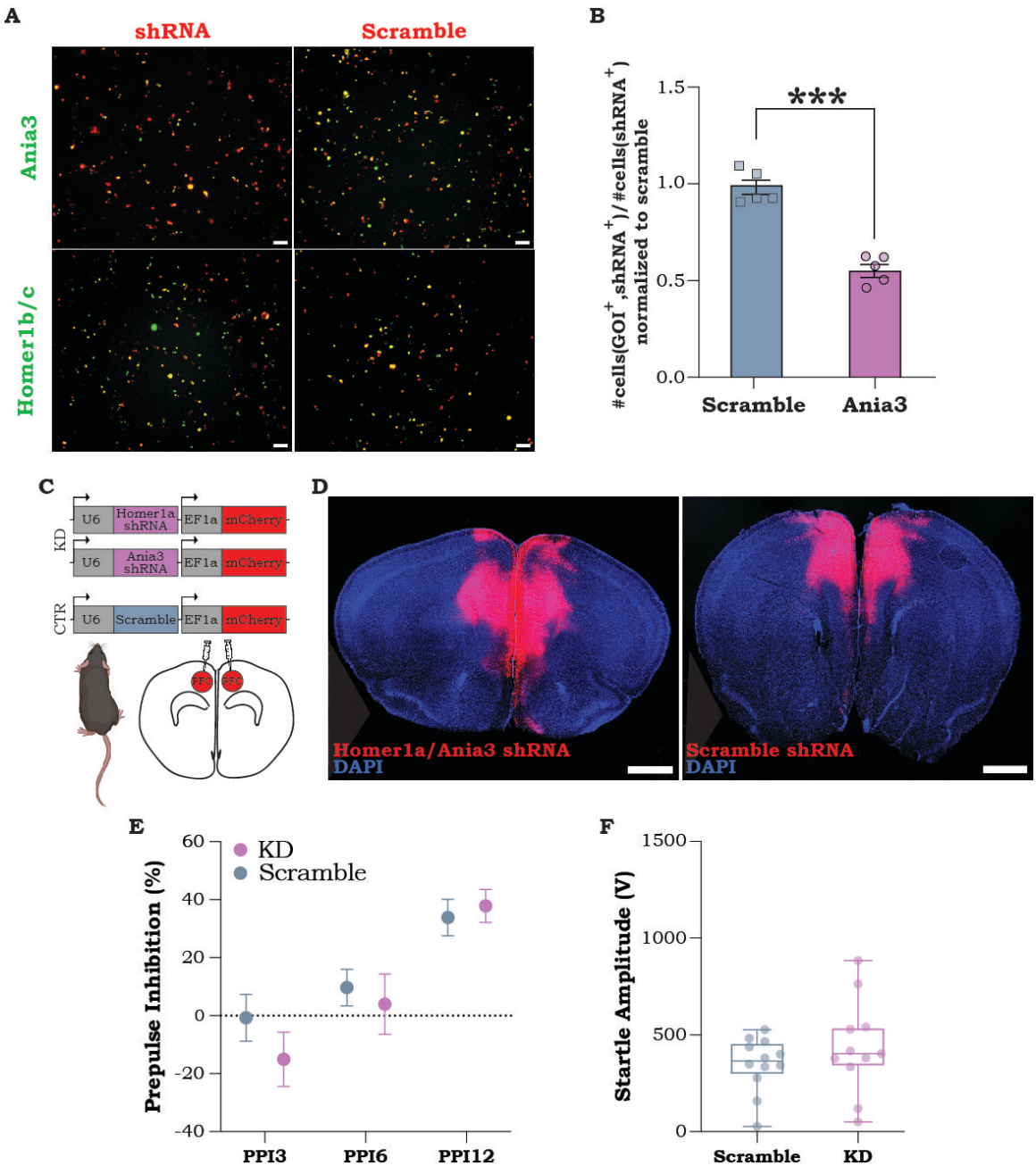
A
shRNA
Scramble
Ania3
Homer1b/c
B
***
#cells(GOI+,shRNA+)/#cells(shRNA+) normalized to scramble
1.5
1.0
0.5
0.0
Scramble
Ania3
C
KD
U6
Homer1a shRNA
EF1a
mCherry
U6
Ania3 shRNA
EF1a
mCherry
CTR
U6
Scramble
EF1a
mCherry
PFC
STR
D
Homer1a/Ania3 shRNA
DAPI
Scramble shRNA
DAPI
E
KD
Scramble
Prepulse Inhibition (%)
60
40
20
0
-20
-40
PPI3
PPI6
PPI12
F
Startle Amplitude (V)
1500
1000
500
0
Scramble
KD

Figure 3.5 *Homer1a/Ania3* adult PFC knockdown has no effect
(**A**) *in vitro* validation of gene knockdown constructs. Representative images of HEK cells co-transfected with *Ania3* (panels 1 and 3 from the left) or Scramble (panels 2 and 4 from the left) shRNA (red) and *Ania3* (panels 1 and 2 from the left) or *Homer1b/c* (panels 3 and 4 from the left) expression constructs (green), Scale bar: 100 µm. (**B**) Quantification of shRNA-mediated gene knockdown, expressed as the fraction of cells co-expressing the *Ania3* expression construct and shRNA or scramble construct relative to the total number cells expressing the shRNA or scramble, normalized to the scramble control experiments. In cells transfected with the *Ania3* expression construct, there was a significant difference in *Ania3* expression between the cells co-transfected with the shRNA (n=5 fields of view), and Scramble (n=5 fields of view) constructs (Unpaired t-test, $p<0.001$). (**C**) Schematic of constructs and injection location (PFC) for knockdown (KD, purple) and control (Scramble, blue) in adult B6 mice. (**D**) Validation histology performed 12 weeks after bilateral injection of pooled AAV-U6-Homer1a_shRNA-EF1A-mCherry and AAV-U6-Ania3_shRNA-EF1A-mCherry for KD (left panel) and AAV-U6-Scramble-EF1A-mCherry control virus for Scramble (right panel) into PFC, showing viral transduction in the target area (DAPI, blue; mCherry, red). Scale bars: 1000 µm. (**E**) PPI in Scramble (n=12) and adult *Homer1a/Ania3* KD, (n=11). (**F**) Startle response in Scramble (n=12) and adult KD (n=11) mice. Boxes indicate 2nd and 3rd quartiles with a line at the median, bars indicate range. Data in **B** and **E** shown as mean ± SEM.

3.3.2 *Homer1a* and *Ania3* mediate variation in pre-attentive and attentional performance during postnatal development

To assess whether the effects of *Homer1a* may be developmental in origin, based on prior work on germline knockouts (Datko et al., 2017; Jaubert et al., 2006; Lominac et al., 2005; Szumlinski et al., 2005), we profiled the expression of *Homer1a*, *Ania3*, and *Homer1b/c* in CC083 and CC025 mice across postnatal development (Figure 3.6A). We found that the expression of *Homer1a* and *Ania3,* but not that of *Homer1b/c*, diverged between the CC lines as early as p14-p21 (Figure 3.6B), suggesting possible developmental roles in regulating attentional processing.

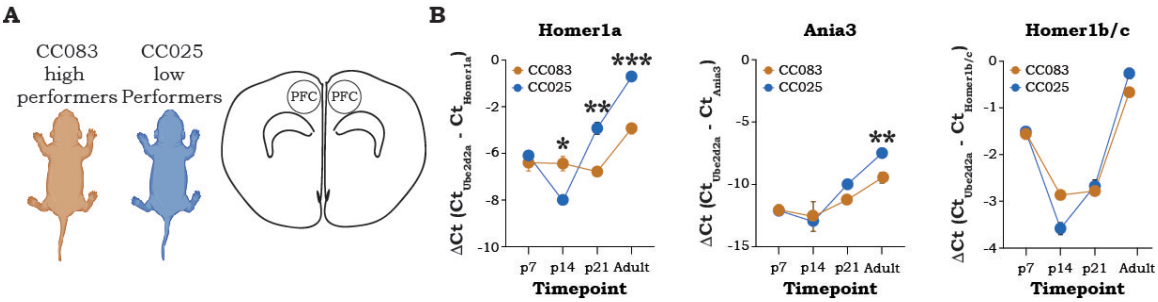

Figure 3.6 CC expression of *Homer1* isoforms across postnatal development
(**A**) Schematic of PFC dissection region in CC high (CC083, tan) and low (CC025, blue) performers for qPCRs across postnatal development. (**B**) PFC expression of *Homer1a*, *Ania3*, and *Homer1b/c* in CC083 and CC025 mice at p7, p14, p21, and in adult by qPCR (n=3 per strain per timepoint), significant differences for *Homer1a* by two-way ANOVA with post hoc Holm-Sidak's test, $p=0.02$ at p14, $p=0.002$ at p21, and $p<0.001$ at adult; and for *Ania3* $p=0.002$ at adult.

To test this hypothesis, we knocked down *Homer1a* and *Ania3* during early developmental stages (p14-p21) to evaluate the effect on adult behavior by bilaterally injecting the pooled *Homer1a* and *Ania3* shRNA AAVs into the PFC of neonatal B6 pups (Figure 3.7A; referred to as KD_{dev}). Despite the developmental *Homer1a* knockdown being less effective than the adult manipulation (~80% in adults and ~60% in pups; Figures 3.4C & 3.7B), we observed significant improvement in measures of pre-attentive processing (PPI, Figure 3.7C). This difference in PPI could not be attributed to startle response or weight (Figures 3.7D-G).

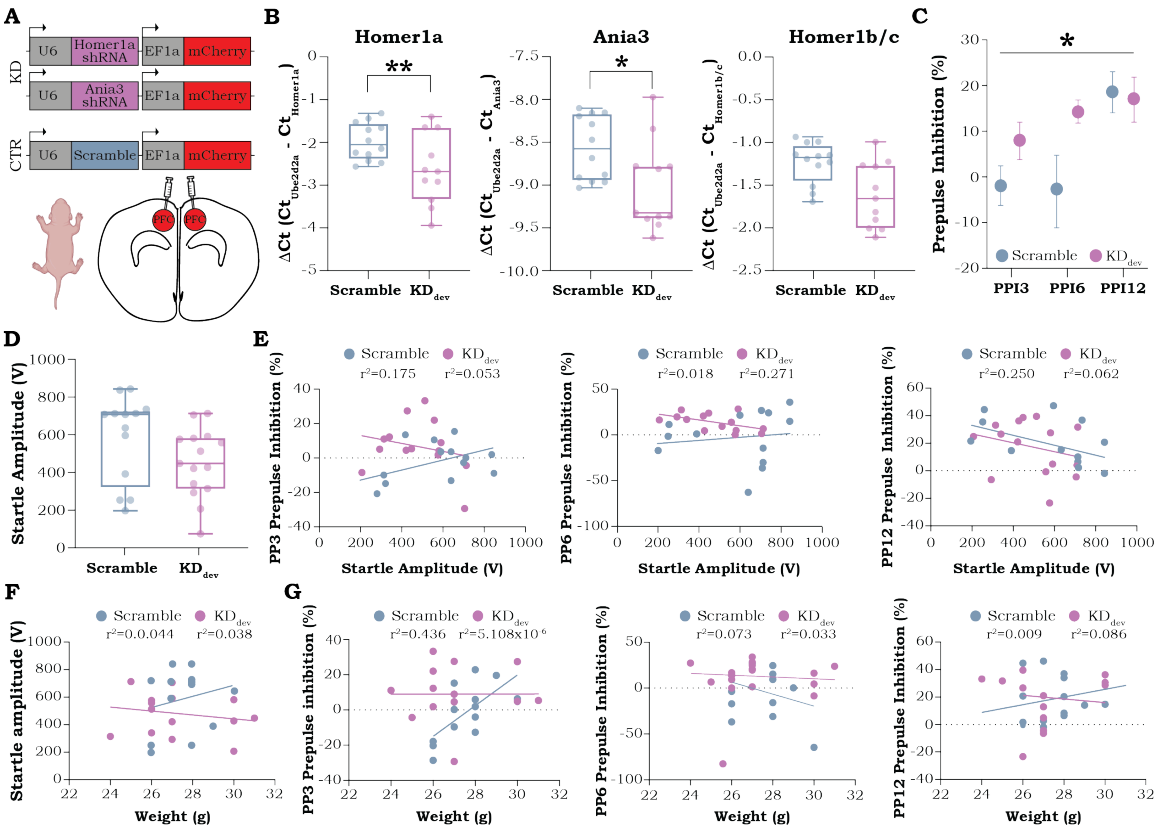

Figure 3.7 Developmental PFC knockdown of *Homer1a/Ania3* improves pre-attentive processing

(**A**) Schematic of constructs and injection location (PFC) for knockdown (KD_{dev}, purple) and control (Scramble, blue) in neonatal B6 mice. (**B**) *ex vivo* validation of developmental knockdown manipulation assessed by quantification of *Homer1a* (left), *Ania3* (center) and *Homer1b/c* (right) levels measured by qPCR in PFC samples dissected from Scramble (n=12) and KD_{dev} (n=15), (two-way ANOVA showed significant main effects for group, $p<0.001$, and *Homer1* isoform expression, $p<0.001$; post hoc Holm-Sidak's test for multiple comparisons shows a significant difference in *Homer1a,* $p=0.004$, and *Ania3,* $p=0.05$, expression). (**C**) PPI in Scramble (n=13) and KD_{dev}, (n=15). Significant differences between KD_{dev} and Scramble groups by two-way ANOVA ($p=0.04$). (**D-G**) Correlations between (**E**) startle response and PPI, measured as percent inhibition, at 3 dB (PP3: Scramble $r^2 = 0.175$, KD_{dev} $r^2 = 0.053$,), 6 dB (PP6: Scramble $r^2 = 0.018$, KD_{dev} $r^2 = 0.271$,), and 12 dB (PP12: Scramble $r^2 = 0.250$, KD_{dev} $r^2 = 0.062$,) above background, (**F**) weight (g) and startle response (Scramble $r^2 = 0.044$, KD_{dev} $r^2 = 0.038$,), and (**G**) weight and PPI (PP3: Scramble $r^2 = 0.436$, KD_{dev} $r^2 = 5.108$ x10-6,; PP6: Scramble $r^2 = 0.073$, KD_{dev} $r^2 = 0.033$; PP12: Scramble $r^2 = 0.009$, KD_{dev} $r^2 = 0.086$).

We next tested the effects of developmental *Homer1a/Ania3* knockdown on multiple, widely-used assays for attention in adult mice including: 1. An operant SDT (Figure 3.8), 2. A head-fixed Go/No-Go task (Figure 3.9), 3. a head-fixed multi-modal SDT (Figure 3.10), and 4. an attentional set shift task (Muzzio et al., 2009) (Figure 3.11). In all cases, we observed that mice with developmental prefrontal *Homer1/Ania3* knockdown performed significantly better on measures of attention than

the corresponding controls. For instance, on the operant SDT task, when comparing response latencies on correct trials, the most sensitive measure of attentional performance, KD_{dev} mice exhibited significantly faster response latencies than controls, particularly on correct trials and when we increased attentional demand, that persisted throughout the extent of both cue length phases (Figure 3.8); repeated-measures two-way ANOVA p(5sec cue)=0.04, p(1sec cue)<0.001).

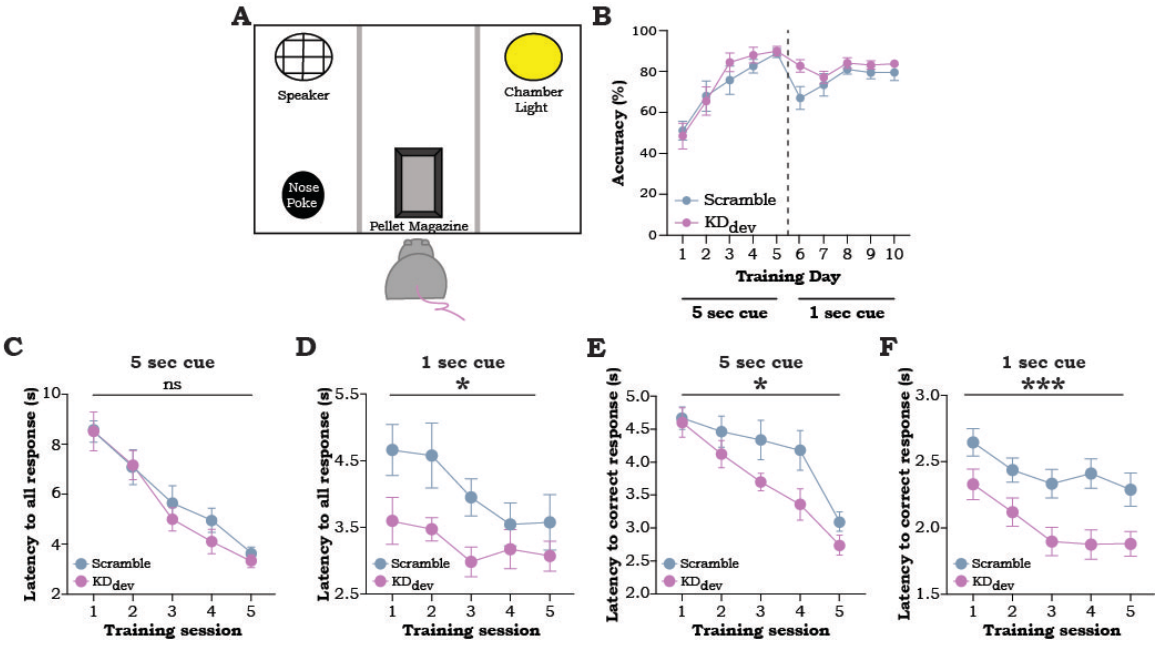

Figure 3.8 KD_{dev} performance on the operant signal detection task
(**A**) Schematic of operant wall of arena used for signal detection task (SDT). (**B**) Percentage of correct responses for Scramble and KD_{dev} mice (5 sec cue: n=13 per group; 1 sec cue: Scramble n=9 KD_{dev} n =11). (**C**-**F**) Performance during SDT across training sessions, shown as (**C**-**D**) mean latency from cue to first response within all trials (p_{1sec}=0.04) and (**E**-**F**) mean latency from cue to first response within correct trials (p_{5sec}=0.03; p_{1sec}<0.001) for 5 sec cue (Scramble n=13 and KD_{dev} n=13, **C** and **E**) and 1 sec cue (Scramble n=9 and KD_{dev} n=11, **D** and **F**). Significant differences between groups measured by repeated-measures two-way ANOVA. Data in **B**-**F** is shown as mean ± SEM.

Furthermore, in a head-fixed Go/No-Go task where mice were trained to respond to one paired tone/odor cue and inhibit response to a different paired tone/odor cue (Figure 3.9A), KD_{dev} mice responded faster (Figures 3.9B and 3.9D) and more reliably (Figure 3.9E) than scramble controls. Notably, the magnitudes of these effect sizes were substantial, for instance, with mean differences in response latency between groups of ~400ms on the operant SDT task (~2.3 s for Scramble controls vs 1.9 s for KD_{dev}, p<0.001 by two-way ANOVA, Figure 3.8F) and ~150 ms for the head-fixed Go/No-Go task (~600 ms for Scramble controls vs ~450 ms for KD_{dev}, p<0.01 by two-way ANOVA, Figure 3.9D, and appreciable qualitatively in the raw lick rasters in Figure 3.9B). These effects between

groups were not present prior to learning, and there were no obvious differences in overall ability to learn the tasks (Figures 3.8B and 3.9C).

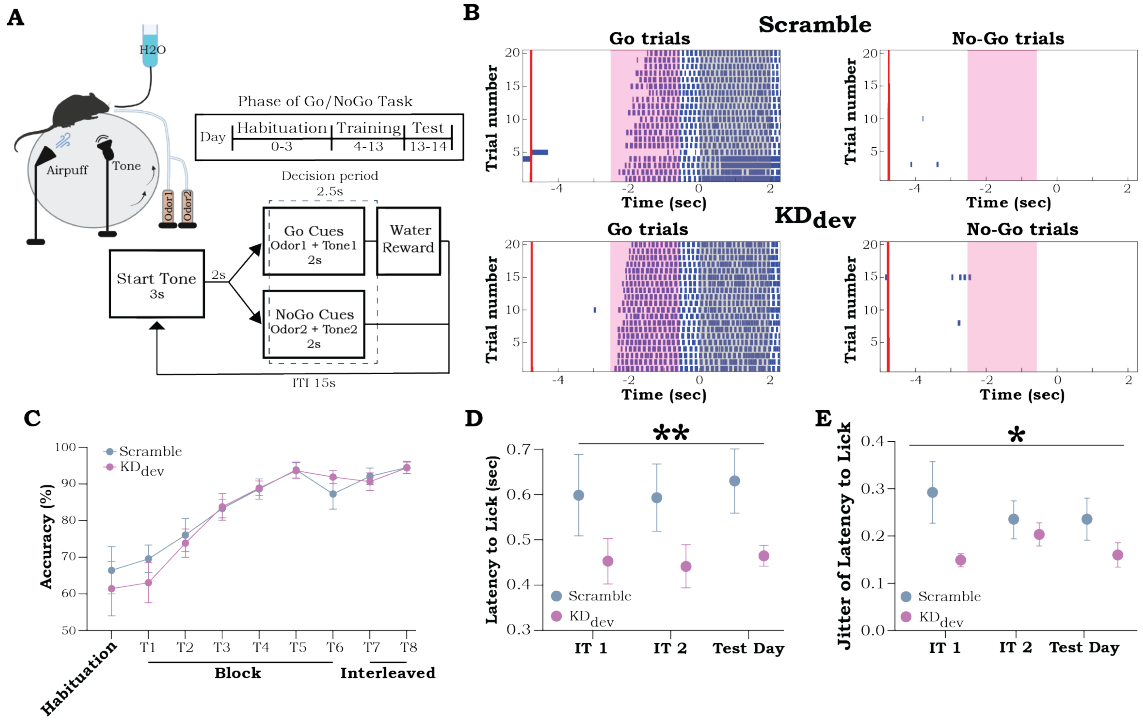

Figure 3.9 KD_{dev} performance on the head-fixed Go/No-Go task
(**A**) Schematic of Go/No-Go task setup (left) and training protocol (right). Below is the task structure for interleaved training days and the testing day. (**B**) Raster plots of licking for the Go/No-Go task for representative Scramble (above) and KD_{dev} (below) mice. Go (right) and No-Go (left) trials were interleaved during testing but are depicted separately. Time 0 is plotted as the end of the decision period. The red bar shows the end of the start tone, pink shading notes the time when cues are delivered, and licks are plotted as blue ticks. (**C**) Go/No-Go task performance accuracy across habituation and training days (n = 8 per group). (**D**) Quantification of the latency to first lick within the decision period of Go trials. Each point is the average latency to first lick for the first 10 Go trials per animal (p=0.005, n=8 per group, significant main effect between groups by two-way ANOVA). (**E**) Quantification of the latency to first lick jitter. Jitter was quantified as the standard deviation of first lick latencies across the first 10 Go trials (significant main effect between groups by two-way ANOVA showed a significant main effect between groups, p=0.01, n=8 per group). Data in **C**-**E** is shown as mean ± SEM.

In a head-fixed multi-modal signal detection task, where mice only had to respond to the presence of a paired tone/odor cue (Figure 3.10), KD_{dev} mice responded only slightly faster but displayed strikingly less variability in their response latency than the scramble control mice (Figures 3.10B-C).

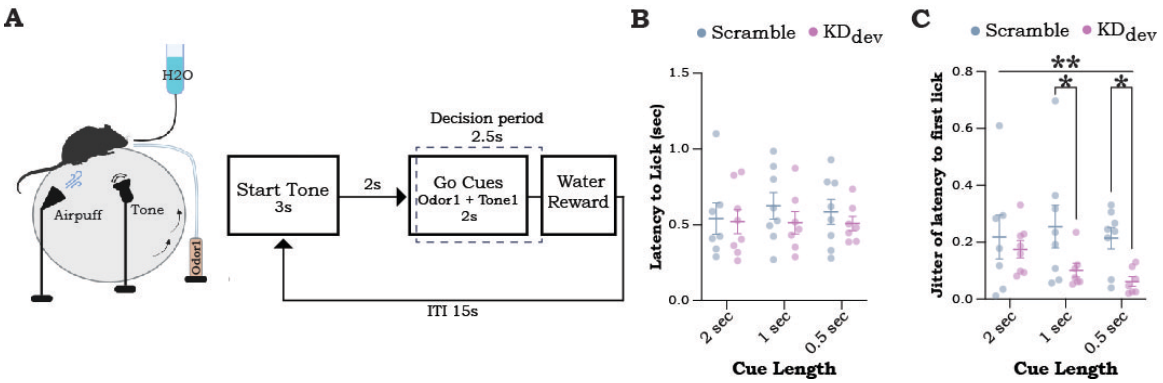

Figure 3.10 KD_{dev} performance on the head-fixed signal detection task

(**A**) Diagram of head-fixed SDT setup (left) and task structure (right). (**B**) Quantification of the latency to first lick (sec) within the decision windows across cue lengths. Each point is the average latency to first lick for the first 3 Go trials per animal (2 sec cue: Scramble n=7, KD_{dev} n=8; 1 sec and 0.5 sec cues: Scramble n=8, KD_{dev} n=7). (**C**) Quantification of the latency to first lick jitter across cue lengths. Jitter is quantified as the standard deviation of first lick latencies across the first 3 Go trials (two-way ANOVA showed a significant main effect for group, p=0.007, and post hoc Holm-Sidak's test for multiple comparisons showed significant differences between groups at 1 and 0.5 sec cues, p=0.04 for both cue lengths, 2 sec cue: Scramble n=7, KD_{dev} n=8; 1 sec and 0.5 sec cues: Scramble n=8, KD_{dev} n=7).

Finally, using an odor-based attentional set shift task we found that KD_{dev} mice displayed significantly shorter latencies to retrieve the food reward than control mice (Figure 3.11), despite having a similar baseline exploratory activity (measured as time spent exploring the four odors during pre-trial when the reward was not present: Scramble 92.2 ± 8.8 and KD_{dev} 100.1 ± 12.7), or bias between odors (measured as % time spent exploring each odor / total exploration time (cloves: Scramble 27.5 ± 3.4, KD_{dev} 23.3 ± 2.7; cumin: Scramble 20.9 ± 1.9, KD_{dev} 21.9 ± 3.2; sage: Scramble 24.2 ± 2.3, KD_{dev} 27 ± 2.6; cinnamon: Scramble 27.4 ± 2.3, KD_{dev} 27.8 ± 2.1).

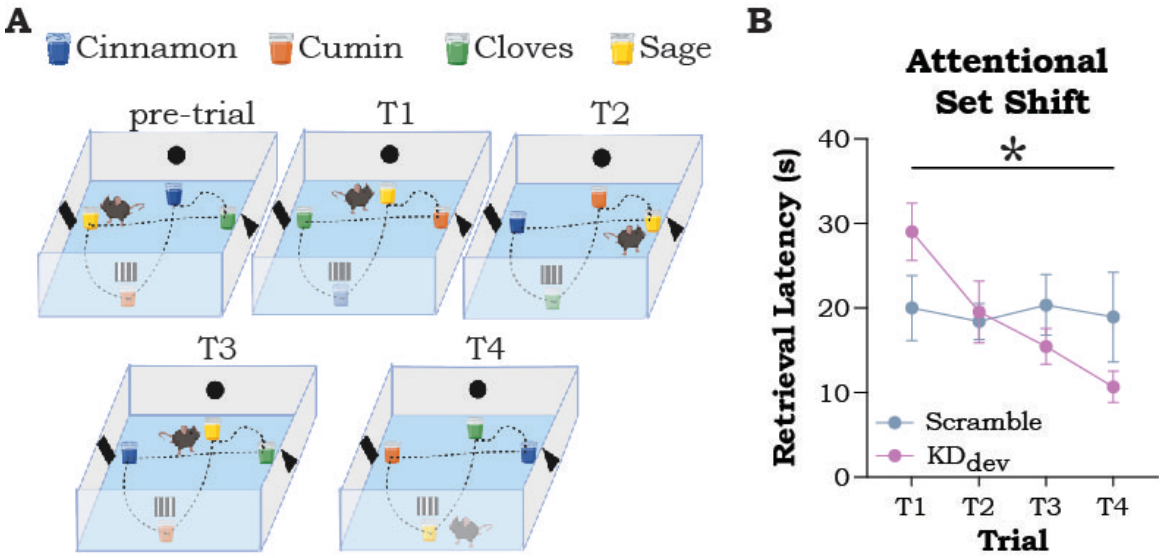

Figure 3.11 KD_{dev} performance on the attentional set shifting task
(**A**) Schematic of the Attentional Set Shift setup and experiment protocol. (**B**) Latency (s) to retrieve the chocolate pellet measured in Scramble (n=14) and KD_{dev}, (n=13) mice during the 4 trials of the Attentional Set Shift test. Significant interaction between trial and group, p=0.04, by repeated-measures two-way ANOVA. Data is shown as mean ± SEM.

We also performed control experiments to assess the sensory or motor confounds to the observed differences in pre-attentive (Figure 3.7D-F) and attentional processing (Figures 3.12A-C). As with CC mice, KD_{dev} and controls displayed no significant differences in gross motor control or motor coordination (Figures 3.12A-B), hearing (Figure 3.12C), nor did they display broad cognitive deficits (Figures 3.12D-E). Notably, however, in contrast to CC mice, they exhibited no significant differences in anxiety-like behavior (Figure 3.12F-G). Altogether, these results demonstrate that reducing the expression of *Homer1a/Ania3* in PFC during early postnatal development is sufficient to improve pre-attentive processing and attentional performance in adulthood. This raised the question: how does the endogenous differential expression of short *Homer1/Ania3* isoforms throughout development affect cellular functions underlying attention in the adult?

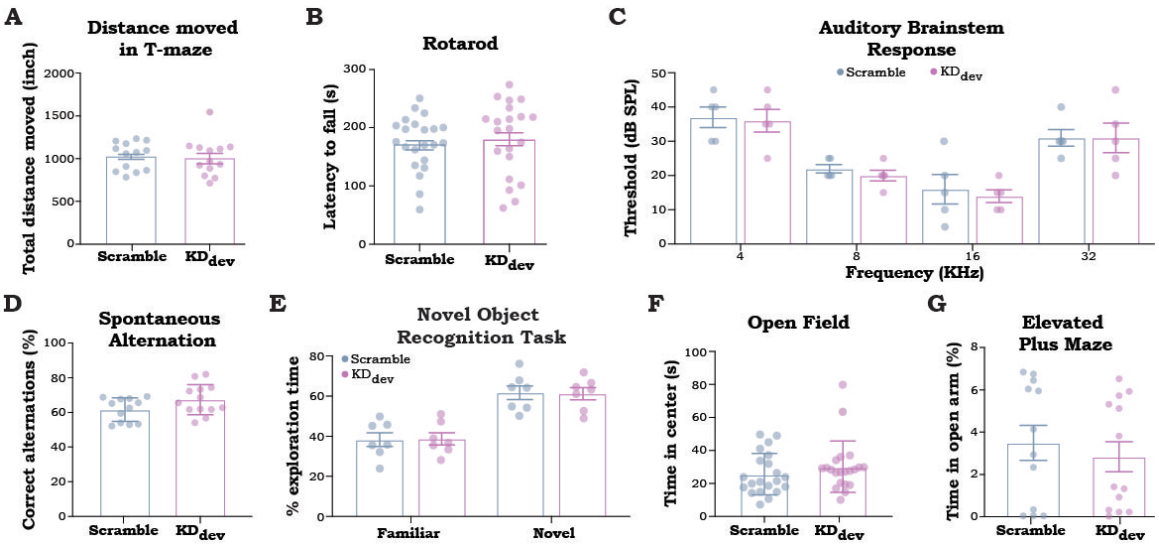

Figure 3.12 Sensory, motor, & cognitive controls in KD_{dev} mice
(**A**) Gross motor activity measured as distance moved (inch) by Scramble (n=15) and KD_{dev} (n=15) during a 6-min spontaneous alternation test in a T-maze apparatus. (**B**) Motor coordination in the Rotarod test for Scramble (n=22) and KD_{dev} (n=21), measured as latency (s) to fall from the rod averaged across 4 consecutive trials. (**C**) Auditory brainstem response measured as minimum thresholds in Scramble (n=5) and KD_{dev} (n=5), as sound pressure level (dB) in response to increasing frequencies (4, 8, 16, 32 kHz). (**D**) Working memory performance assessed in a T-maze apparatus for Scramble (n=12) and KD_{dev}, (n=13) mice, measured as correct alternations performed, expressed as a percentage total alternations. (**E**) Short-term memory tested by a novel object recognition test in Scramble (n=7) and KD_{dev}, (n=7) mice, measured as time spent exploring the novel object *vs* the familiar one and expressed as a percentage of total exploration time during a 5-min test. Two-way ANOVA showed significant main effect for novelty ($p<0.001$), but not for line. (**F**-**G**) Anxiety-like behavior measured as (**F**) time (in seconds) spent in the center of an open field arena during a 5-min test in Scramble (n=21) and KD_{dev}, (n=21) mice, and (**G**) time spent in the open arm (%) of an elevated plus maze during a 5-min test in Scramble (n=12) and KD_{dev}, (n=13) mice**.**

3.4 Low *Homer1a/Ania3* expressing neurons up-regulate GABA-receptors

To better understand the differences in transcriptional programs associated with *Homer1* we performed single-cell RNAseq from PFC of adult CC083 and CC025 mice (Figure 3.13A). After applying quality control filters (Chapter 6 – Methods) we obtained 70,920 total cells (Figure 3.13B; 40,897 from CC083 and 30,023 from CC025, n=2 biological replicates per CC line of 3 mice pooled per replicate). We performed graph-based weighted nearest neighbors clustering analysis and identified major cell types based on the cluster-wide expression of several canonical marker genes (Figures 3.13C-E) (Zeisel et al., 2018). Since *Homer1* is primarily expressed in neurons(Shiraishi-Yamaguchi & Furuichi, 2007), we sub-clustered the neurons (4,633 cells) and re-clustered them based on the first 50 principal components, identifying 10 distinct neuronal clusters (Figure 3.13F; Chapter 6 – Methods). We

determined that 9 of the clusters were glutamatergic and 1 was GABAergic based on the expression of marker genes *Slc17a6*, *Slc17a7*, *Slc32a1*, and *Gad1* (Figure 3.13G). Consistent with previous studies (Ango et al., 2000; Petralia et al., 2001), *Homer1* expression was primarily restricted to glutamatergic neurons (Figure 3.13H). Of the 9 glutamatergic clusters, 4 showed substantial downregulation of *Homer1* in CC083 cells compared to CC025 cells (Figure 3.13I; clusters 0, 1, 5, & 6 – referred to as *Homer1* Differentially Expressed (DE) clusters).

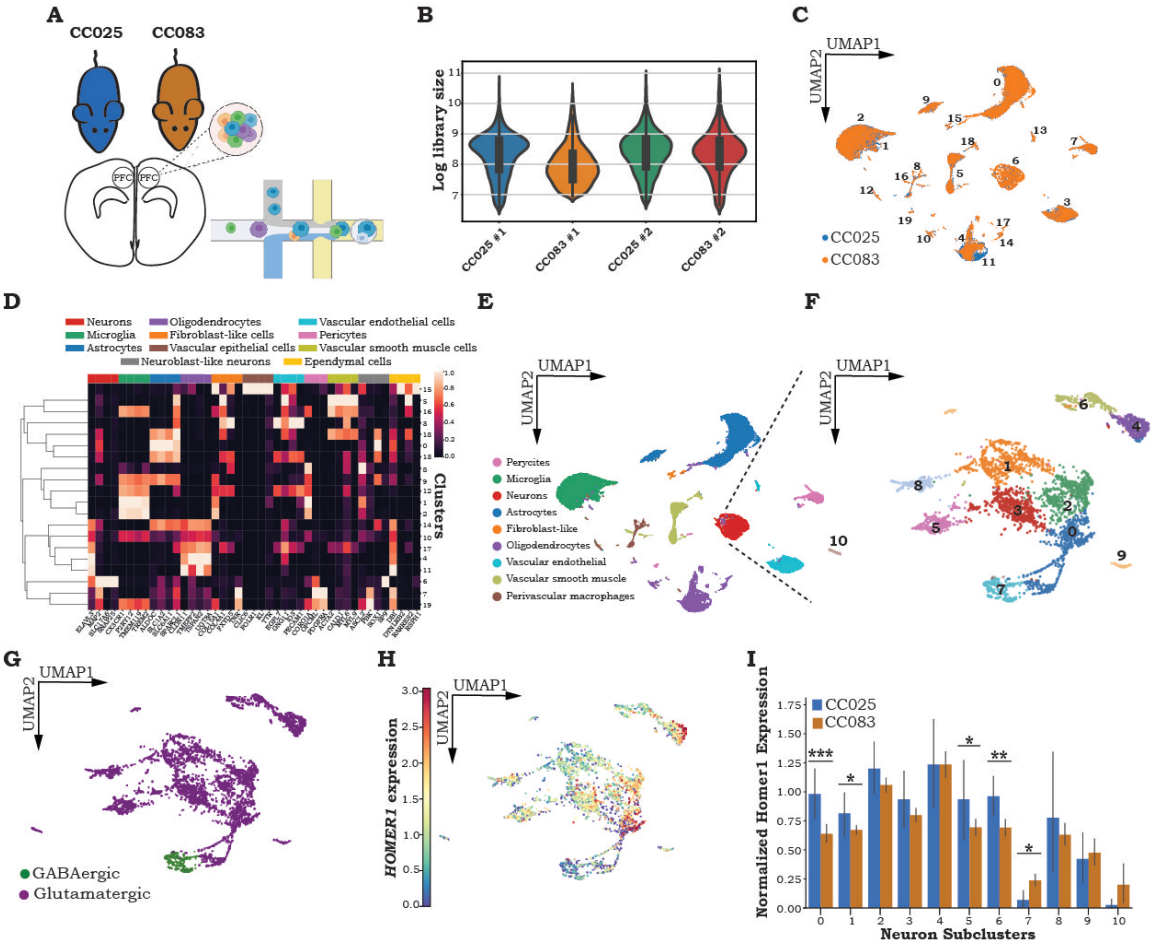

Figure 3.13 Single-cell sequencing in PFC of CC mice
(**A**) Schematic representation of scSeq workflow. (**B**) Violin Plots of library size for each biological replicate. (**C**) UMAP visualization of initial clusters colored by line. (**D**) Heatmap of select cell type marker genes for clusters shown in **C**. (**E**) UMAP visualization of all cells collected from CC025 (n=6) and CC083 (n=6) mice clustered based on transcriptional profile. (**F**) UMAP visualization sub-clustering all cells identified as neurons. (**G**) Identification of excitatory (glutamatergic) and inhibitory (GABAergic) neuron clusters based on expression of canonical marker genes. (**H**) UMAP visualization of scaled *Homer1* expression in neuronal clusters. (**I**) Differential *Homer1* expression between CC083 and CC025 neurons by cluster shown as mean ± SD (*p≤0.1, **p≤0.01, ***p≤0.001).

To define the gene expression patterns associated with varying levels of *Homer1* we performed differential expression analysis on the *Homer1* DE clusters between CC lines (Finak et al., 2015). Gene ontology (GO) analysis of molecular function for genes upregulated in the CC083 cells from the *Homer1* DE clusters showed an enrichment of pathways related to inhibitory GABA signaling, while CC025 terms overrepresented glutamatergic signaling, driven by GABA and glutamate receptor subunits, respectively (Figure 3.14A). In fact, CC083 cells uniformly upregulate several GABA receptor sub-types (Figure 3.14C), specifically in the *Homer1* DE clusters (Figure 3.14D), further apparent when analyzing the Homer1+ cells within those clusters (Figure 3.14E), and meanwhile downregulating several glutamatergic receptor subtypes with almost no differential expression of other neurotransmitter receptors or transporters (Figure 3.14B). These data indicate that lower expression of *Homer1* in a subset of prefrontal excitatory neurons yields enhanced GABAergic to glutamatergic receptor balance in those same neurons, suggesting enhanced inhibitory receptivity.

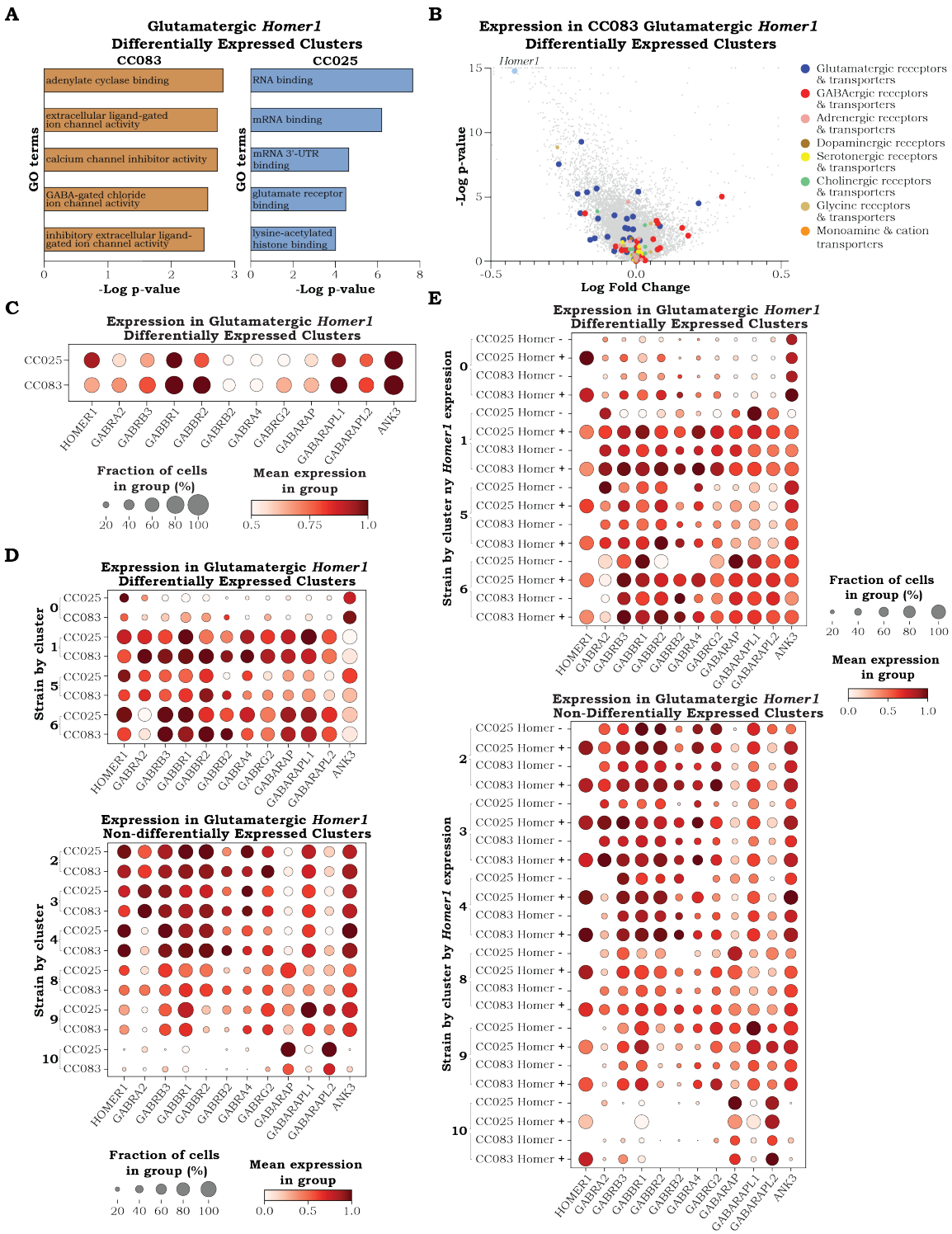
A
Glutamatergic Homer1
Differentially Expressed Clusters
CC083
CC025
adenylate cyclase binding
extracellular ligand-gated ion channel activity
calcium channel inhibitor activity
GABA-gated chloride ion channel activity
inhibitory extracellular ligand-gated ion channel activity
RNA binding
mRNA binding
mRNA 3'-UTR binding
glutamate receptor binding
lysine-acetylated histone binding
GO terms
-Log p-value
B
Expression in CC083 Glutamatergic Homer1
Differentially Expressed Clusters
Homer1
-Log p-value
Log Fold Change
Glutamatergic receptors & transporters
GABAergic receptors & transporters
Adrenergic receptors & transporters
Dopaminergic receptors & transporters
Serotonergic receptors & transporters
Cholinergic receptors & transporters
Glycine receptors & transporters
Monoamine & cation transporters
C
Expression in Glutamatergic Homer1
Differentially Expressed Clusters
CC025
CC083
HOMER1 GABRA2 GABRB3 GABBR1 GABBR2 GABRB2 GABRA4 GABRG2 GABARAP GABARAPL1 GABARAPL2 ANK3
Fraction of cells in group (%)
Mean expression in group
D
Expression in Glutamatergic Homer1
Differentially Expressed Clusters
Strain by cluster
Expression in Glutamatergic Homer1
Non-differentially Expressed Clusters
Strain by cluster
Fraction of cells in group (%)
Mean expression in group
E
Expression in Glutamatergic Homer1
Differentially Expressed Clusters
Strain by cluster ny Homer1 expression
CC025 Homer -
CC025 Homer +
CC083 Homer -
CC083 Homer +
Fraction of cells in group (%)
Mean expression in group
Expression in Glutamatergic Homer1
Non-Differentially Expressed Clusters
Strain by cluster by Homer1 expression

Figure 3.14 Low *Homer1*-expressing PFC glutamatergic neurons upregulate GABA receptors

(**A**) GO analysis of molecular function for genes upregulated in the *Homer1* DE clusters from CC083 mice (left) and CC025 mice (right). (**B**) Volcano plot depicting differential gene expression in the CC083 *Homer1* DE clusters relative to CC025. Colored dots indicate genes encoding receptors and transporters of common neurotransmitter systems. Triangles indicate points beyond axes' bounds. (**C**) Dot plots showing expression of GABAergic genes driving GO analysis (from **A**) in the *Homer1* DE clusters by CC line. (**D**-**E**) Dot plots of select GABAergic receptor expression in all glutamatergic clusters (**D**) by cluster and CC line and (**E**) by cluster, CC line, and *Homer1* positivity. For **C**-**E**, the size of each dot corresponds to the percentage of cells expressing each gene, and color intensity indicates the relative, scaled expression of that gene.

We next assessed the transcriptional programs of upstream GABAergic neurons. To do so, we performed differential expression analysis on the GABAergic cluster, in which, interestingly, *Homer1* is significantly upregulated in the CC083s (Figure 3.13I, cluster 7, p=0.02). Due to the well-studied contributions of neuromodulation in attentional processing (Thiele & Bellgrove, 2018), we assessed expression differences of markers for the most common neuromodulatory systems and found that CC083 GABAergic neurons had higher expression of genes associated with adrenergic and cholinergic signaling than the CC025s (Figure 3.15A). Furthermore, pathway enrichment analysis (Chen et al., 2013; Kuleshov et al., 2016; Xie et al., 2021) indicated a significant overrepresentation of genes related to noradrenergic signaling in CC083s (Figure 3.15B). Given its historical significance in attentional regulation (Arnsten et al., 2012; Aston-Jones & Cohen, 2005; de Lecea et al., 2012; Lovett-Barron et al., 2017), as well as its role as a target of medications to treat ADHD (Banaschewski et al., 2004; Cinnamon Bidwell et al., 2010), we further analyzed the expression of adrenergic receptors. We found that the higher expression of adrenergic marker genes in CC083 GABAergic cells is driven primarily by the adrenergic receptor *Adra1b*, which, along with *Adrb1*, appears to be preferentially expressed in the GABAergic cluster (Figure 3.15C).

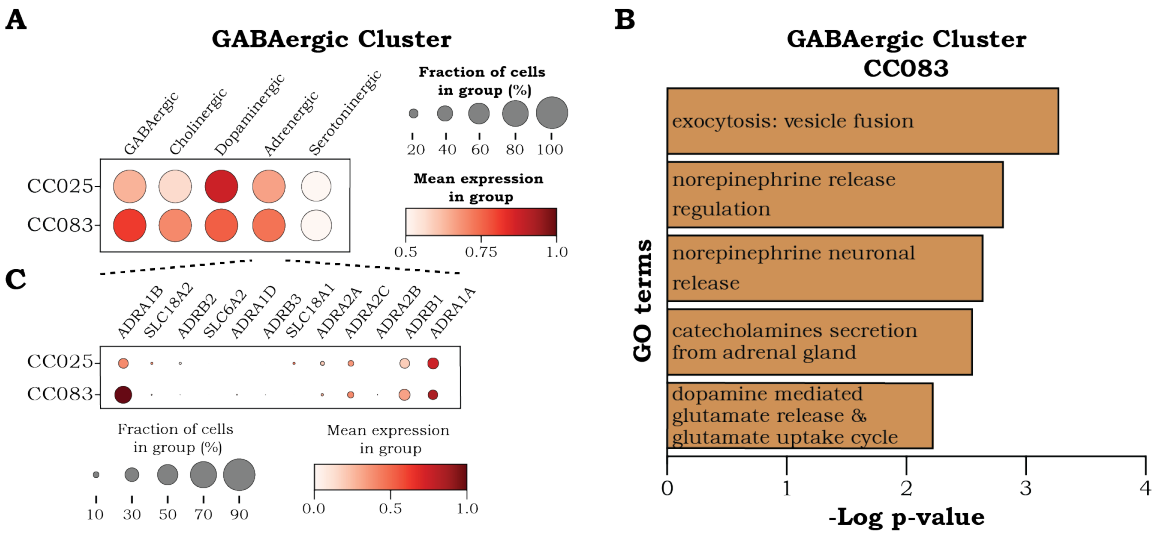

Figure 3.15 Low *Homer1*-expressing PFC GABAergic neurons upregulate adrenergic receptors

(**A**) Dot plot showing the expression of markers for common neuromodulatory systems in GABAergic cluster 7 by line. (**B**) Functional pathway enrichment analysis for CC083 cells in the GABAergic cluster using the Elsiver_Pathway_Collection gene set library in Enrichr. (**C**) Dot plots showing scaled expression of select GABAergic receptors in the glutamatergic cluster by group. For **A** and **C,** the size of each dot corresponds to the percentage of cells from each group expressing each gene or gene set, and the color intensity indicates the relative, scaled expression of the gene/gene set.

To determine whether these differences between strains were causally driven by developmental changes in *Homer1a/Ania3* expression, we prepared another cohort of mice with bilateral injection of either *Homer1a/Ania3* shRNA or scrambled controls at P0. We then performed scSeq from adult mice and performed similar analyses as with the CC mice. We found that within the cluster of excitatory neurons (Figures 3.16A-B), *Homer1* was significantly downregulated in cells from the KD_{dev} mice (Figure 3.16C), while indeed in those same cells, similar GABA receptor genes to those upregulated in the CC083 were significantly upregulated. Notably, in both the CC083 and KD_{dev} mice, excitatory neurons downregulating *Homer1* substantially upregulated the $GABA_B$ receptor subunit *GABBR2* (Figures 3.16D and 3.14C-E). Furthermore, KD_{dev} mice displayed strong enrichment of adrenergic receptor subtypes within the inhibitory neuron cluster.

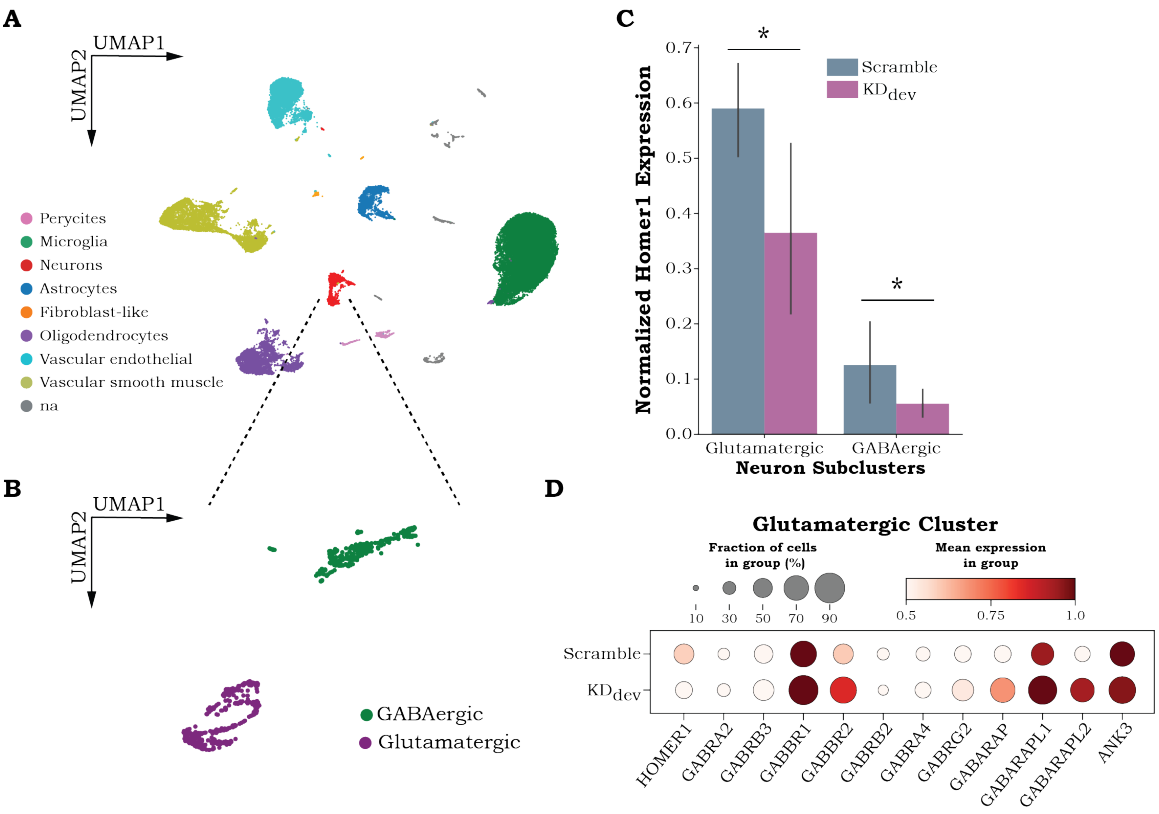

Figure 3.16 KD_{dev} PFC glutamatergic neurons upregulate GABA receptors

(**A**) UMAP visualization of all cells collected from Scramble and KD_{dev} mice (n=3 mice pooled per group) clustered based on transcriptional profile. (**B**) UMAP visualization sub-clustering all cells identified as neurons, identified as excitatory (glutamatergic) and inhibitory (GABAergic) neuron clusters based on expression of canonical marker genes. (**C**) Differential *Homer1* expression between Scramble and KD_{dev} neurons by cluster shown as mean ± SD (p=0.03 for both glutamatergic and GABAergic clusters). (**D**) Dot plots showing scaled expression of select GABAergic receptors in the glutamatergic cluster by group. The size of each dot corresponds to the percentage of cells from each group expressing each gene and the color intensity indicates the relative, scaled expression of the gene.

3.5 Summary

In this chapter, we demonstrate that knocking down *Homer1a* and *Ania3* during postnatal development, but not adulthood, is sufficient to improve both preattive processing and attentional behavior. Unbiased RNAseq from multiple regions important for attention showed that *Homer1* is the only locus gene differentially expressed between DO high- and low-performers, and only within PFC. This differential expression was also observed in the PFC of CC083 and CC025 mice, our recombinant inbred high- and low-performers, respectively. Importantly, the differential expression between both DO performance groups and CC lines was driven by a downregulation of two short, activity-dependent

Homer1 isoforms – *Homer1a* and *Ania3*. However, *in vivo* manipulations in adult mice did not have any effect on pre-attentive processing. Instead, knocking down prefrontal *Homer1a* and *Ania3* during postnatal development via p0 viral injections proved sufficient to improve not only pre-attentive processing, but overall attention across multiple behavioral paradigms.

We also used scSeq to show that excitatory neurons from CC083 mice that downregulate *Homer1* relative to their counterparts from CC025 mice upregulate GABA receptors, indicating an increased inhibitory influence on these cells. Additionally, CC083 inhibitory neurons upregulate adrenergic receptors, important functional constituents during attention (Viggiano et al., 2004). To identify a causal link between reduced *Homer1a* and *Ania3* with GABAergic and adrenergic signaling, we also performed single-cell RNA seq on our KD_{dev} mice. Similar to the CC mice, GABAergic receptors were upregulated in excitatory neurons of the KD_{dev} mice, while adrenergic receptors were upregulated in their inhibitory neurons. Together, these data demonstrate that developmental prefrontal *Homer1/Ania3* knockdown is causally related to increased prefrontal receptivity to adrenergic and inhibitory input. Further, this poses the question of how these cellular and molecular changes influence neural dynamics supporting attention. To answer this question, we next explored the consequences of these effects on neural dynamics in the behaving animal during an attention task.

CHAPTER 4. *Homer1* regulates prefrontal inhibitory tone and dynamic range to alter attention

4.1 Introduction

How do the *Homer1a*-associated molecular and cellular changes contribute to changes in neural dynamics underlying attentional processing? Are there roles for long-range inhibitory recurrence via the thalamus, neuromodulation via locus coeruleus, or both linked to attentional performance? And are there contributions of non-neuronal cells (i.e., oligodendrocyte precursor cells (OPCs) or mature oligodendrocytes (OLs)) in regulating prefrontal dynamics and attentional processing? To answer these questions, we needed to record neural dynamics during attentional behavior in PFC and connected, attention-related brain regions.

Neural activity during top-down attention in the PFC serves to determine which stimuli are task-relevant and transmit that information to improve the efficacy of processing related sensory information and coordinate any necessary motor actions. In practice, this often works as a type of neural gain control to amplify the intensity of the prefrontal signal. These mechanisms can be observed by measuring neural activity both at single-cell and population resolution. While electrophysiological methods are the most direct method of assessing neural activity, it is difficult to implement in a cell-type- or projection-specific manner. Since *Homer1* is predominantly expressed in excitatory neurons (Sjöstedt et al., 2020; Thul et al., 2017), we were interested in the interactions between excitatory neurons of PFC and the activity patterns of inputs to PFC such as MD and LC. Further, as the top 20 upregulated genes in the DO high-performers from bulk RNAseq (Figure 3.1A) were primarily genes almost exclusively expressed in OL-lineage cells (Figure 4.1A-B) and GO analysis from CC bulk and single-cell RNAseq (Figures 3.2A and 3.13A) suggested similar OL-lineage cell involvement (Figure 4.1C-D), we also wanted to explore interactions between PFC excitatory neurons and local OLs.

Calcium imaging utilizes the influx of calcium ions during neuronal firing as well as the release of intracellular calcium stores during cellular activity to infer how cells are behaving over time by optically recording fluorescence changes of genetically encoded calcium indicators (Chen et al., 2013; Dana et al., 2016). Since these fluorescent indicators are genetically encoded, we could restrict their expression using cell type- or projection-specific promotors and enhancers. To collect calcium signals from multiple brain areas in freely moving animals, we performed multi-fiber photometry during behavior (Kim et al., 2016), which would allow us to assign neural activity to behavioral epochs and assess the functional connectivity of brain areas and how they change over time.

4.2 Low *Homer1*-expressing mice have enhanced LC-PFC functional correlations at the start of an attention task

We aimed to target neurons in PFC, MD, and LC as well as OLs in PFC of CC083 and CC025 mice. Since there was not a commercially available construct that would restrict GCaMP expression only to oligodendrocytes, we designed our own. Using sequence conservation and OL lineage-specific transcription factor binding site data, we identified a 2.5 Kb putative myelin-associated glycoprotein (*MAG*) promoter region (Figure 4.1E; Chapter 6 – Methods) and cloned it upstream of a GCaMP6f coding sequence. After AAV packaging, we validated the AAV-MAG-GCaMP6f expression *in vivo* (Figures 4.1F-G).

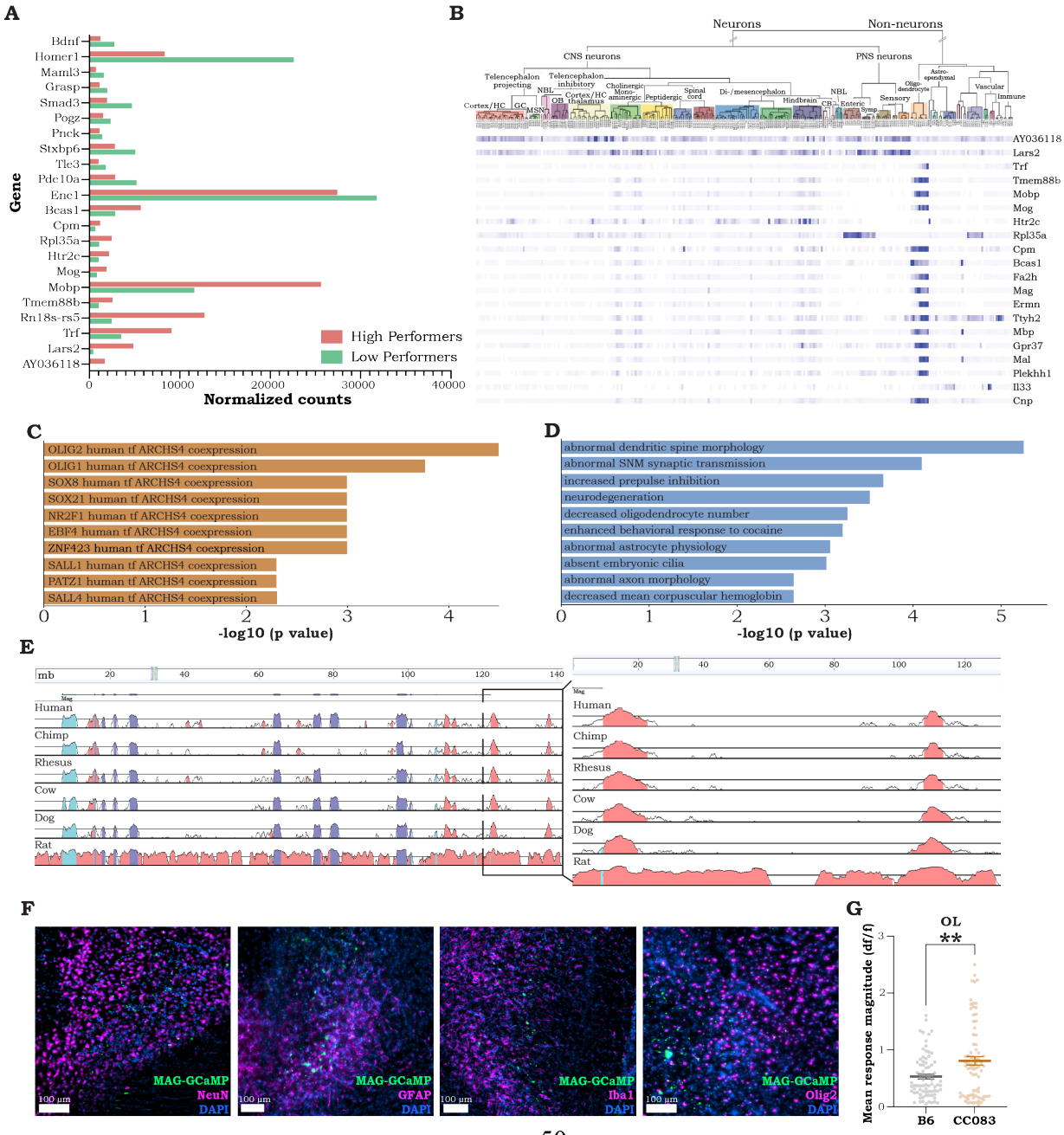

Figure 4.1 DO & CC PFC RNAseq reveals potential oligodendrocyte contribution to Chr13 QTL effect & validation of AAV-MAG-GCaMP6f
(**A**) The most differentially expressed genes between DO high- (n=3) and DO low- (n=3) performers from bulk PFC RNAseq (Figure 3.1C). Genes are ordered by Log2FC relative to high-performers (11 upregulated and 11 downregulated). (**B**) Typical cell-type expression patterns for the 20 most upregulated genes in PFC of DO mice with high PPI performance. Differential gene expression between performance groups was determined by DESeq2, n=6 biologically independent samples. Cell-type expression patterns were determined by the Linnarsson Lab adult mouse single cell gene expression database (http://www.mousebrain.org). Genes selected for each group had log2 fold change ≥ 0.7 and adjusted p value ≤ 0.05. (**C**) Transcription factor co-expression enrichment analysis (from ARCHS4 database) of genes significantly upregulated in the PFC of CC083 mice (n=3) relative to CC025 mice (n=3) from bulk RNAseq data (Figure 3.2B). (**D**) Mammalian phenotype ontology enrichment analysis (from MGI Mammalian Phenotype database with Level 4 cutoff) of genes upregulated in CC025 cells within neuron subcluster 0 from scSeq (Figure 3.13F). (**E**) VISTA plots of mouse sequence at the MAG locus and its genomic sequence conservation in humans, chimpanzees, rhesus macaques, cows, dogs, and rats. The box indicates the 2.3 kb upstream promoter region zoomed-into on the right with 2 regions of high conservation, which suggests they are likely functionally important. Purple shading indicates coding sequence conservation, blue shading indicates UTR sequence conservation, and pink shading indicates non-coding sequence conservation. (**F**) Immunohistochemistry performed 4 weeks after PFC injections of AAV-MAG-GCaMP6f (green) showing viral transduction in the target area. 20x images were collected of sections stained with antibodies (magenta) raised against the microglial marker Iba1 (top left), neuronal marker NeuN (bottom left), oligodendrocytes lineage marker Olig2 (top right), and astrocytic marker GFAP (bottom right), as well as DAPI (blue). (**G**) Average activity (area under responses) in home cage for B6 (n=5) vs CC083 (n=4) during 1 min recordings from PFC oligodendrocytes (OLs, Welch-corrected t-test p=0.004).

To begin, we injected AAV1/9-GCaMP or JRGECO1a into locus coeruleus (LC, GCaMP6f), mediodorsal thalamus (MD, GCaMP6f), PFC oligodendrocytes (OL, GCaMP6f) and PFC excitatory neurons (PFC, jRGECO1a), implanted optical fibers above each region, and used a custom dual-color fiber photometry system to record bulk calcium signals from these regions simultaneously in behaving mice (Figure 4.2A). Because CC025 mice did not tolerate intracranial implants we used B6 mice as “low-performers” in their place, since they have comparable *Homer1a* expression and behavioral performance to CC025s (Figures 4.2C, 2.1B, and 2.4B). Multi-area neural activity recordings from a given animal were frame projected onto a camera sensor, and custom scripts (Chapter 6 – Methods) were used to extract time-series data, regress out motion-related artifacts, and align to behavioral data (example alignment from one trial of a CC083 mouse in Figure 4.2B).

We first analyzed baseline activity patterns by quantifying the area under the curve (AUC) of the calcium traces (similar to the example trace in Figure 4.2B) from all recorded regions and cell types in CC083 and B6 mice when they were not engaged in the SDT. Interestingly, we noticed substantially depressed PFC activity ($p<0.001$, Welch-corrected t-test),

moderately depressed MD activity (p=0.002, Welch-corrected t-test), and elevated LC activity (p=0.002, Welch-corrected t-test) in CC083 mice (Figure 4.2E). The diminished PFC activity, along with the upregulation of GABAergic receptors in PFC excitatory neurons (Figure 3.14C) indicates increased inhibitory tone, and this lower PFC activity in concert with the reduced MD activity suggests that this increased prefrontal inhibition may affect PFC-MD recurrent activity. Further, the increased LC activity, together with the observation from scSeq data of increased adrenergic *Adra1b* reception onto PFC GABAergic cells (Figure 3.15), suggested that LC may contribute to baseline inhibitory tone in PFC. Indeed, we found that LC-PFC functional correlations when not engaging in the SDT were close to Pearson's r=0 in CC083s compared to ~0.7 in B6 (Figure 4.2F, p<0.001, Welch-corrected t-test). However, as mice started training on the signal detection task, we noticed a steady increase in LC-PFC functional correlations in CC083 mice (Figure 4.2G) that mirrored their steady improvement in task performance (Figure 4.2D), and which were unlikely to be due to contamination of LC fibers in PFC (since these recordings were made on contralateral sides, using separate sensors and imaging filters, and emerged only in certain phases of the task, Chapter 6 – Methods). This steady increase in LC-PFC correlations was not observed in B6 mice, presumably due to already high baseline correlations precluding further enhancements during the task (Figure 4.2G, multiple Welch-corrected t-tests p(block 1)=0.009, p(blocks 2-5)<0.001; example raw traces from day 3 and day 11 are shown). This improved LC-PFC coupling in CC083 mice was strongest in the first four minutes (block 1) of each day's session (Figure 4.2G, left panel), after which these correlations reduced back toward baseline (blocks 2-5; Figure 4.2G, right panel).

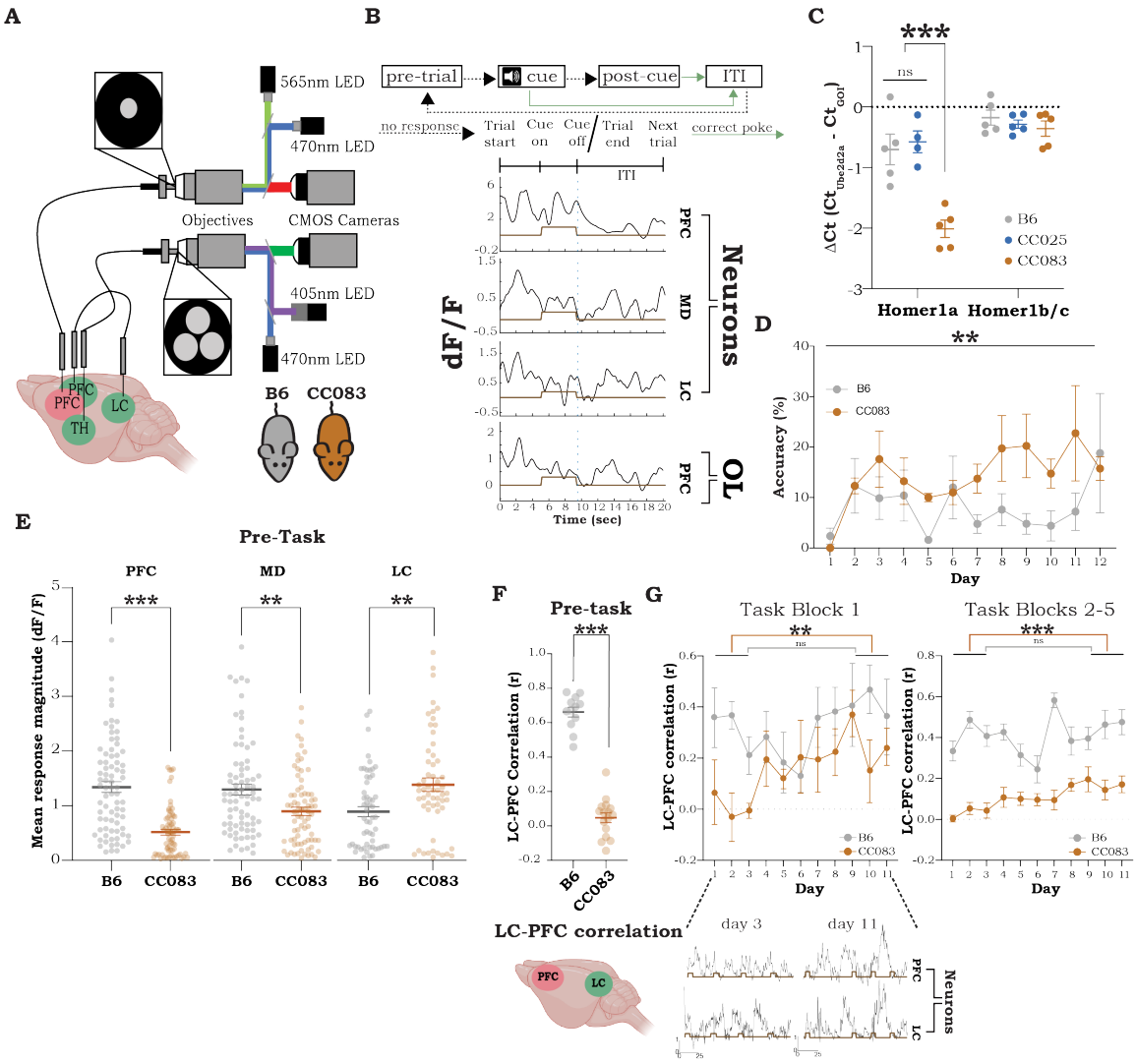
A
565nm LED
470nm LED
Objectives
CMOS Cameras
405nm LED
470nm LED
PFC
PFC
LC
TH
B6
CC083
B
pre-trial
cue
post-cue
ITI
no response
Trial start
Cue on
Cue off
Trial end
Next trial
correct poke
ITI
dF/F
PFC
MD
LC
Neurons
PFC
OL
Time (sec)
C
***
ns
ΔCt (Ct Ube2d2a - Ct Gol)
B6
CC025
CC083
Homer1a
Homer1b/c
D
**
Accuracy (%)
B6
CC083
Day
E
Pre-Task
PFC
MD
LC
***
**
**
Mean response magnitude (dF/F)
B6
CC083
B6
CC083
B6
CC083
F
Pre-task
***
LC-PFC Correlation (r)
B6
CC083
G
Task Block 1
Task Blocks 2-5
**
***
ns
LC-PFC correlation (r)
Day
B6
CC083
LC-PFC correlation
day 3
day 11
PFC
LC
PFC
LC
Neurons

Figure 4.2 Lower developmental expression of *Homer1a/Ania3* improves PFC-LC synchrony at the start of the task across training
(**A**) Schematic of dual-color, 4-region photometry system. Simultaneous 565 nm, 470 nm, and 405 nm recordings were taken from PFC neurons (jRGECO, red), MD neurons, LC neurons, and PFC oligodendrocytes (GCaMP, green) in B6 (grey) or CC083 (tan) strains. (**B**) Top: Schematic representation of SDT trial structure. Bottom: example jRGECO (PFC neurons, row 1) and GCaMP (MD neurons, LC neurons, and PFC oligodendrocytes (OL; rows 2-4, respectively) traces aligned to a SDT trial. (**C**) PFC expression of *Homer1a* and *Homer1b/c* by qPCR in B6, CC025, and CC083 adult mice (*Homer1a*: n(B6)=5, n(CC025)=4, and n(CC083)=5; *Homer1b/c:* n=5 per line; two-way ANOVA showed significant main effects for strain, *Homer1* isoform, and a significant interaction between those variables, $p<0.001$ for all; post-hoc Holm-Sidak's test showed significant differences for B6 *vs* CC083 and CC025 vs CC083, $p<0.001$ for both). (**D**) Performance of B6 (n=5) and CC083 (n=4) mice during SDT across days showing the percentage of correct responses (two-way ANOVA, $p=0.002$). Tethering mice to fibers impacted performance for both lines equally. (**E**) Average activity during baseline for B6 (n=4) and CC083 (n=4 for PFC and MD, n=3 for LC) during 1 min recordings (Welch-corrected t-test, $p(PFC)<0.001$, $p(MD)=0.002$, $p(LC)=0.002$). (**F**) Pairwise Pearson's correlations between LC and PFC neuronal activity at baseline (Welch-corrected t-test for B6 *vs* CC083, n=4 each, 5 min recordings, $p<0.001$). (**G**) Top: pairwise Pearson's correlations between LC and PFC activity during SDT sessions. Each 20 min session was split into 5, 4 min blocks. Bottom: representative traces from PFC (top) and LC neurons (bottom) from day 3 (left) and 11 (right), Y-axis is *z*-scored dF/F and X-axis is time (s). Brown rectangles indicate cues. Data is shown from the first 4-minute block (left) and for blocks 2-5 (right) as mean ± SEM (Welch-corrected t-tests for days 1-3 *vs* days 9-11 within strain, for CC083 $p(block1)=0.003$ and $p(blocks\ 2\text{-}5)<0.001$).

4.3 Reduced developmental *Homer1a/Ania3* improves prefrontal inhibitory input and SNR

In addition to increased LC-PFC coupling, we found that during the task CC083s exhibited large increases in PFC activity before and at cue-onset, which were greater on shorter latency correct trials compared to long latency trials and omissions (Figure 4.3A, example raw traces from correct and incorrect trials shown). More strikingly, this cue-related activity rapidly diminished during inter-trial intervals (ITIs) (Figure 4.3A). Such dynamic task-related fluctuations in CC083s led to consistently high levels of PFC signal-to-noise (SNR: trial averaged neural activity in cue vs baseline periods of the task) throughout the task (Figure 4.3B). Notably, these dynamic task-related fluctuations in PFC activity, and enhanced SNR, were not observed in B6 mice, which exhibited relatively constant PFC responses at baseline as well as before trials with either short or long latency responses (Figures 4.2E and 4.3).

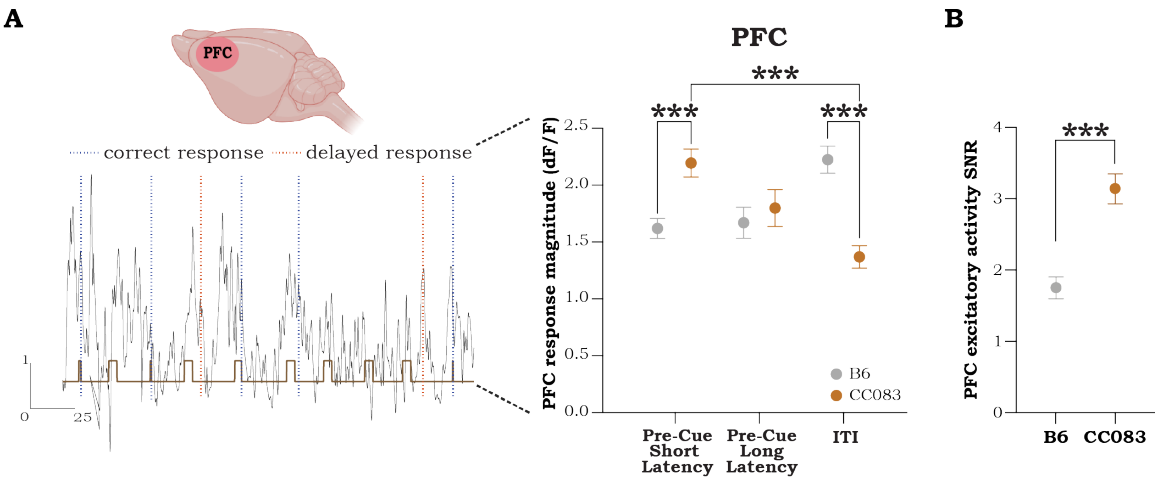

Figure 4.3 Downregulation of *Homer1/Ania3* expression during development improves prefrontal SNR
(**A**) Left: Representative trace from PFC, Y-axis is z-scored dF/F and X-axis is time (s). Brown rectangles indicate cues, blue dotted lines indicate correct responses, orange dotted lines indicate delayed responses. Right: PFC activity in task during the 5 sec before cue onset of short and long latency response trials, respectively, and during the last 5 seconds of ITIs for trials on all days in B6 (n=5) and CC083 (n=4) mice (two-way ANOVA, followed by Holm-Sidak's test for multiple comparisons, *** indicates $p<0.001$). (**B**) PFC neuronal signal to noise (SNR: trial pre-cue maximum - task baseline mean) / task baseline SD) 5 seconds before cue onset in B6 (n=5) and CC083 (n=4) mice for correct trials on all days (Welch-corrected t-test, $p<0.001$).

To test whether these dynamic task-related fluctuations and enhanced SNR in CC083 mice were causally driven by changes in *Homer1*, we prepared a new cohort of B6 mice for photometry with developmental knockdown of prefrontal *Homer1a/Ania3* compared with Scramble controls. We simultaneously recorded excitatory neurons in PFC using jRGECO and inhibitory neurons in PFC using mDlx-GCaMP as mice performed the operant SDT (Figure 4.4). The results from these experiments beautifully recaptured the excitatory SNR effects we had observed in CC083 vs B6 mice (Figures 4.3 and 4.4F-G). Specifically, PFC excitatory responses were substantially higher at cue presentation than during ITI in KD_{dev} mice compared with controls (Figures 4.4E-F), leading to significant improvements in SNR during task performance (Figure 4.4G). One notable difference between the CC083s and KD_{dev} mice is that the baseline inhibitory tone in KD_{dev} mice was reflected acutely during the task (during ITIs), whereas more chronic inhibitory tone was observed in the CC083s, which was apparent even outside of the task and during home-cage (Figure 4.2E vs Figure 4.4C). This may reflect acute compensation of Homer1 knockdown in KDdev mice or that other effects beyond the locus and gene contribute to a more chronic inhibitory tone in CC083s.

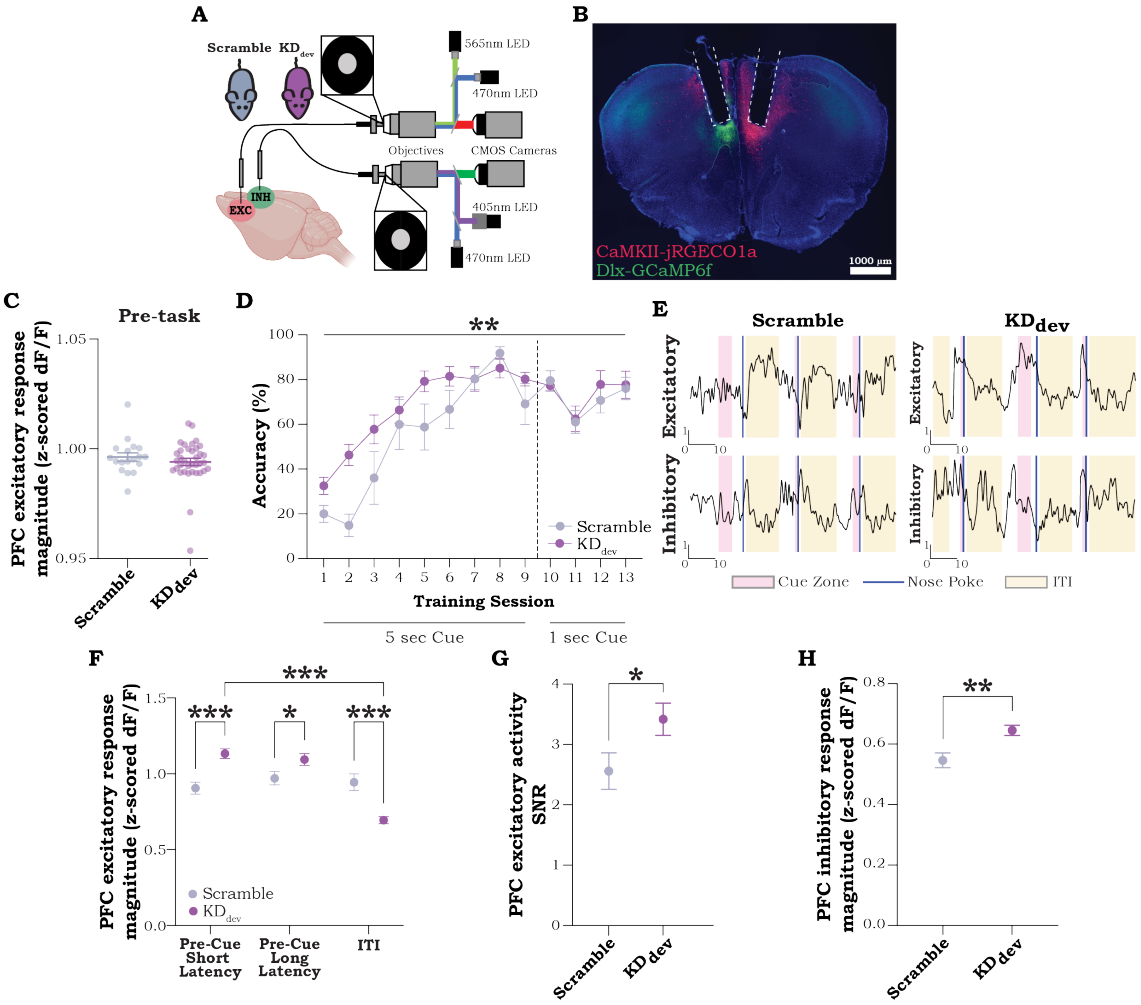

Figure 4.4 Prefrontal *Homer1a/Ania3* developmental knockdown alters inhibitory influence, enhances SNR, and improves attention

(**A**) Schematic of dual-color recordings from PFC excitatory neurons (jRGECO, red) and inhibitory neurons (GCaMP, green) in Scramble and KD_{dev} mice. (**B**) Representative DAPI-stained (blue) histology image of dual-color photometry surgical preparation to simultaneously record from excitatory and inhibitory neurons in PFC by injecting AAV-mDlx-GCaMP6f (green) contralateral to AAV-CaMKII-Cre + AAV-CAG-FLEX-jRGECO1a (red) and implanting fibers above the injection site (indicated by white dashed outlines). (**C**) Average activity (area under responses) in home cage for Scramble (n=6) vs KD_{dev} (n=10) during 1 min recordings from PFC excitatory neurons. (**D**) Accuracy (percentage of correct responses) for Scramble (n=6) and KD_{dev} mice (n=10). Two-way ANOVA showed a significant interaction between training session and group (p=0.002). (**E**) Example traces from excitatory (top) and inhibitory (bottom) neurons across 3 trials in Scramble (left) and KD_{dev} (right) mice. (**F**) PFC excitatory activity in task during the 5 sec before cue onset of short and long latency response trials, respectively, and during the last 5 seconds of ITIs for trials on all days in Scramble (n=6) and KD_{dev} (n=10) mice (two-way ANOVA, followed by Holm-Sidak's test, *** indicates p<0.001, * indicates p=0.03). (**G**) PFC excitatory neuronal SNR 5 seconds before cue onset in Scramble (n=6) and KD_{dev} (n=10) mice for correct trials on all days (Welch-corrected t-test, p=0.04). (**H**) PFC inhibitory activity in task during the last 5 seconds of ITIs for trials on all days in Scramble (n=6) and KD_{dev} (n=10) mice (Welch-corrected t-test, p=0.001).

Focusing next on the inhibitory neurons, we found a small but significant increase in the activity of inhibitory neurons during ITIs in KD_{dev} mice compared with controls (Figure 4.4H), though these were not as striking as the large magnitude changes in excitatory responses during the task (Figure 4.4F, short latency cue vs ITI). Together, these data suggest that reducing *Homer1a/Ania3* improves prefrontal SNR by dynamically scaling excitatory neuron activity (low during ITIs but high at cue-presentation), which is in part facilitated by an increase in inhibitory activity (Figures 4.4E and 4.4G), but also a greater sensitivity of excitatory neurons to this inhibition (Figures 4.4 F and H, also supported by striking elevations of GABARs specifically in KD_{dev} excitatory cells, Figure 3.16D).

4.4 Summary

In this chapter, I discussed using a custom, dual-color multifiber photometry system to record the neural dynamics of multiple cell types, across multiple brain regions *in vivo* from mice with differing developmental *Homer1a* and *Ania3* expression during an attention task. We showed that in mice with endogenously lower short-form *Homer1* expression (CC083), there was an increase in LC-PFC functional correlations during the beginning of the task across training that we did not observe in mice with higher short *Homer1* expression (B6). The CC083 mice also had higher PFC excitatory activity before and at cue onset, which quickly moderated during ITI periods, a phenomenon not present in the B6 mice. These dynamic activity resets in which activity is amplified surrounding signal periods (cue) but swiftly and greatly reduced during task baseline epochs (ITI) constitute the superior prefrontal SNR of the CC083 mice.

To causally link *Homer1* and heightened SNR, we next used the dual-color photometry system to simultaneously record from prefrontal excitatory and inhibitory neurons in the KD_{dev} mice. Just as with the CC083 mice, PFC excitatory responses were significantly larger at cue presentation than during ITI in KD_{dev} mice, compared with Scramble controls. Furthermore, KD_{dev} prefrontal inhibitory neurons had significant increases in activity, albeit of smaller magnitude change than the excitatory neurons, during ITI periods compared to control mice. Taken together, these results suggest a model in which low *Homer1a/Ania3* during development enhances inhibitory receptivity, allowing for dynamic scaling of prefrontal activity, and targeted elevations at cue-onset, linked to short-latency correct responses (Figure 4.5). These results therefore reveal that the critical component of prefrontal processing during attention may not be overall increases in activity, but rather frequent cue vs ITI resets that enable increased SNR and targeted behavioral responses.

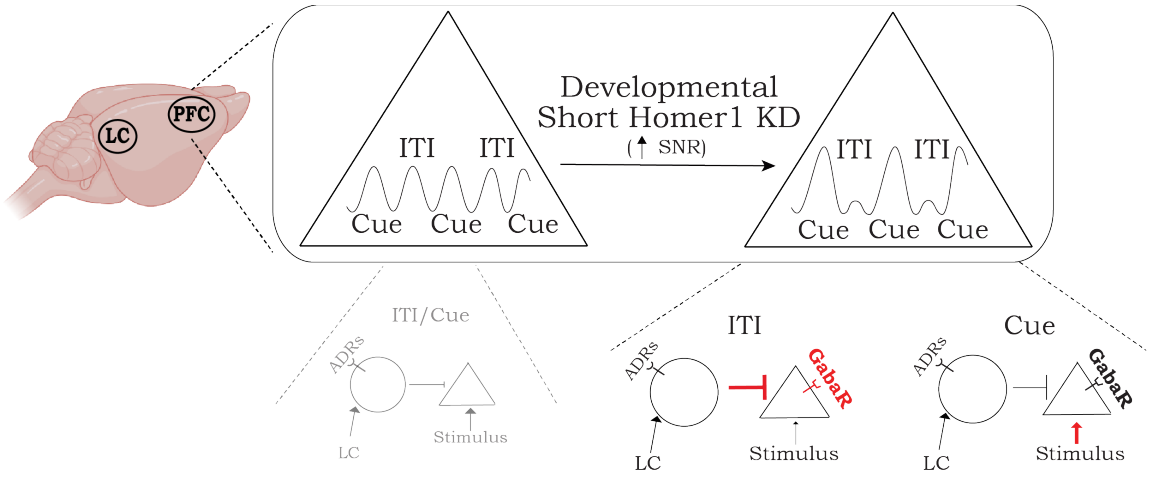

Figure 4.5 Putative model for developmental knockdown of *Homer1a/Ania3* improvement of prefrontal SNR

Knockdown of short *Homer1* isoforms (*Homer1a/Ania3*) during postnatal development improves SNR by reducing PFC activity during non-attentive periods of a task (here depicted as inter-trial intervals, ITIs) but dynamically elevating activity during cue-presentations. Reduced *Homer1/Ania3* levels leads to increased GABA receptor expression in excitatory neurons, and increased inhibitory tone in PFC (either by increasing feed-forward inhibition from LC, or how the excitatory neurons sense ongoing inhibition, or both) during non-attentive baseline periods of a task. When attention is required, incoming excitatory input overrides ongoing inhibition to provide targeted cue-related responses.

CHAPTER 5. Discussion

The prefrontal cortex is a critical module for carrying out top-down attention. It exerts its control through a complex network of intracortical and longer-range cellular communications, facilitated by an equally complicated series of molecular interactions serving as gain modulation for goal-related signals. Both cellular and molecular circuitries can be regulated bidirectionally at several nodes. This thesis has detailed my work to mechanistically study attention at multiple scales, through a genes-to-circuits-to-behavior approach. More specifically, the goal was to identify genes of relatively large effect, which may point to key circuits within a complex network that have outsized contributions to attentional processing.

First, my collaborators and I completed high-resolution genetic mapping on the highly outbred Diversity Outbred (DO) mouse population, identifying a discrete genomic locus of large effect on chromosome 13 for an innate, pre-attentive processing phenotype, prepulse inhibition (PPI). Using partially outbred collaborative cross (CC) lines, which share their genomic origins with the DO, we validated the locus effect on pre-attentive processing and found that the locus also contributed to attentional variation, without obvious effects on confounding sensory (i.e. hearing) or motor (i.e. locomotion or hyperactivity) processes. The locus effects were also specific to attention, but not to other related cognitive processes such as short-term memory. To determine the gene(s) within the locus responsible for this observed variation in attention, I focused my study on the only gene (out of 18 at this locus), that was differentially expressed in high- vs low-performing DO or CC mice – *Homer1*. I discovered substantial downregulation of *Homer1*, and in particular its two short, activity-dependent isoforms *Homer1a/Ania3*, in PFC linked to improvements in attention. Indeed by artificially manipulating these short *Homer1* isoform levels, during a developmental window, I was able to substantially improve multiple measures of attention in adult mice.

To gain further insight into molecular changes corresponding to the developmental downregulation of *Homer1a/Ania3*, my collaborators and I undertook single-cell RNA sequencing in high- and low-performing CC mice as well as mice with *Homer1a/Ania3* knocked down during development and associated controls. In both experiments, we found that low *Homer1* expression was associated with upregulation of inhibitory GABA receptors. Accordingly, when performing neural activity recordings in mice with endogenous and induced reductions in *Homer1a/Ania3* levels, I identified greater prefrontal inhibitory tone and significantly improved signal-to-noise ratios (SNRs) leading to improved attentional performance. In this chapter, I will explore the implications of my thesis

work on the mechanisms of attention. Since there are no clear functional distinctions between *Homer1a* and *Ania3*, the remainder of this section will primarily focus on the more thoroughly studied isoform, *Homer1a*.

5.1 Short *Homer1* isoforms and excitatory/inhibitory balance across development

A wide history of work on *Homer1* and its isoforms has revealed important roles in excitatory neurotransmission affecting multiple cognitive domains (Datko et al., 2017; Jaubert et al., 2006; Lominac et al., 2005; Szumlinski et al., 2005), but little is known about its isoform and cell type-specific role in attention, especially during a circumscribed developmental stage. Importantly, my work led me to focus on changing SNR through noise reduction, as opposed to signal amplification, where the latter has been the primary focus of mechanistic understanding and therapeutic strategies. While my thesis begins to explore how *Homer1* affects inhibitory tone, SNR, and behavioral modification, future work will require a deeper investigation.

One promising avenue of further study may be on the role of *Homer1a* in homeostatic scaling. Over long time scales, neurons hold their excitability in a homeostatic equilibrium using several mechanisms, collectively known as homeostatic plasticity (Turrigiano, 2012). Of the methods neurons use to stabilize their activity, *Homer1a* is known to be a key component of one such pathway known as synaptic scaling (Diering et al., 2017; Hu et al., 2010). Such synaptic scaling pathways serve as negative feedback mechanisms that allow neurons to sense alterations in their firing rates in a calcium-dependent manner and then up or downregulate receptor trafficking to or from the membrane, respectively (Turrigiano, 2012). Paul Worley's group first identified a homeostatic scaling mechanism dependent on Homer1a in 2010(Hu et al., 2010). Using primary cortical neuron cultures and slice electrophysiology from *Homer1a* knockout and wild type mice, they found that *Homer1a* reduces the quantity of α-amino-3-hydroxy-5-methyl-4-isoxazolepropionic acid receptors (AMPARs) at the dendritic membrane by inducing the dephosphorylation of tyrosine residues on the c-terminus of the AMPAR subunits GluA2/3 in a metabotropic glutamate receptor 5 (mGluR5)-dependent manner. Thus, in cortical neurons from *Homer1a* knockout mice, AMPA receptor surface expression and miniature excitatory postsynaptic current (mEPSC) amplitudes were elevated, both of which were reversed when transduced with a virus carrying *Homer1a*. Similarly, when wild type cortical neurons were transduced with the *Homer1a* virus, they also showed a decrease in AMPAR surface expression and a reduction in mEPSCs (Hu et al., 2010). This suggests a model where elevated activity in neurons triggers alternative splicing of the *Homer1* transcript, allowing for the production

of Homer1a (Bottai et al., 2002), which then binds to a proline-rich sequence at the c-terminus of group I mGluRs, interfering with their crosslinking to the longer, constitutively expressed Homer proteins (Tu et al., 1998). Homer1a-mGluR interaction can prompt agonist-independent activation of the group1 mGluRs (Ango et al., 2001), which would lead to the dephosphorylation of the c-terminal GluA2/3 tyrosine residues, an action known to be required for AMPAR endocytosis (Ahmadian et al., 2004).

Interestingly, Worley's group induced the synaptic scaling in wild type neurons by treating the primary cells with bicuculline, a $GABA_A$ receptor antagonist. Further, the bicuculline induction of Homer1a lasted several hours (the maximum quantity was measured at 12 hours of drug treatment). This indicates that 1) GABA signaling is likely a mechanism for maintaining postsynaptic neuronal homeostasis; although, unlike the *Homer1a*-dependent mechanism, it is not cell-autonomous, and 2) a homeostatic mechanism involving inhibitory neurotransmission likely would require chronic inhibition to bring the postsynaptic cell to its firing set point. While there have been no reports to date of such a circuit feedback mechanism acting in a homeostatic capacity, it may be operationally inferred through physiology studies of an MD-PFC circuit during an attention and cognitive flexibility task (Mukherjee et al., 2021).

In the single-cell RNA sequencing, I found that excitatory neurons with developmentally reduced *Homer1* expression upregulated GABA receptor expression (Figures 3.14 and 3.16). Increased inhibition may serve as a compensatory homeostatic mechanism when Homer1a is reduced. Under this paradigm, PFC neurons with less Homer1a would be hyperexcitable, as the Homer1a-mGluR mechanism of synaptic scaling would not be as effective. This would lead to over-excitation of downstream circuit components, which would relay the need for increased inhibition back to PFC interneurons, strengthening their inhibitory synaptic input to the hyperexcitable pyramidal cells. In response to the elevated inhibitory tone, the excitatory neurons would raise their baseline rate of GABA receptor expression. This model is supported by the reduced prefrontal activity we observed at baseline in the CC083 mice (Figure 4.3E). Furthermore, there is a clear attentional implication for this model. If a PFC projection neuron is hyperexcitable and regulated through inhibitory input, all that would be required to adjust its firing would be small changes in inhibition; i.e. reducing the inhibition by a small amount would cause it to fire more and applying a small amount of inhibition would rein it back in. This would serve as a method of tightly controlling SNR. Our data also fit this aspect of the model, as we found small but significant increases in inhibitory neural activity that corresponded to large reductions in excitatory activity during non-attentive periods of our task (Figure 4.5H).

As detailed in Chapter 3, *Homer1a/Ania3* knockdowns only improved attention when performed during postnatal development, not in adulthood (Figures 3.4-5 and 3.7-11). If increased inhibitory tone is a compensatory homeostatic mechanism, why would it be restricted to specific developmental stages? There are multiple mechanisms of homeostatic plasticity (Turrigiano, 2012) but aside from a need for upscaling or downscaling activity, little work has been done to elucidate the differential circumstances for their activation. Nonetheless, one recent study explored age-dependent differences in homeostatic plasticity and found that overstimulation in the visual cortical neurons resulted in increased inhibitory input in young mice (3 months old), but not in older mice (12 months old). Additionally, overstimulation led to a mGluR5-dependent decrease in dendritic spine size in young mice as well as a reduction in GluA2 localized to the dendritic spines. In the older animals, visual overstimulation led to elevated excitatory activity levels that persisted over several days and a decrease in inhibitory input relative to controls (Radulescu et al., 2023). These data suggest that synaptic scaling mechanisms change with age. It is likely that this also holds, or perhaps is even exaggerated, during postnatal development since that time window holds critical periods, defined epochs when synaptic changes are most flexible to shape neural circuits in response to sensory experience.

5.2 Norepinephrine and the stress-arousal-attention axis

While *Homer1* alterations in PFC do not cause increases in anxiety-like behavior (Figures 3.12F-G), the low-attention CC025 mice do have an increased anxiogenic susceptibility compared to the high-attention CC083s (Figures 2.6D-E), prompting some discussion of the associations between anxiety, or stress more generally, and attention. Stress is a physiologic reaction to stimuli that challenge homeostasis, whether real or perceived (Del Giudice et al., 2018). Its impacts on cognition vary depending on the time scale of its presentation, i.e. acute stress has been demonstrated to have positive effects (Yuen et al., 2009), whereas chronic stress can lead to cognitive impairment (S. Li et al., 2008; Liston et al., 2006). This can be viewed as a modified Yerkes-Dodson curve in which acute stress improves attentional performance relative to baseline but chronic stress can impair attention relative to baseline (Figure 5.1A). This is reminiscent of how the relationship between arousal and attention is thought of (Yerkes & Dodson, 1908). Arousal can be thought of as acting on attention following a Yerkes-Dodson curve, where extremely low arousal levels correspond to a sleep state and gradually increasing arousal will induce a transition through fatigue, to a level of alertness optimal for attention, until ultimately reaching a stressful, hypervigilant state where attention is easily diverted by new stimuli in a bottom-up manner (Figure 5.1B).

The neuromodulatory neurotransmitter norepinephrine (NE) is inextricably linked with both arousal (Aston-Jones & Bloom, 1981; Berridge, 2008; Carter et al., 2010) and stress (Valentino & Van Bockstaele, 2008; Van Bockstaele et al., 1998). Its overlap between these two systems has led to the idea that NE and its source, locus coeruleus (LC), are the neural substrates coordinating the influence of stress on arousal (Bouras et al., 2023). Just as with stress and anxiety, NE is understood to impact attention in a Yerkes-Dodson fashion. In fact, NE-releasing LC neurons follow this activity pattern corresponding to attentional performance(Aston-Jones et al., 1999). Given the role of LC NE release in stress and arousal as well as in attention via PFC (Aston-Jones & Cohen, 2005; Eldar et al., 2013), it stands to reason that LC could be a hub modulating the stress-arousal-attention axis (Figure 5.1C).

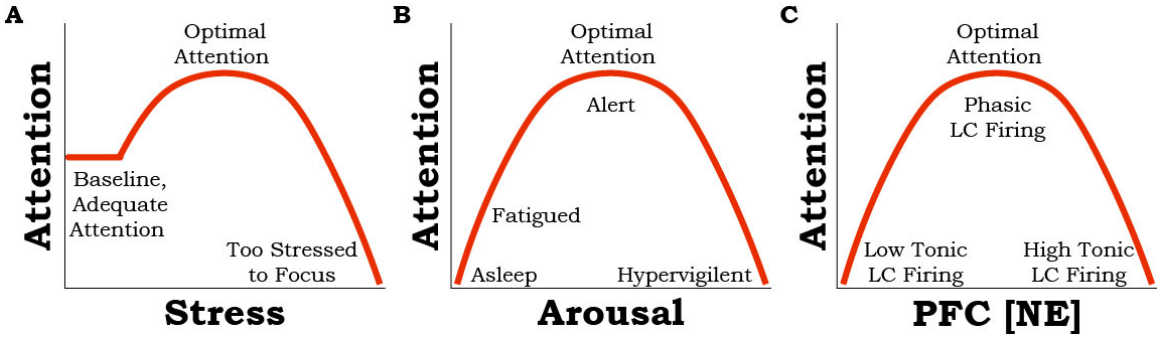

Figure 5.1 The relationships of stress, arousal, and norepinephrine with attention

(**A**) A schematic representation of the modified Yerkes-Dodson relationship between stress and attention. (**B**) A schematic representation of the relationship between arousal and attention. (**C**) A schematic representation of the relationship between the concentration of NE in the PFC and attention. NE release is assumed based on LC firing patterns.

Interestingly, NE signaling has also been shown to be involved with the Homer1a-mGluR mechanism of homeostatic synaptic downscaling. It has been shown that Homer1a expression and targeting to the postsynaptic density are linked with circadian rhythm, so they are upregulated during sleep (or after sleep deprivation) and downregulated during wakefulness (Maret et al., 2007; Diering et al., 2017). There is evidence that this rhythmic expression facilitates Homer1a-mGluR synaptic scaling during sleep, promoted by adenosine receptor A1 receptor signaling and inhibited during wakefulness by noradrenergic signaling (Diering et al., 2017). Thus, it's possible that this mechanism could account for, in part, the poor attention of high-*Homer1a*-expressing mice in a PFC-specific manner, such that elevated Homer1a levels prompted the additional removal of AMPARs, reducing excitatory input to PFC. Remarkably, the CC025 glutamatergic neurons with elevated

Homer1 expression upregulate the A1 receptor (data not shown), which could act as a non-locus amplifier of the *Homer1a*-dependent attentional effect by increasing the excitatory downscaling even further, which may explain the larger differences in signal detection task response latencies for the CCs compared to the KD_{dev} mice (Figures 2.5D-E and 3.8C-F). Additionally, this reduced excitation in CC025 PFC could impact the PFC projections to the basolateral amygdala that are thought to mediate anxiety (Liu et al., 2020), an area in which NE release from LC projections has been shown to promote anxiogenic behavior (McCall et al., 2017).

5.3 Glial contributions to attention and cognition

Cognition has typically been studied in the context of neuron activity. Yet in recent years, it has become clear that glia, the non-neuronal brain cells traditionally thought to simply support neuronal function, play important, active roles in enabling and modifying circuit dynamics. Astrocytes, oligodendrocytes, oligodendrocyte precursor cells, and microglia do so through several mechanisms, including modifying synaptic architecture to alter circuit plasticity, flexibly adjusting axonal conductance velocity, as well as regulating neurotransmitter levels at the synapse and altering the ion concentrations in the extracellular space (Allen & Lyons, 2018). There is also evidence that patients with psychiatric disorders involving impaired attention often exhibit white matter abnormalities (Kubicki et al., 2005; Q. Li et al., 2021; Parlatini et al., 2023). Given the implications from our sequencing data that oligodendrocytes may have some influence on attentional variation (Figure 4.1), it is worthwhile considering the potential roles glia may play in attention.

Derived from oligodendrocyte precursor cells (OPCs; also known as NG2 cells or polydendrocytes), oligodendrocytes (OLs) comprise approximately 25% of all cells in the human brain (Allen & Lyons, 2018; Von Bartheld et al., 2016). OLs are best known as the myelinating cells of the brain – a function in which they segmentally wrap axons in multilayered sheathes of a lipid-rich material called myelin, insulating axons to improve their conduction. However, oligodendrocytes also regulate extracellular potassium ions through the inward-rectifying potassium channel Kir4.1, which affects the firing rates of local neurons (Battefeld et al., 2016) as well as broader network function and behavior (Larson et al., 2018). Nonetheless, it appears that myelination is the more dynamic contribution oligodendrocytes provide to circuit function. Thickening of myelin increases axonal transmembrane resistance thereby increasing action conduction velocity, and improving the efficiency of neuronal communication. Further, the formation of new myelin is generally thought to occur in response to neural activity

(Gibson et al., 2014) and has been demonstrated to be related to cognition (Geraghty et al., 2019). Interestingly, activity-dependent myelination appears to be a process in which OPCs receive synaptic input from neurons, prompting them to mature into myelinating OLs through a brain-derived neurotrophic factor (BDNF)-dependent pathway (Geraghty et al., 2019). Considering that almost all of the top 20 upregulated genes in the high-performing DO mice were genes primarily expressed by OL-lineage cells and related transcriptional shifts were noted in the CC high-performers, it's possible that there was an attentional contribution of OL-lineage cells. However, it is also possible, that these observations could reflect a highly consistent, transcriptionally active population of cells, namely OPCs or pre-myelinating OLs. Regardless, the question of whether these transcriptional differences implicate OPCs for activity-dependent myelination requires further study.

Astrocytes, another class of glia, make up approximately 20% of cells in the human brain (Von Bartheld et al., 2016) and are part of what is known as the tripartite synapse, a term used to describe the bidirectional flow of information between neurons and astrocytes at the synapse (Perea et al., 2009). Astrocytes express receptors for almost all neurotransmitters and release several neuroactive chemicals themselves, including glutamate, GABA, as well as purinergic and peptidergic signaling molecules (Perea et al., 2009). Further, astrocyte-secreted synaptogenic factors may play a role in attention (Nagai et al., 2019). Since astrocytes are large cells that engage with multiple synapses across a relatively large area, it has been proposed that astrocytes may act to coordinate larger local neural network activity (Allen & Lyons, 2018). Further, it has been observed that calcium activity within astrocytes differs between cellular compartments (Lia et al., 2021). These calcium microdomains appear to have different time constants, ranging from shorter time scales similar to that of neurons in astrocytic endfeet and fine processes to tens of seconds in the soma (Stobart, Ferrari, Barrett, Stobart, et al., 2018). This suggests that astrocytes may serve to coordinate spatiotemporal neuronal synchrony in longer-term cognitive processes such as sustained attention. To do so, neural activity would stimulate astrocytes and induce intracellular calcium-dependent signaling cascades that, at the synapse would occur at a rate compatible with neuronal processing, but the long-lasting somatic response would keep those synaptic-scale modulations continuing over time, temporally regulated by the distance necessary for the signaling molecules to travel. This would also align with how the neural signatures of sustained attention appear to oscillate rhythmically (Fiebelkorn et al., 2013, 2018).

Finally, comprising roughly 15% of human brain cells (Von Bartheld et al., 2016), microglia are the resident immune cells of the brain. During

development, microglia modify circuit architecture by engulfing excess synapses in a neural activity-dependent thereby eliminating them (Paolicelli et al., 2011; Schafer et al., 2012). Still, microglia are also involved in enabling cognitive function in adulthood. Microglia are thought to be involved in synaptic plasticity, since knocking out the microglia-specific CX3C chemokine receptor 1, the receptor for neuronally secreted fractalkine, impairs long-term potentiation and motor learning (Rogers et al., 2011). Motor learning and synaptic accumulation of ionotropic glutamate receptors were also impaired in a study depleting microglia brain-wide (Parkhurst et al., 2013). Interestingly, conditionally knocking out microglial BDNF substantially reduced synaptic levels of the N-Methyl-D-aspartic acid receptor (NMDAR) subunit GluN2B and similarly impaired motor learning (Parkhurst et al., 2013). This raises the question of whether microglia may play a role in adaptive myelination as well. Microglia have also been found to exert an inhibitory influence on excitatory neurons in a negative feedback mechanism believed to prevent excess synchrony by highly active neurons, which can lead to seizures (Badimon et al., 2020). While synchronous activity can promote optimal attention, too much synchrony is thought to underly stress-induced hypervigilance, similar to that seen in patients with post-traumatic stress disorder (Dunkley et al., 2018). This could indicate a role for microglia in the stress-arousal-attention axis to help maintain an optimal attentional state during stressful periods.

5.4 Limitations, future directions, and concluding thoughts

As with all studies, the work I discussed in this thesis faced some limitations. While we benefitted from genetic mapping using innate behavioral measures of attention (indeed, using learned measures of attention introduced too many confounds and was not successful), in retrospect we may have further benefitted from including multiple innate behavioral measures of attention in our initial screen. This is challenging since few such measures have been well characterized or are easily quantifiable, but this effort may be worthwhile for future QTL mapping studies. Furthermore, due to a lack of appropriate reagents, we were not able to assess the functional roles of Homer1a and Ania3 at the protein levels and resolved at synapses, nor distinguish between their functions in our high- and low-performing mouse models, which will be important future avenues for study. Additionally, in our neural activity recordings, we opted to perform bulk photometry-based neural recordings for ease of initial exploration and understanding of cross-region neural dynamics, however, in the future, we will benefit from an approach with greater spatial and temporal resolution to further resolve the inhibitory/excitatory dynamics in PFC microcircuits. Relatedly, the potential adrenergic contribution to our model is based on both single-

cell sequencing data and LC recordings, but simultaneous, direct measurements of local norepinephrine release would be ideal for future studies to provide a more accurate representation of neurotransmitter dynamics affecting PFC microcircuits and output. Finally, emerging work from many labs, including preliminary findings in this thesis, suggests functional roles for glia in attention, which, with incipient technologies, is ripe for in-depth study.

CHAPTER 6. Methods

6.1 Animals

C57Bl6/J (B6) and Diversity Outbred (DO, 25th generation) male mice were purchased from The Jackson Laboratory. Collaborative Cross (CC) male mice from the CC083 and CC025 lines were purchased from the University of North Carolina at Chapel Hill. All mice were bought at six to eight weeks old, group-housed three to five per cage, and kept under a 12 hr light-dark cycle in a temperature-controlled environment with ad libitum food and water, unless mice were food restricted for behavioral assays. All procedures were done in accordance with guidelines approved by the Institutional Animal Care and Use Committees (protocol #22087-H) at The Rockefeller University. The number of mice used for each experiment was determined based on expected variance and effect size from previous studies and no statistical method was used to predetermine sample size. DO phenotyping was performed with all males to sufficiently power the study at an affordable cost, but future studies will use female-only or mixed cohorts.

6.2 Surgical procedures

Surgical procedures and viral injections were carried out under protocols approved by Rockefeller University IACUC and were performed in mice anesthetized with 1%–2% isoflurane using a stereotactic apparatus (Kopf) under a heating pad. Paralube vet ointment was applied to the eyes to prevent drying.

6.2.1 Viral injections

Viruses were injected using a 34–35 G beveled needle in a 10ul NanoFil Sub-Microliter Injection syringe (World Precision Instruments) controlled by an injection pump (Harvard Apparatus). All viruses were injected at a volume of 1 μL and a rate of 100nL/min (unless otherwise mentioned), and the needle was removed 10 min after the injection was done to prevent backflow of the virus. All injection coordinates were relative to bregma.

For adult knockdown manipulations: B6 mice were bilaterally injected at the age of 8 weeks in the PFC (A/P: 1.8 mm, M/L: ±0.3 mm, D/V: -1.75 mm) with a scAAV9 expressing either a U6-scramble (non-targeting) shRNA-CMV-mCherry (titer: 9.87. x 10^{12} GC/mL, VectorBuilder) or U6-Homer1a-targeted shRNA-CMV-mCherry (titer: 4.8 x 10^{12} GC/mL, VectorBuilder) construct.

For adult overexpression manipulations: B6 mice were bilaterally injected (2 injections/hemisphere) at the age of 8 weeks in the PFC (A/P: 1.8 mm, M/L1: ±0.3 mm, M/L2: ±0.45 mm, D/V: -1.75 mm) with an AAV9 expressing either CaMKII(1.3)-eYFP (titer: 1.0 x 10^{13} GC/mL) or CaMKII(1.3)-Homer1a-eYFP (titer: 1.0 x 10^{13} GC/mL) construct at a volume 0.5 µL for each injection. pAAV.CamKII(1.3).eYFP.WPRE.hGH was a gift from Karl Deisseroth (Addgene plasmid# 105622; http://n2t.net/addgene:105622; RRID: Addgene_105622).

For developmental knockdown experiments: Injections in pups were performed according to previously described anesthesia and injection protocols(Che et al., 2018). Here, B6 pups were bilaterally injected in PFC at p0 (A/P: ~0.3 mm, M/L: ~±0.15-0.2 mm, ~-0.7-0.8 mm) and again at p11 (A/P: 0.51, M/L: ±0.17, D/V: -1.5 mm) with an AAV9 expressing either a U6-scramble (non-targeting) shRNA-EF1a-mCherry (titer: 4.8. x 10^{12} GC/mL) or pooled U6-Homer1a-targeted shRNA-EF1a-mCherry and U6-Ania3-targeted shRNA-EF1a-mCherry construct (titer: 2.8 x 10^{12} GC/mL, Vector Biolabs) construct at a volume of 0.1 µL both times.

For multi-fiber photometry experiments: A mixture of AAV9-CaMKII(0.4)-Cre (titer: 1.0 x 10^{13}) and AAV1-Cag-Flex-JRGECO1a (titer: 1.0 x 10^{13}) was injected into PFC (A/P: 1.85 mm, M/L: 0.35 mm, D/V: -2.55 mm) at a combined volume of 1 µL. AAV9-Syn-GCaMP6f (titer: 1.4 x 10^{13} GC/mL) was injected ipsilaterally into MD (A/P: -1.6 mm, M/L: 0.45 mm, D/V: -3.2 mm). AAV(Olig001)-MAG-GCaMP6f (titer: 1 x 10^{13} GC/mL, Univ. Arizona Viral Production Core) was injected into PFC contralaterally (coordinates: A/P: 1.85 mm, M/L: -0.35 mm, D/V: -2.55 mm). AAV1-Cag-GCaMP6f (titer: 2.6 x 10^{12}) was also injected contralaterally to the initial injection (Cag-Flex-JRGECO1a) into LC (A/P: -5.4 mm, M/L: -0.85 mm, D/V: -3.6 mm). pENN.AAV.CamKII 0.4.Cre.SV40 was a gift from James M. Wilson (Addgene viral prep # 105558-AAV9; http://n2t.net/addgene:105558; RRID: Addgene_105558), pAAV.CAG.Flex.NES-jRGECO1a.WPRE.SV40 was a gift from Douglas Kim & GENIE Project (Addgene viral prep # 100852-AAV1; http://n2t.net/addgene:100852; RRID: Addgene_100852;) (Dana et al., 2016), pAAV.Syn.GCaMP6f.WPRE.SV40 was a gift from Douglas Kim & GENIE Project (Addgene viral prep # 100837-AAV9; http://n2t.net/addgene:100837; RRID: Addgene_100837), pAAV.CAG.GCaMP6f.WPRE.SV40 was a gift from Douglas Kim & GENIE Project (Addgene viral prep # 100836-AAV1; http://n2t.net/addgene:100836 ; RRID:Addgene_100836)(T.-W. Chen et al., 2013), Olig001 was a gift from Thomas McCown (Addgene plasmid # 170716; http://n2t.net/addgene:170716; RRID:Addgene_170716) (Powell et al., 2016).

6.2.2 Cannula implants

Immediately following viral injections, mice undergoing photometry experiments were implanted with 1.25 mm ferrule-coupled optical fibers (0.48 NA, 400 μm diameter, Doric Lenses) cut to the desired length so that the implantation site is ~0.2 mm dorsal to the injection site. Cannula implants were slowly lowered using a stereotaxic cannula holder (Doric) at a rate of 1 mm/min until they reached the implantation site, 0.2 mm dorsal to the injection site. Optic glue (Edmund Optics) was then used to seal the skull/cannula interface and a custom titanium headplate was glued to the skull using adhesive cement (Metabond).

Mice recovered for 5 weeks after Homer1 manipulations and 3 weeks after photometry implants before experiments began.

6.3 Animal behaviors

6.3.1 Acoustic startle response and prepulse inhibition

Acoustic startle response and prepulse inhibition testing were performed as described previously (Jin et al., 2019). Startle was measured using a San Diego Instruments SR-Lab Startle Response System. Mice were placed into Plexiglas cylinders resting on a Plexiglas platform with the chamber light on for the entire duration of the experiment. Acoustic stimuli were produced by speakers placed 33 cm above the cylinders. Piezoelectric accelerometers mounted under the cylinders transduced the movements of the mice, which were digitized and stored by an interface and computer assembly. Beginning at startle stimulus onset, 65 consecutive 1 ms readings were recorded to obtain the amplitude of the mouse's startle response. For the acoustic startle sessions, the intertrial interval between stimulus presentations averaged 15 sec (range: 7–23 s). A 65 dB background was presented continuously throughout the session. Startle pulses were 40 ms in duration, prepulses were 20 ms in duration, and prepulses preceded the pulse by 100 ms (onset–onset). The Plexiglas holders were wiped clean and allowed to dry between runs. The acoustic startle sessions consisted of three blocks. Sessions began with a 5 min acclimation period followed by delivery of five startle pulses (120 dB). This block allowed the startle response to reach a stable level before specific testing blocks. The next block tested the response threshold and included four each of five different acoustic stimulus intensities: 80, 90, 100, 110, and 120 dB (data not shown) presented in a pseudorandom order. The third block consisted of 42 trials including 12 startle pulses (120 dB) and 10 each of 3 different prepulse trials (i.e., 68, 71, and 77 dB preceding a 120 dB pulse). PPI was calculated as follows using the trials in the third block: 100 − ([(average startle of the prepulse + pulse trials)/average startle in the

pulse alone trial] × 100). In all experiments, the average startle magnitude over the record window (i.e., 65 ms) was used for all data analysis.

6.3.2 Spontaneous alternations in a T-maze

Tests consisted of a single 5 min trial, in which the mouse was allowed to explore all three arms of a Y maze (arm dimensions: 12" x 3" x 5" in (L x W x H) for 6 minutes while being recorded using a ceiling mounted camera under red light illumination. Mice were acclimated to the experimental site for 1 hr before all experiments. Whenever possible, the experimenter was blind to the viral condition of all mice during behavioral testing, with the exception of CC083 vs CC025 tests due to the difference in their coat color. The animal behavior was automatically tracked and analyzed by the EthoVision XT (Noldus) software for 1) total number of entries into each arm, 2) sequences of arm entries, 3) and distance moved (inch). Correct alternation (% of the total number of arm entries) was defined as consecutive entries in 3 different arms. The total number of entries into each arm as well as the total distance moved in the apparatus served as controls to exclude confounding factors to the memory performance, such as arm bias and/or differences in gross motor activity.

6.3.3 Rotarod

For this task, on day 1 the mice were habituated to the apparatus by being placed on a rod moving at a constant speed of 4 RPM for 5 min. On day 2, the mice were placed on the rod that this time is moving with an accelerating speed from (4 to 40 RPM), for 4 consecutive trials. In each trial, the latency (sec) to fall from the rod was measured by an experimenter. The cut-off time was 300 seconds. The latency to fall was averaged across trials and used as a measure of motor coordination.

6.3.4 Signal detection task (SDT)

Three days before the experiment, mice were gradually food-restricted to 85% of their body weight by providing ~2g of food per mouse per day and habituated to chocolate pellets by providing 2/3 pellets per mouse per day in their home cage. From the start of food deprivation and for the entire duration of the experiment, body weight and overall well-being were monitored by daily observation and weighting. All training and testing occur immediately before daily feeding.

The protocol is divided into multiple phases:

- ***Magazine Shaping.*** The box is configured to have the chocolate pellet magazine and dispenser, the white LED chamber light, speaker. The mouse enters the box with the chamber light off. A reward pellet is dispensed into the magazine on a variable 7-13 sec (VI10) schedule and at the same time the magazine light goes on. If the mouse retrieves the pellet, the program returns to the VI10 schedule of reward delivery. Alternatively, if the mouse does not retrieve the pellet within a variable 1-5 min period, the program returns to the VI10 schedule of reward. The session ends after 20 min. When 75% of the cohort are retrieving ≥15 pellets during the magazine shaping phase, the experiment moves to the next phase (usually 1 or 2 days).

- ***Nose Poke Shaping.*** The box configuration is enriched by the nosepoke port and will stay unchanged until the end of the experiment. The mouse enters the box with the chamber light off and is left to explore the box with the new element. Whenever the mouse pokes in the nosepoke port, a reward is dispensed. The session ends when the mouse receives 80 rewards or 20 min has elapsed. When 75% of the cohort is retrieving ≥15 pellets during the nosepoke shaping phase, the experiment moves to the next phase (usually ~3 days).

- ***SDT– 5 sec Cue Training.*** The mouse enters the box with the chamber light off. The session begins with an initial pre-cue delay period of the variable duration of 3-5 sec. If the mouse pokes during this time, the program moves to anticipatory response contingency (see below). Otherwise, it is followed by an 8 kHz pure tone auditory cue (~71 dB) that lasts for up to 5 sec. If the mouse pokes during the cue, the magazine lights up, a chocolate pellet is dispensed and the program moves to ITI contingency (see below). If, on the other hand, the mouse doesn't poke during the 5 sec cue, the cue turns off and the program moves to the post-cue response period that lasts up to 5 sec. If the mouse pokes during this phase, the magazine lights up, a chocolate pellet is dispensed and the program moves to ITI contingency. If, on the other hand, the mouse doesn't poke during the post-cue response period, the program moves to time-out contingency (see below).

- ***SDT– 1 sec Cue Training.*** This phase is exactly as the 5 sec cue training, with the only exception that the tone (cue) stays on for up to 1 sec vs 5 sec. The session ends when either the mouse has reached 100 correct responses or 20 min elapses.

ITI contingency: the magazine light turns off, and after a VI10 schedule delay, the program returns to the pre-cue delay period. If, on the other

hand, the mouse pokes during ITI contingency, the program goes to anticipatory response contingency.

Anticipatory response contingency: the chamber light turns on for 10 sec. If the mouse pokes during this time, the program restarts anticipatory response contingency. If, on the other hand, it doesn't poke, the chamber light turns off and the program moves to the pre-cue delay period.

Time-out contingency: the chamber light turns on for 10 sec. If the mouse pokes during this time, the program moves to delayed response contingency. If it doesn't, the chamber light turns off, the trial is considered omitted and the program moves to the pre-cue delay period.

Delayed response contingency: the chamber light turns on for 10 sec. If the mouse pokes during this time, the program restarts the delayed response contingency. If it doesn't, the chamber light turns off, the trial is considered omitted and the program moves to the pre-cue delay period. The session ends when either the mouse has reached 100 correct responses or 20 min elapses. When 75% of the cohort is getting ≥70% trials rewarded for 2 consecutive days in SDT Training 1, the experiment moves to the next phase.

All SDT experiments were performed within a Habitest Modular Arena and controlled, recorded, and analyzed by Graphic State 4 software (Coulbourn Instruments). If there was a statistically significant difference between cohorts by three-way ANOVA, data was normalized across cohorts and experimental groups relative to 5 sec cue training day 1.

6.3.5 Attentional set shift

One week before the test day, mice started a food deprivation protocol to achieve 80-85% of the initial weight. On day 1 and each consecutive day, they are handled, weighted, and fed ~20 g of food pellets and a few chocolate pellets (Bio-Serv). On the day of the experiment, the mice were placed in a squared open field arena (16 x 16 x 16 inch) for 5 consecutive trials and their behavior was recorded by a camera and analyzed by EthoVision XT (Noldus) software, similar to previous studies(Muzzio et al., 2009). Each of the arena walls has a different visual cue, and in front of each of them, on the floor and ~3 in from the wall, there is a medicinal cup containing bedding mixed with either sage, cinnamon, cumin, or cloves (2 gr of spice in 500gr bedding). During the pre-trial (T0), the mice were introduced in the arena for 5 min and allowed to explore the cups. This phase was necessary to assess the mice's exploratory activity and exclude any odor bias as well as differences between groups in sensitivity to the odors. For each of the successive 4 trials (T1-T4), the mice were re-

introduced in the arena for 5 min, and the cup containing sage was enriched by adding a chocolate pellet (reward). From trial to trial, the cups' positions were randomly shifted so that the odor/visual cue pair was always different, but it was kept fixed for all mice. To correctly perform the task, the mice had to learn to ignore the visual cues that remained at fixed locations and selectively pay attention to the odor as they changed position in the maze from trial to trial. During ITI, the mice were moved to a holding cage while the experimenter cleaned the arena with 10% ethanol, replaced the cups with clean ones, and re-baited the sage cup. The exploration time spent by the mice on each cup was recorded, as well as the latency to reach the correct cup (sage) and retrieve the pellet. Mice that did not locate the chocolate pellet in the initial 3 minutes of trial 1 were excluded from the analysis.

6.3.6 Novel object recognition task (NORT)

This test began with 2 days of habituation where the mice were allowed to explore an empty square arena (16" x 16" x 14" (L x W x H) for 15 minutes. During training (day 3), mice are re-introduced in the arena where are now present two identical objects positioned in the back left and right corners of the cage. Each animal was placed in the middle point of the wall opposite the objects and allowed to explore them for 15 min. At the end of the training phase, mice returned to their home cage for 15 min, while the box and the objects were cleaned with 10% Ethanol and then water. Successively, the mice were re-entered into the arena for the test, during which one of the two (familiar) objects was replaced with a new one (novel), totally different in color, texture, and shape. Each mouse was left free to explore the objects for 5 min. The entire experiment was recorded using a ceiling-mounted camera and the animal behavior was automatically tracked and analyzed by the EthoVision XT (Noldus) software. Two measures were considered: 1) total exploration time (sec) spent by the animal interacting with the two familiar objects during training, to evaluate object bias and 2) the exploration time spent by the animal interacting with the novel object over total exploration time (e.g., [novel/(familiar + novel)] × 100) during the test. Object exploration time is defined as the time during which the mouse nose was in contact with the object or directed toward it at a distance ≤ 2 cm.

6.3.7 Open field (OF)

Thigmotaxis was determined in an open field box (16 × 16 × 16 in), virtually divided into a peripheral and a central zone 50% smaller. Each mouse was allowed to explore the apparatus for 15 min and its behavior was recorded by a camera and analyzed by Ethovision. The time spent by the animal in the center of the arena was measured. In this test, the

preferential exploration of the peripheral zone of the open field is considered an index of anxiety.

6.3.8 Elevated plus maze (EPM)

This test is commonly used to evaluate anxiety-like behavior in rodents (Lister, 1987). The apparatus was composed of four black plastic arms, arranged as a cross, located 55 cm above the plane of a laboratory bench, and illuminated by a 60 w lamp located above the apparatus. Two closed arms, opposite to each other were enclosed by lateral walls (50 × 6 × 40 cm), whereas the other two open arms were without walls (50 × 6 × 0.75 cm); the closed and open arms delimited a small squared area (6 × 6 cm) called center. Each mouse was placed into the center of the maze, facing one of the two open arms, and its behavior was video-recorded for 5 min and automatically analyzed by the EthoVision XT software (Noldus) for the time spent by the mice in each of the three compartments (open, close, center), which was measured by an observer blind to the experimental groups.

6.3.9 3-chamber social interaction

Tests used an 18” x 18” x 12” (L x W x H) clear acrylic arena, which was divided into 3 chambers of equal area (18” x 6” x 12” (L x W x H) that were separated by walls 6” in length on each side so that there was a 6” long separation in each wall that a mouse could pass through. Mice were habituated to the testing area for 1 hr prior to the start of the experiment. The test began with a 5 min habituation phase to the center chamber, in which the openings in the walls were obstructed so that the mice could not see or enter either opening. Mice were then put in a transfer cage for 1 minute as the center walls were opened, after which the mice were returned to the center chamber for a 5 min habituation phase to all 3 chambers of the arena. Mice were then returned to the transfer cage for 5 min and the arena was wiped down with 10% ethanol, and wire cups were placed upside down in the center of the outer 2 chambers either with a non-social stimulus (foam figurine) or a novel, age- and strain-matched mouse underneath. Mice were then placed back in the center chamber and allowed to explore for 15 min. Behavior was video-recorded and automatically analyzed by the EthoVision XT Software (Noldus) for time spent in each chamber and time spent exploring a 3 cm proximity to the social or the non-social stimuli (social and non-social zones, respectively). The social discrimination index was calculated as the difference between the mouse’s time in the social zone and the non-social zone, divided by the total time exploring both zones.

6.3.10 Go/No-Go task

Mice were head-fixed in place above the center styrofoam ball (axially fixed with a rod passing through the center of the ball and resting on post holders) and allowed to move freely forward and backward. MATLAB engine ViRMEn was used to design the virtual task landscape and a National Instruments Data Acquisition (NIDAQ) device provided TTL pulses to trigger the Arduino Unos controlling the tones, odors, airpuff, and lick port. Capacitance changes of the lick port during licking were recorded through the NIDAQ as well.

Prior to behavioral training (2-3 days), homecage water was replaced with water containing 1% citric acid to increase motivation to receive water rewards throughout the task. Habituation began with mice receiving water rewards during Go cues presentation (odor: isoamyl acetate, pure tone: 6kHz). After 3-4 days, mice would be trained using blocks of Go and No-Go cue (odor: lavender oil, pure tone: 1kHz) trials. Delivery of water rewards required mice to lick during the Go cues presentation and an aversive airpuff punishment (25 psi) would be delivered to the flank of the mouse for licking during No-Go cues. After mice completed the block trials with 70% or greater accuracy, Go and No-Go trials would be pseudo-randomly interleaved (60-80 trials in total).

$$accuracy = \frac{\#\ correctly\ selected\ Go\ trials\ +\ \#\ correctly\ rejected\ NoGo\ trials}{total\ trials}$$

Mice completing the trials with 70% or greater accuracy for two consecutive days would then move on to testing. The testing trial structure is as follows: A 2 sec trial start tone (pure tone: 3kHz) begins each trial followed by a 2 sec delay then either Go or No-Go cues will be presented (2 sec presentation). At the onset of the cue presentation, a decision window will begin and last 2.5 seconds. A correct selection of the Go cues is made by licking within this decision window and a water reward is delivered at the end of correctly identified decision periods. Correct rejections of No-Go cues are measured by the absence of licking within the decision window. Each trial is followed by a 15 sec ITI.

6.3.11 Head-fixed signal detection task

Following the completion of Go/No-Go testing, mice were tested on a signal detection task. Each trial began with the 2 sec trial start tone (pure tone: 3kHz) and following a 2 sec delay mice were presented with

increasingly shortened Go cues (odor: isoamyl acetate, pure tone: 6kHz; cue length: 2 sec, 1 sec, 0.5 sec). After the Go cues presentation began, a decision window of 2.5 seconds opened and mice that licked within this window received a water reward.

6.4 Auditory brainstem recording thresholds (ABRs)

The mice were anesthetized with ketamine (110 mg/kg) and xylazine (11 mg/kg) via intraperitoneal injection prior to all procedures. Once a suitable plane of anesthesia was reached, one mL of chilled 0.9% sodium chloride was injected into the mouse's back for hydration. Both eyes also were moistened with ophthalmic ointment (Puralube®, Dechra Veterinary Products). The anesthetized animal was then placed in a sound-isolated, electrically shielded box on top of a heating pad (40-90-2-05, FHC, Inc.). In conjunction with the heating pad, a rectal probe and DC temperature controller (41-90-8D, FHC, Inc.) were used to maintain the mouse's temperature near 38 °C. Needle electrodes (GRD-SAF, The Electrode Store) were subdermally placed behind the pinna of the tested ear (reference electrode), in the scalp between the ears (active electrode), and in the back near the tail (ground electrode). ABRs were evoked by tone bursts of 4, 8, 16, and 32 kHz produced by a closed-field magnetic speaker connected to a power amplifier (MF1 and SA1, Tucker-Davis Technologies). Each 5-ms burst was presented 33.3 times per second with alternating polarity. The onset and offset of each burst were tapered with a squared cosine function. For each frequency, the sound pressure level was lowered from 80 dB SPL in 5–10 dB steps until the threshold was reached. If 80 dB SPL was not enough to elicit a response, higher intensities were produced. The entire sound delivery system was calibrated with a ¼ inch condenser microphone (4939-A-011 and 2690-A-0S1, Brüel & Kjær). The electrical response evoked by the tone bursts and measured by the needle electrodes was amplified 10,000 times and bandpass filtered at 0.3–3 kHz (P55, Astro-Med Inc.). The amplified response was then digitally sampled at 10-µs intervals with a data acquisition device (PCI-6259, National Instruments) controlled by custom software (LabVIEW 2019, National Instruments). The electrical responses to 1,000 bursts were averaged at each intensity level to determine the threshold, which was defined as the lowest level at which any response peak was distinctly and reproducibly present. Visual inspection of the vertically stacked responses facilitated threshold determination.

6.5 QTL mapping in Diversity Outbred mice

6.5.1 Genotype identification & haplotype reconstruction

SNP locations and genotypes for the eight founder strains were acquired from ftp.jax.org/MUGA and the consensus genotype for each

founder strain and each SNP was determined from the multiple individuals that were genotyped. SNP genotypes for the 182 DO mice were determined using a high-density mouse universal genotyping array, GigaMUGA (GeneSeek). A total of 114,184 SNPs were detected on the 19 autosomes and X chromosomes. Using R/qtl2 (Broman et al., 2019), founder haplotype probabilities were reconstructed for all samples and then converted to additive allelic dosages and scaled to 1. Realized genetic relationship matrices, often referred to as kinship matrices, were estimated using the leave-one-chromosome-out (LOCO) method so that the kinship term does not absorb variation explained by the putative QTL. Another QTL mapping software package for multiparental populations (MPPs), miQTL, was used to confirm findings from R/qtl2 and to visualize and assess the level of heterozygosity at the locus of interest.

6.5.2 QTL mapping

Phenotype values from the prepulse inhibition performance were subject to Box-Cox transformation. Then, using R/qtl2, an additive single locus linear mixed model was fit at positions across the genome, producing a genome scan. Potential population structure was controlled for through the inclusion of a random effect to account for correlation structure measured by the kinship matrix. This was performed in R/qtl2 using the leave one chromosome out (LOCO) method (Kang et al., 2010). For confirmation of the QTL results, we performed a multiple imputation genome scan (11 imputations) using miQTL, to assess whether uncertainty in founder haplotype reconstruction was strongly influencing the results. Genome-wide significance thresholds (alpha = 0.05) for the genome scans were determined through 1000 permutations of the diplotype.

6.5.3 Analysis of founder contributions

To determine the founder haplotype effects driving the Chr13QTL, we first estimated the best linear unbiased predictors (BLUPs), which constrain potentially unstable effects by fitting the QTL term as a random effect. To further confirm these results, we used Diploffect, to estimate posterior credible intervals for the haplotype effects as well as the proportion of variance explained by the QTL (sometimes referred to as the locus heritability).

6.6 RNA expression analysis

6.6.1 RNA extraction from brain tissues

For tissue extraction, p28 and adult (up to p120) mice were sacrificed by cervical dislocation and immediately decapitated, while p7, p14, and p21 mice were sacrificed by decapitation in compliance with IACUC protocol # 22087-H. The targeted brain regions were harvested from 1 mm brain slices, obtained by brain matrices (ZIVIC) using 1.0 mm tissue punches and transferred to a tube containing 300 mL of ice-cold lysis buffer and 3 mL ß-mercaptoethanol (Total RNA Purification kit, NORGEN; following the manufacturer's protocol). Samples were then homogenized by passing a 25G insulin syringe six times and left on ice. For RNA extraction, the total RNA Purification kit was used according to the manufacturer's instructions (NORGEN). RNA quality was evaluated by Bioanalyzer 2100 (Eukaryote Total RNA Nano chip, Agilent) at the Rockefeller University Genomic Resource Center (RIN > = 7.50 and free of genomic DNA contamination). RNA samples were then aliquoted and stored at -80°C.

6.6.2 Bulk RNA sequencing (RNAseq) and analysis

For RNAseq, RNA libraries were prepared from 100ng of total RNA per sample for 6 DO mice, 3 brain regions per mouse using the TruSeq stranded mRNA LT kit (Cat# RS-122-2101, Illumina). These synthetic RNAs cover a range of concentrations, lengths, and GC content for validation of the fidelity and dose-response of the library prior to downstream procedures. Libraries prepared with unique barcodes were pooled at equal molar ratios following the manufacturer's protocol (Cat# 15035786 v02, Illumina). The pool was denatured and subject to paired-end 50x (DO samples) or single-end 100x (CC samples) sequencing on the NovaSeq SP platform. An average of 67 million reads per sample were obtained. Sequencing reads were aligned to the mouse genome (mm10) using STAR (v2.4.2a) and aligned reads were quantified using Salmon (v0.8.2). Approximately 90% of the reads were uniquely mapped. Hierarchical clustering and Principal Components Analysis were performed following Variance Stabilizing Transformation (VST) from DESeq2, which is on the log2 scale and accounts for library size differences. The hierarchical clustering heatmap shows the Euclidean distances of VST of the counts between samples.

6.6.3 Quantitative PCR (qPCR)

For quantitative PCR, each reverse transcription was performed with 0.2 mg RNA using the High-Capacity RNA-to-cDNA kit (Applied Biosystems # 4387406), in a final volume of 20 µL. Primers for reverse

transcription were equal mixtures of poly-T nucleotides and random hexamers. Negative controls (omitting reverse transcriptase enzyme) were performed for each sample. The cDNA products were diluted 1:1 and 2 µL was analyzed by qPCR using custom primer sets and PowerUp SYBR Green Master Mix (10 µL total reaction, Applied Biosystems # A25742). RT-qPCRs were performed on a Quantstudio3 from Applied Biosystems. Every reaction was systematically run in triplicate. Conditions were the following: 50ºC 2 min, 95ºC 10 min, 40 x (95ºC 15 s, 60ºC 1 min). qPCR Ct values were analyzed using the LightCycler software. The detection threshold was set at DRn = 0.3, with this limit always within the 2n exponential amplification phase of genes. The means of technical triplicate values were reported. All mice gene expression Ct values were normalized with the reference gene Ube2d2a using the dCt method to determine the relative mRNA expression of each gene. Developmental knockdown mice that expressed both *Homer1a* and *Ania3* at levels higher than the average scramble expression by half a standard deviation or more were post hoc excluded from downstream analyses.

6.7 Single-Cell sequencing

6.7.1 Single-cell dissociation and single-cell RNA sequencing

Single-cell suspensions of the prefrontal cortex were prepared as described previously (Zeisel et al., 2018). Briefly, mice were sacrificed with an overdose of isoflurane, followed by transcardial perfusion with carbogenated (95% O_2, 5% CO_2) Hanks' Balanced Salt Solution (HBSS). Brains were removed, 500µm sections were collected, and the prefrontal cortex region was isolated. The tissue was dissociated using papain (LS003124, Worthington) dissolved in Hibernate A buffer (NC1787837, Fisher Scientific) and incubated for 25-30 min at 37ºC, followed by manual trituration using fire-polished Pasteur pipettes and filtering through a 40µm cell strainer (BAH136800040, Millipore Sigma). Cells were washed with wash buffer (PBS + 1% BSA) and centrifuged at 200 g for 5 min, the supernatant was carefully removed, and cells were resuspended in ~500ul wash buffer and 10% DAPI. Flow cytometry was done using a BD FACS Aria III Cell Sorter (BD FACSDiva Software, v8.0.1) with a 100-µm nozzle. The cell suspensions were first gated on forward scatter, then within this population based on lack of DAPI staining. Cells were collected in wash buffer and manually counted using a Burker chamber, and suspension volumes were adjusted to a target concentration of 700 -1000 cells/µl. Single-cell RNA sequencing was carried out with the Chromium Next GEM Single Cell 3' Kit v3.1 (10X Genomics, 1000268). The manufacturer's instructions were followed for downstream cDNA synthesis (12-14 PCR cycles) and library preparation. Final libraries were sequenced on the Illumina NovaSeq S4 platform (R1 – 28 cycles, i7 – 8 cycles, R2 – 90 cycles).

6.7.2 Single-cell RNA sequencing data analysis

Raw sequencing reads were aligned to the GRCm38/mm10 mouse reference genome and a custom cell-gene count matrix was constructed using the Sequence Quality Control (SEQC) package (Azizi et al., 2018). Viable cells were identified based on library size and complexity, whereas cells with >20% of transcripts derived from mitochondria were excluded from further analysis. The Python Scanpy package (v1.9.3) was used to further analyze the data. Replicates were merged and doublets were removed using Scrublet (Wolock et al., 2019). Cells with <2,500 UMIs per cell and <1,000 genes per cell, and genes detected in <3 cells were removed. Per-cell counts were normalized to equal the median of total counts per cell and log-transformed. Principal component analysis was used to reduce the dimensionality to 50 principal components. A nearest-neighbor graph was computed between cells using these principal components, and Leiden clustering was applied to separate the cells into distinct clusters of major cell types. Known gene markers were used (Zeisel et al., 2018) to assign cell types. Once the neuronal cluster was identified, it was subsetted and re-clustered using the first 50 principal components to identify inhibitory and excitatory neurons. Clusters with differential *Homer1* expression between cc083 and cc025 strains were identified using t-tests. Clusters with significantly different *Homer1* expression between strains were merged, and the "MAST" R package (Finak et al., 2015) was used to identify differentially expressed genes between strains for the merged cluster as well as all individual clusters. Gene set enrichment analysis was performed using the fast gene set enrichment analysis (GSEA) package (fgsea v1.18.0), the GO_Molecular_Function_2021 gene set, and the Elsevier_Pathway_Collection gene-set libraries using Enrichr (E. Y. Chen et al., 2013; Kuleshov et al., 2016; Xie et al., 2021). In Scanpy, dot plots scaled from 0 to 1 were scaled using the "standard_scale" function, while dot plots scaled from 0.5 to 1 were scaled by setting "vmin" to 0.5 and "vmax" to 1.

6.8 Gene expression manipulation experiments *in vitro* & *in vivo*

We used the following shRNAs for gene knockdown (which were then subcloned into a pscAV-U6-mCherry construct, VectorBuilder/Vector Biolabs):

Homer1a (GenBank: NM_011982.4), Targeting sequence: GGTTTCAGAAACTCTTGAA;

Ania3 (GenBank: NM_001347598.1), Targeting sequences: GGAGACATAGTTCTTCTTA, GCTAAGCTAGAGCCATCTA.

For gene expression, coding sequences of Homer1a and Ania3 were cloned from mouse cortical cDNA and subsequently subcloned into a pAAV.CamKII(1.3).eYFP.WPRE.hGH expression vector using standard molecular cloning techniques. Constructs were verified first by Sanger sequencing, and then diagnostics for ITR integrity, by digestion with SmaI, before AAV production.

6.9 Generation of AAV-MAG-GCaMP6f

We identified the mouse *MAG* gene locus (including introns and a 3 kb upstream potential promoter region) using the UCSC genome browser, as others have done previously (von Jonquieres et al., 2016), on the reverse strand of Chr 7qB1: 30,899,176-30,917,832 in the July 2007 mm9 alignment (Chromosome 7: 30,598,601-30,617,298 in the GRC38/mm10 alignment). Sequence conservation was assessed using the VISTA genome browser (Frazer et al., 2004) and the putative *MAG* promoter was screened for regions of >50% interspecies sequence similarity, which were then evaluated for transcription factor binding sites, especially OL-lineage specific *Olig1* and *Olig2*, using the Wilmer Bioinformatics Resource (S. Hu et al., 2009) and the P-match 1.0 program (http://gene-regulation.com/pub/programs.html#pmatch). This method yielded a 2.5 Kb putative *MAG* promoter region. The putative *MAG* promoter was cloned from mouse cortical cDNA using standard molecular cloning techniques and replaced the Syn promoter from the pAAV.Syn.GCaMP6f.WPRE.SV40 plasmid. The pAAV-MAG-GCaMP6f construct was packaged using the Olig001 capsid (Powell et al., 2016), which has high oligodendrocyte tropism. (Univ. of Arizona Viral Production Core).

6.10 Histology & immunohistochemistry

Mice were transcardially perfused with PBS and 4% paraformaldehyde in 0.1M PB, then brains were post-fixed by immersion for 24 h in the perfusate solution followed by 30% sucrose in 0.1M PB at 4°C. The fixed tissue was cut into 40 mm coronal sections using a freezing microtome (Leica SM2010R), stained with DAPI (1:1000 in PBST), and mounted on slides with ProLong Diamond Antifade Mountant (Invitrogen). For immunostaining, the fixed sections were permeabilized with 70% methanol for 15 min before blocking with 5% normal donkey serum in PBS for 1 h and incubated with primary antibodies overnight at 4°C. Sections were washed three times in PBS and incubated with appropriate secondary antibodies overnight at 4°C. Afterward, coverslips were mounted using ProLong Diamond Antifade mounting medium for image collection. Primary and secondary antibodies include rabbit polyclonal

anti-NeuN (Millipore ABN78), rabbit polyclonal anti-Iba1 (Wako, 019-19741), rabbit polyclonal anti-Olig2 (Millipore, AB9610), and mouse monoclonal anti-GFAP (Millipore MAB360), Alexa Fluor 647 donkey anti-rabbit IgG (Jackson ImmunoResearch, Cat # 711-606-152), Alexa Fluor 647 donkey anti-mouse IgG (Jackson ImmunoResearch, Cat # 715-606-151), and DAPI (Cayman Chemical, Cat#28718-90-3). For immunohistochemistry staining, epifluorescent images were obtained at room temperature on a Nikon Eclipse T*i* microscope using a Nikon 4x (NA 0.13, dry), 10x (NA 0.30, dry), or 20x (NA 0.45, dry), objectives with the same settings and configurations for each objective across all samples within each experiment.

6.11 *In vivo* multi-site photometry recordings

6.11.1 Photometry setup

A custom dual-color, multi-fiber photometry setup was built. For GCaMP6f imaging, excitation of the 470 nm (imaging) and 405 nm (isosbestic control) wavelengths was provided by LEDs (Thorlabs M470F3, M405FP1), which were collimated into a dichroic mirror holder with a 425 nm long pass filter (Thorlabs DMLP425R). This was coupled to another dichroic mirror holder with a 495 nm long pass dichroic (Semrock FF495-Di02-25x36) which redirected the excitation light onto a custom branching low-autofluorescence fiberoptic patchcord of three bundled 400 mm diameter 0.57NA fibers (BFP(3)_400/440/PKMJ-0.57_1m_SMA-3xFC_LAF, Doric Lenses) using a 20x/0.5NA Objective lens (Nikon CFI SFluor 20X, Product No. MRF00100). GCaMP6f fluorescence from neurons below the fiber tip in the brain was transmitted via this same cable back to the mini-cube, where it was passed through a GFP emission filter (Semrock FF01-520/35-25), amplified, and focused onto a high-sensitivity sCMOS camera (Prime 95b, Photometrics). For jRGECO1a imaging, a second light path was built so that excitation of the 565 nm (imaging) and 470 nm (isosbestic control) wavelengths were provided by LEDs (Thorlabs M565F3^{h}, M470F3), which were collimated into a dichroic mirror holder with a 505 nm long pass dichroic (Thorlabs DMLP505R). This was coupled to another dichroic mirror holder with a 573 nm long pass dichroic (Semrock Di02-R561-25x36), which redirected the excitation light onto a low-autofluorescence monofiberoptic patchcord with a 400 mm diameter 0.57NA fiber (MFP_400/440/PKMJ-0.57_1m_SMA-FC_LAF, Doric Lenses) using a 20x/0.5NA Objective lens (Nikon CFI SFluor 20X, Product No. MRF00100). jRGECO1a fluorescence from neurons below the fiber tip in the brain was transmitted via this same cable back to the mini-cube, where it was passed through an RFP emission filter (Semrock

FF01-607/36-25), amplified, and focused onto a high-sensitivity CMOS camera (BFS-PGE-50S5M-C, Teledyne FLIR).

Each of the multiple branch ends of the branching fiber optic patchcord, as well as the monofiberoptic patchcord, were coupled to four 2 m low-autofluorescence patchcords (MFP_400/430/1100-0.57_2m_FCZF1.25_LAF, Doric Lenses) which is used to collect emission fluorescence from 1.25mm diameter lightweight ferrules (MFC_400/430-0.48_ZF1.25, Doric Lenses) using a mating sleeve (SLEEVE_BR_1.25, Doric Lenses). A microcontroller (Arduino Uno) was programmed to take trigger inputs from the Operant Behavior Setup or MATLAB and synchronize the camera shutters and alternate triggering of the 405 nm and 565 nm LEDs together and both 470 nm LEDs together. Custom TTL converters were used to read in-frame acquisition times to the Habitest Modular system (above), which were integrated with events from the behavior in Graphic State 4. Bulk activity signals were collected using the PVCAM (GCaMP) and Spinnaker (jRGECO) software, and data were further post-processed and analyzed using custom MATLAB scripts.

6.12 Quantification and statistical analysis

6.12.1 Behavior statistical reporting

Sample sizes were selected based on expected variance and effect sizes from the existing literature, and no statistical methods were used to determine sample size a priori. Before experiments were performed, mice were randomly assigned to experimental or control groups. The investigator was blinded to all behavioral studies (except for CC083 versus CC025 cohorts, where coat color differences prevent blinding during experimentation). Homer1a/Ania3 shRNA mice were removed from the developmental knockdown experiments if they did not have sufficiently reduced expression relative to the scramble groups or were extreme outliers from the remainder of the knockdown mice. Data analyses for calcium imaging were automated using MATLAB scripts. Statistical tests were performed in MATLAB 2022b or GraphPad Prism 9.

6.12.2 Gene expression statistics

Differential gene expression between high- and low-performing DO mice as well as between CC025 and CC083 mice from bulk RNAseq data was determined in R (3.5.0) using the DESeq2. P values were determined using a Wald test and p values were corrected using the Benjamini-Hochberg (BH) method.

6.12.3 Multi-fiber photometry data processing

For analysis, the images captured by the sCMOS camera were post-processed using custom MATLAB scripts. Regions of interest were manually drawn for each fiber to extract fluorescence values throughout the experiment. The 405 nm (GCaMP) or 470 nm (jRGECO) reference traces were scaled to best fit the 470 nm (GCaMP) or 565 nm. (jRGECO) signal using least-squares regression. The normalized change in fluorescence (dF/F) was calculated by subtracting the scaled 405 nm or 470. nm reference traces from the 470 nm or 565 nm signals, respectively, and dividing those values by the scaled reference traces. The true baseline of each dF/F trace was determined and corrected by using the MATLAB function "msbackadj" to estimate the baseline over a 200-frame sliding window, regressing varying baseline values to the window's data points using a spline approximation, then adjusting the baseline in the peak range of the dF/F signal. Task events (e.g., cue on/offsets, and nosepokes), were time stamped via the Graphic State 4 software.

6.12.4 Multi-fiber photometry data analysis

Total mean activity for non-task baseline periods as well as for different task phases and different strains was quantified as the area under the curve (AUC) of dF/F responses shifted above 0. AUC was calculated using MATLAB "trapz" function and normalized with the recorded time. Pearson Correlation of the dF/F responses was performed between different regions using the "corr" (MATLAB) function. To ensure that correlation values were significantly more than chance, each time series was scrambled 10,000 times randomly, for each session across all mice. All such chance correlation coefficients were pooled to calculate the mean (all of which were at or near zero) and standard deviation of chance correlations. To quantify signal-to-noise ratio (SNR), we calculated the mean and standard deviation of each region's neural activity (z-scored dF/F) during baseline periods of the task, i.e. all omission trials (from cue onset to the onset of the pre-trial delay phase, calculated values referred to as baseline_mean and baseline_SD) for each mouse for a given day. Trial SNR was calculated as the difference between the maximum pre-cue activity (z-scored dF/F for the 5 sec immediately before cue onset) and the baseline_mean value for that mouse, divided by the baseline_SD value.

$$SNR = \frac{trial\ pre\text{–}cue\ maximum - baseline\_mean}{baseline\_SD}$$

For cohorts that progressed to the 1 sec cue training phase, only mice remaining above 70% performance accuracy were included in the

analyses. Additionally, the first training session and any training sessions under 15 minutes long were not included in the analyses.

CHAPTER 7. References

Aceves-Piña, E. O., & Quinn, W. G. (1979). Learning in Normal and Mutant *Drosophila* Larvae. *Science*, *206*(4414), 93–96. https://doi.org/10.1126/science.206.4414.93

Adams, M. D., Celniker, S. E., Holt, R. A., Evans, C. A., Gocayne, J. D., Amanatides, P. G., Scherer, S. E., Li, P. W., Hoskins, R. A., Galle, R. F., George, R. A., Lewis, S. E., Richards, S., Ashburner, M., Henderson, S. N., Sutton, G. G., Wortman, J. R., Yandell, M. D., Zhang, Q., … Venter, J. C. (2000). The Genome Sequence of *Drosophila melanogaster*. *Science*, *287*(5461), 2185–2195. https://doi.org/10.1126/science.287.5461.2185

Ahmadian, G., Ju, W., Liu, L., Wyszynski, M., Lee, S. H., Dunah, A. W., Taghibiglou, C., Wang, Y., Lu, J., Wong, T. P., Sheng, M., & Wang, Y. T. (2004). Tyrosine phosphorylation of GluR2 is required for insulin-stimulated AMPA receptor endocytosis and LTD. *The EMBO Journal*, *23*(5), 1040–1050. https://doi.org/10.1038/sj.emboj.7600126

Allada, R., White, N. E., So, W. V., Hall, J. C., & Rosbash, M. (1998). A Mutant Drosophila Homolog of Mammalian Clock Disrupts Circadian Rhythms and Transcription of period and timeless. *Cell*, *93*(5), 791–804. https://doi.org/10.1016/S0092-8674(00)81440-3

Allen, N. J., & Lyons, D. A. (2018). Glia as architects of central nervous system formation and function. *Science*, *362*(6411), 181–185. https://doi.org/10.1126/science.aat0473

Alsene, K. M., Rajbhandari, A. K., Ramaker, M. J., & Bakshi, V. P. (2011). Discrete Forebrain Neuronal Networks Supporting Noradrenergic Regulation of Sensorimotor Gating. *Neuropsychopharmacology*, *36*(5), 1003–1014. https://doi.org/10.1038/npp.2010.238

Ango, F., Pin, J. P., Tu, J. C., Xiao, B., Worley, P. F., Bockaert, J., & Fagni, L. (2000). Dendritic and axonal targeting of type 5 metabotropic glutamate receptor is regulated by homer1 proteins and neuronal excitation. In *J Neurosci* (Vol. 20, Issue 23, pp. 8710–8716). https://doi.org/10.1523/JNEUROSCI.20-23-08710.2000

Ango, F., Prézeau, L., Muller, T., Tu, J. C., Xiao, B., Worley, P. F., Pin, J. P., Bockaert, J., & Fagni, L. (2001). Agonist-independent activation of metabotropic glutamate receptors by the intracellular protein Homer. *Nature*, *411*(6840), 962–965. https://doi.org/10.1038/35082096

Arnsten, A. F. T. (2000). Through the Looking Glass: Differential Noradenergic Modulation of Prefrontal Cortical Function. *Neural Plasticity*, *7*(1–2), 133–146. https://doi.org/10.1155/NP.2000.133

Arnsten, A. F., Wang, M. J., & Paspalas, C. D. (2012). Neuromodulation of thought: Flexibilities and vulnerabilities in prefrontal cortical network synapses. In *Neuron* (Vol. 76, Issue 1, pp. 223–239). https://doi.org/10.1016/j.neuron.2012.08.038

Aston-Jones, G., & Bloom, F. (1981). Activity of norepinephrine-containing locus coeruleus neurons in behaving rats anticipates fluctuations in the sleep-waking cycle. *The Journal of Neuroscience*, *1*(8), 876–886. https://doi.org/10.1523/JNEUROSCI.01-08-00876.1981

Aston-Jones, G., & Cohen, J. D. (2005). An Intigrative Theory Of Locus Coeruleus-Norepinephrine Function: Adaptive Gain and Optimal Performance. *Annual Review of Neuroscience*, *28*(1), 403–450. https://doi.org/10.1146/annurev.neuro.28.061604.135709

Aston-Jones, G., Rajkowski, J., & Cohen, J. (1999). Role of locus coeruleus in attention and behavioral flexibility. In *Biol Psychiatry* (Vol. 46, Issue 9, pp. 1309–1320). https://doi.org/10.1016/s0006-3223(99)00140-7

Aston-Jones, G., Rajkowski, J., & Kubiak, P. (1997). Conditioned responses of monkey locus coeruleus neurons anticipate acquisition of discriminative behavior in a vigilance task. *Neuroscience*, *80*(3), 697–715. https://doi.org/10.1016/S0306-4522(97)00060-2

Atienza, M., Cantero, J. L., & Escera, C. (2001). Auditory information processing during human sleep as revealed by event-related brain potentials. *Clinical Neurophysiology*, *112*(11), 2031–2045. https://doi.org/10.1016/S1388-2457(01)00650-2

Azizi, E., Carr, A. J., Plitas, G., Cornish, A. E., Konopacki, C., Prabhakaran, S., Nainys, J., Wu, K., Kiseliovas, V., Setty, M., Choi, K., Fromme, R. M., Dao, P., McKenney, P. T., Wasti, R. C., Kadaveru, K., Mazutis, L., Rudensky, A. Y., & Pe'er, D. (2018). Single-Cell Map of Diverse Immune Phenotypes in the Breast Tumor Microenvironment. In *Cell* (Vol. 174, Issue 5, pp. 1293-1308 e36). https://doi.org/10.1016/j.cell.2018.05.060

Badimon, A., Strasburger, H. J., Ayata, P., Chen, X., Nair, A., Ikegami, A., Hwang, P., Chan, A. T., Graves, S. M., Uweru, J. O., Ledderose, C., Kutlu, M. G., Wheeler, M. A., Kahan, A., Ishikawa, M., Wang,

Y.-C., Loh, Y.-H. E., Jiang, J. X., Surmeier, D. J., … Schaefer, A. (2020). Negative feedback control of neuronal activity by microglia. *Nature*, *586*(7829), 417–423. https://doi.org/10.1038/s41586-020-2777-8

Banaschewski, T., Roessner, V., Dittmann, R. W., Santosh, P. J., & Rothenberger, A. (2004). Non-stimulant medications in the treatment of ADHD. In *Eur Child Adolesc Psychiatry: Vol. 13 Suppl 1* (pp. I102-16). https://doi.org/10.1007/s00787-004-1010-x

Bargiello, T. A., Jackson, F. R., & Young, M. W. (1984). Restoration of circadian behavioural rhythms by gene transfer in Drosophila. *Nature*, *312*(5996), 752–754. https://doi.org/10.1038/312752a0

Bargiello, T. A., & Young, M. W. (1984). Molecular genetics of a biological clock in Drosophila. *Proceedings of the National Academy of Sciences of the United States of America*, *81*(7), 2142–2146. https://doi.org/10.1073/pnas.81.7.2142

Bari, A., Xu, S., Pignatelli, M., Takeuchi, D., Feng, J., Li, Y., & Tonegawa, S. (2020). Differential attentional control mechanisms by two distinct noradrenergic coeruleo-frontal cortical pathways. *Proceedings of the National Academy of Sciences*, *117*(46), 29080–29089. https://doi.org/10.1073/pnas.2015635117

Battefeld, A., Klooster, J., & Kole, M. H. P. (2016). Myelinating satellite oligodendrocytes are integrated in a glial syncytium constraining neuronal high-frequency activity. *Nature Communications*, *7*(1), 11298. https://doi.org/10.1038/ncomms11298

Benzer, S. (1967). BEHAVIORAL MUTANTS OF *Drosophila* ISOLATED BY COUNTERCURRENT DISTRIBUTION. *Proceedings of the National Academy of Sciences*, *58*(3), 1112–1119. https://doi.org/10.1073/pnas.58.3.1112

Berger, B., Gaspar, P., & Verney, C. (1991). Dopaminergic innervation of the cerebral cortex: Unexpected differences between rodents and primates. *Trends in Neurosciences*, *14*(1), 21–27. https://doi.org/10.1016/0166-2236(91)90179-X

Berridge, C. W. (2008). Noradrenergic modulation of arousal. *Brain Research Reviews*, *58*(1), 1–17. https://doi.org/10.1016/j.brainresrev.2007.10.013

Berridge, C. W., & Spencer, R. C. (2016). Differential cognitive actions of norepinephrine a2 and a1 receptor signaling in the prefrontal

cortex. *Brain Research*, *1641*, 189–196. https://doi.org/10.1016/j.brainres.2015.11.024

Birnbaum, S. G., Yuan, P. X., Wang, M., Vijayraghavan, S., Bloom, A. K., Davis, D. J., Gobeske, K. T., Sweatt, J. D., Manji, H. K., & Arnsten, A. F. T. (2004). Protein Kinase C Overactivity Impairs Prefrontal Cortical Regulation of Working Memory. *Science*, *306*(5697), 882–884. https://doi.org/10.1126/science.1100021

Boekhoudt, L., Omrani, A., Luijendijk, M. C. M., Wolterink-Donselaar, I. G., Wijbrans, E. C., Van Der Plasse, G., & Adan, R. A. H. (2016). Chemogenetic activation of dopamine neurons in the ventral tegmental area, but not substantia nigra, induces hyperactivity in rats. *European Neuropsychopharmacology*, *26*(11), 1784–1793. https://doi.org/10.1016/j.euroneuro.2016.09.003

Boekhoudt, L., Voets, E. S., Flores-Dourojeanni, J. P., Luijendijk, M. C., Vanderschuren, L. J., & Adan, R. A. (2017). Chemogenetic Activation of Midbrain Dopamine Neurons Affects Attention, but not Impulsivity, in the Five-Choice Serial Reaction Time Task in Rats. *Neuropsychopharmacology*, *42*(6), 1315–1325. https://doi.org/10.1038/npp.2016.235

Botstein, D., White, R. L., Skolnick, M., & Davis, R. W. (1980). Construction of a genetic linkage map in man using restriction fragment length polymorphisms. *American Journal of Human Genetics*, *32*(3), 314–331.

Bottai, D., Guzowski, J. F., Schwarz, M. K., Kang, S. H., Xiao, B., Lanahan, A., Worley, P. F., & Seeburg, P. H. (2002). Synaptic Activity-Induced Conversion of Intronic to Exonic Sequence in Homer 1 Immediate Early Gene Expression. *The Journal of Neuroscience*, *22*(1), 167. https://doi.org/10.1523/JNEUROSCI.22-01-00167.2002

Bouras, N. N., Mack, N. R., & Gao, W.-J. (2023). Prefrontal modulation of anxiety through a lens of noradrenergic signaling. *Frontiers in Systems Neuroscience*, *17*, 1173326. https://doi.org/10.3389/fnsys.2023.1173326

Bouret, S., & Sara, S. J. (2004). Reward expectation, orientation of attention and locus coeruleus-medial frontal cortex interplay during learning. *European Journal of Neuroscience*, *20*(3), 791–802. https://doi.org/10.1111/j.1460-9568.2004.03526.x

Braff, D. L., Geyer, M. A., Light, G. A., Sprock, J., Perry, W., Cadenhead, K. S., & Swerdlow, N. R. (2001). Impact of prepulse characteristics

on the detection of sensorimotor gating deficits in schizophrenia. *Schizophrenia Research*, *49*(1), 171–178. https://doi.org/10.1016/S0920-9964(00)00139-0

Brakeman, P. R., Lanahan, A. A., O'Brien, R., Roche, K., Barnes, C. A., Huganir, R. L., & Worley, P. F. (1997). Homer: A protein that selectively binds metabotropic glutamate receptors. In *Nature* (Vol. 386, Issue 6622, pp. 284–288). https://doi.org/10.1038/386284a0

Brenner, S. (1974). The Genetics Of *Caenorhabditis elegans*. *Genetics*, *77*(1), 71–94. https://doi.org/10.1093/genetics/77.1.71

Broadbent, D. E. (1958). *Perception and communication*. Pergamon.

Broman, K. W., Gatti, D. M., Simecek, P., Furlotte, N. A., Prins, P., Sen, S., Yandell, B. S., & Churchill, G. A. (2019). R/qtl2: Software for Mapping Quantitative Trait Loci with High-Dimensional Data and Multiparent Populations. In *Genetics* (Vol. 211, Issue 2, pp. 495–502). https://doi.org/10.1534/genetics.118.301595

Bushnell, P. J. (1998). Behavioral approaches to the assessment of attention in animals. *Psychopharmacology*, *138*(3–4), 231–259. https://doi.org/10.1007/s002130050668

Bushnell, P. J., & Strupp, B. J. (2009). Assessing Attention in Rodents. In J. J. Buccafusco (Ed.), *Methods of Behavior Analysis in Neuroscience* (2nd ed.). CRC Press/Taylor & Francis. http://www.ncbi.nlm.nih.gov/books/NBK5234/

Caldarone, B., Saavedra, C., Tartaglia, K., Wehner, J. M., Dudek, B. C., & Flaherty, L. (1997). Quantitative trait loci analysis affecting contextual conditioning in mice. *Nature Genetics*, *17*(3), 335–337. https://doi.org/10.1038/ng1197-335

Callahan, P. M., & Terry, A. V. (2015). Attention. *Handbook of Experimental Pharmacology*, *228*, 161–189. https://doi.org/10.1007/978-3-319-16522-6_5

Carter, M. E., Yizhar, O., Chikahisa, S., Nguyen, H., Adamantidis, A., Nishino, S., Deisseroth, K., & De Lecea, L. (2010). Tuning arousal with optogenetic modulation of locus coeruleus neurons. *Nature Neuroscience*, *13*(12), 1526–1533. https://doi.org/10.1038/nn.2682

Chalfie, M., & Au, M. (1989). Genetic Control of Differentiation of the *Caenorhabditis elegans* Touch Receptor Neurons. *Science*, *243*(4894), 1027–1033. https://doi.org/10.1126/science.2646709

Chalfie, M., & Sulston, J. (1981). Developmental genetics of the mechanosensory neurons of Caenorhabditis elegans. *Developmental Biology*, *82*(2), 358–370. https://doi.org/10.1016/0012-1606(81)90459-0

Che, A., Babij, R., Iannone, A. F., Fetcho, R. N., Ferrer, M., Liston, C., Fishell, G., & De Marco Garcia, N. V. (2018). Layer I Interneurons Sharpen Sensory Maps during Neonatal Development. In *Neuron* (Vol. 99, Issue 1, pp. 98-116 e7). https://doi.org/10.1016/j.neuron.2018.06.002

Chen, E. Y., Tan, C. M., Kou, Y., Duan, Q., Wang, Z., Meirelles, G. V., Clark, N. R., & Ma'ayan, A. (2013). Enrichr: Interactive and collaborative HTML5 gene list enrichment analysis tool. In *BMC Bioinformatics* (Vol. 14, Issue 1, p. 128). https://doi.org/10.1186/1471-2105-14-128

Chen, T.-W., Wardill, T. J., Sun, Y., Pulver, S. R., Renninger, S. L., Baohan, A., Schreiter, E. R., Kerr, R. A., Orger, M. B., Jayaraman, V., Looger, L. L., Svoboda, K., & Kim, D. S. (2013). Ultra-sensitive fluorescent proteins for imaging neuronal activity. *Nature*, *499*(7458), 295–300. PMC. https://doi.org/10.1038/nature12354

Chesler, E. J. (2014). Out of the bottleneck: The Diversity Outcross and Collaborative Cross mouse populations in behavioral genetics research. *Mammalian Genome*, *25*(1–2), 3–11. https://doi.org/10.1007/s00335-013-9492-9

Churchill, G. A., Gatti, D. M., Munger, S. C., & Svenson, K. L. (2012). The diversity outbred mouse population. *Mammalian Genome*, *23*(9), 713–718. https://doi.org/10.1007/s00335-012-9414-2

Cinnamon Bidwell, L., Dew, R. E., & Kollins, S. H. (2010). Alpha-2 adrenergic receptors and attention-deficit/hyperactivity disorder. In *Curr Psychiatry Rep* (Vol. 12, Issue 5, pp. 366–373). https://doi.org/10.1007/s11920-010-0136-4

Clark, K., Squire, R. F., Merrikhi, Y., & Noudoost, B. (2015). Visual attention: Linking prefrontal sources to neuronal and behavioral correlates. *Progress in Neurobiology*, *132*, 59–80. https://doi.org/10.1016/j.pneurobio.2015.06.006

Correns, C. (1900). G. Mendel's Regel über das Verhalten der Nachkommenschaft der Rassenbastarde. *Berichte Der Deutschen Botanischen Gesellschaft*, *18*(4), 158–168. https://doi.org/10.1111/j.1438-8677.1900.tb04893.x

Dana, H., Mohar, B., Sun, Y., Narayan, S., Gordus, A., Hasseman, J. P., Tsegaye, G., Holt, G. T., Hu, A., Walpita, D., Patel, R., Macklin, J. J., Bargmann, C. I., Ahrens, M. B., Schreiter, E. R., Jayaraman, V., Looger, L. L., Svoboda, K., & Kim, D. S. (2016). Sensitive red protein calcium indicators for imaging neural activity. In *Elife* (Vol. 5). https://doi.org/10.7554/eLife.12727

Datko, M. C., Hu, J.-H., Williams, M., Reyes, C. M., Lominac, K. D., von Jonquieres, G., Klugmann, M., Worley, P. F., & Szumlinski, K. K. (2017). Behavioral and Neurochemical Phenotyping of Mice Incapable of Homer1a Induction. In *Frontiers in Behavioral Neuroscience* (Vol. 11, p. 208). https://doi.org/10.3389/fnbeh.2017.00208

Dayan, P., Kakade, S., & Montague, P. R. (2000). Learning and selective attention. *Nature Neuroscience*, *3*(S11), 1218–1223. https://doi.org/10.1038/81504

de Bono, M., & Bargmann, C. I. (1998). Natural Variation in a Neuropeptide Y Receptor Homolog Modifies Social Behavior and Food Response in C. elegans. *Cell*, *94*(5), 679–689. https://doi.org/10.1016/S0092-8674(00)81609-8

de Lecea, L., Carter, M. E., & Adamantidis, A. (2012). Shining light on wakefulness and arousal. In *Biol Psychiatry* (Vol. 71, Issue 12, pp. 1046–1052). https://doi.org/10.1016/j.biopsych.2012.01.032

de Vries, H. (1900). Das Spaltungsgesetz der Bastarde. *Berichte Der Deutschen Botanischen Gesellschaft*, *18*(3), 83–90. https://doi.org/10.1111/j.1438-8677.1900.tb04884.x

Del Giudice, M., Buck, C. L., Chaby, L. E., Gormally, B. M., Taff, C. C., Thawley, C. J., Vitousek, M. N., & Wada, H. (2018). What Is Stress? A Systems Perspective. *Integrative and Comparative Biology*. https://doi.org/10.1093/icb/icy114

Dembrow, N., & Johnston, D. (2014). Subcircuit-specific neuromodulation in the prefrontal cortex. *Frontiers in Neural Circuits*, *8*. https://doi.org/10.3389/fncir.2014.00054

Deutsch, J. A., & Deutsch, D. (1963). Attention: Some theoretical considerations. *Psychological Review*, *70*(1), 80–90. https://doi.org/10.1037/h0039515

Diering, G. H., Nirujogi, R. S., Roth, R. H., Worley, P. F., Pandey, A., & Huganir, R. L. (2017). Homer1a drives homeostatic scaling-down of excitatory synapses during sleep. *Science*, *355*(6324), 511–515. https://doi.org/10.1126/science.aai8355

Doesburg, S. M., Green, J. J., McDonald, J. J., & Ward, L. M. (2012). Theta modulation of inter-regional gamma synchronization during auditory attention control. *Brain Research*, *1431*, 77–85. https://doi.org/10.1016/j.brainres.2011.11.005

Doesburg, S. M., Roggeveen, A. B., Kitajo, K., & Ward, L. M. (2008). Large-Scale Gamma-Band Phase Synchronization and Selective Attention. *Cerebral Cortex*, *18*(2), 386–396. https://doi.org/10.1093/cercor/bhm073

Dudai, Y., Jan, Y. N., Byers, D., Quinn, W. G., & Benzer, S. (1976). Dunce, a mutant of Drosophila deficient in learning. *Proceedings of the National Academy of Sciences*, *73*(5), 1684–1688. https://doi.org/10.1073/pnas.73.5.1684

Dunkley, B. T., Wong, S. M., Jetly, R., Wong, J. K., & Taylor, M. J. (2018). Post-traumatic stress disorder and chronic hyperconnectivity in emotional processing. *NeuroImage: Clinical*, *20*, 197–204. https://doi.org/10.1016/j.nicl.2018.07.007

Eldar, E., Cohen, J. D., & Niv, Y. (2013). The effects of neural gain on attention and learning. *Nature Neuroscience*, *16*(8), 1146–1153. https://doi.org/10.1038/nn.3428

Emery, P., So, W. V., Kaneko, M., Hall, J. C., & Rosbash, M. (1998). CRY, a Drosophila Clock and Light-Regulated Cryptochrome, Is a Major Contributor to Circadian Rhythm Resetting and Photosensitivity. *Cell*, *95*(5), 669–679. https://doi.org/10.1016/S0092-8674(00)81637-2

Esterman, M., & Rothlein, D. (2019). Models of sustained attention. *Current Opinion in Psychology*, *29*, 174–180. https://doi.org/10.1016/j.copsyc.2019.03.005

Fawcett, G. L., Jarvis, J. P., Roseman, C. C., Wang, B., Wolf, J. B., & Cheverud, J. M. (2010). Fine-mapping of Obesity-related Quantitative Trait Loci in an F $_{9/10}$ Advanced Intercross Line. *Obesity*, *18*(7), 1383–1392. https://doi.org/10.1038/oby.2009.411

Fiebelkorn, I. C., Pinsk, M. A., & Kastner, S. (2018). A Dynamic Interplay within the Frontoparietal Network Underlies Rhythmic Spatial Attention. *Neuron*, *99*(4), 842-853.e8. https://doi.org/10.1016/j.neuron.2018.07.038

Fiebelkorn, I. C., Saalmann, Y. B., & Kastner, S. (2013). Rhythmic Sampling within and between Objects despite Sustained Attention at a Cued Location. *Current Biology*, *23*(24), 2553–2558. https://doi.org/10.1016/j.cub.2013.10.063

Finak, G., McDavid, A., Yajima, M., Deng, J., Gersuk, V., Shalek, A. K., Slichter, C. K., Miller, H. W., McElrath, M. J., Prlic, M., Linsley, P. S., & Gottardo, R. (2015). MAST: a flexible statistical framework for assessing transcriptional changes and characterizing heterogeneity in single-cell RNA sequencing data. In *Genome Biology* (Vol. 16, Issue 1, p. 278). https://doi.org/10.1186/s13059-015-0844-5

Frazer, K. A., Pachter, L., Poliakov, A., Rubin, E. M., & Dubchak, I. (2004). VISTA: computational tools for comparative genomics. In *Nucleic Acids Res* (Vol. 32, Issue Web Server issue, pp. W273-9). https://doi.org/10.1093/nar/gkh458

Fritz, J. B., Elhilali, M., David, S. V., & Shamma, S. A. (2007). Auditory attention—Focusing the searchlight on sound. *Current Opinion in Neurobiology*, *17*(4), 437–455. https://doi.org/10.1016/j.conb.2007.07.011

Funato, H. (2020). Forward genetic approach for behavioral neuroscience using animal models. *Proceedings of the Japan Academy, Series B*, *96*(1), 10–31. https://doi.org/10.2183/pjab.96.002

Gailey, D. A., & Hall, J. C. (1989). Behavior and cytogenetics of fruitless in Drosophila melanogaster: Different courtship defects caused by separate, closely linked lesions. *Genetics*, *121*(4), 773–785. https://doi.org/10.1093/genetics/121.4.773

Gao, W. J., Krimer, L. S., & Goldman-Rakic, P. S. (2001). Presynaptic regulation of recurrent excitation by D1 receptors in prefrontal circuits. *Proceedings of the National Academy of Sciences of the United States of America*, *98*(1), 295–300. https://doi.org/10.1073/pnas.98.1.295

Gatti, D. M., Svenson, K. L., Shabalin, A., Wu, L.-Y., Valdar, W., Simecek, P., Goodwin, N., Cheng, R., Pomp, D., Palmer, A., Chesler, E. J., Broman, K. W., & Churchill, G. A. (2014). Quantitative Trait Locus Mapping Methods for Diversity Outbred

Mice. *G3: Genes|Genomes|Genetics*, *4*(9), 1623. https://doi.org/10.1534/g3.114.013748

Gazzaniga, M. S., Ivry, R. B., & Mangun, G. R. (2014). *Cognitive neuroscience: The biology of the mind* (Fourth edition). W. W. Norton & Company, Inc.

Geraghty, A. C., Gibson, E. M., Ghanem, R. A., Greene, J. J., Ocampo, A., Goldstein, A. K., Ni, L., Yang, T., Marton, R. M., Paşca, S. P., Greenberg, M. E., Longo, F. M., & Monje, M. (2019). Loss of Adaptive Myelination Contributes to Methotrexate Chemotherapy-Related Cognitive Impairment. *Neuron*, *103*(2), 250-265.e8. https://doi.org/10.1016/j.neuron.2019.04.032

Ghosh, R., Bloom, J. S., Mohammadi, A., Schumer, M. E., Andolfatto, P., Ryu, W., & Kruglyak, L. (2015). Genetics of Intraspecies Variation in Avoidance Behavior Induced by a Thermal Stimulus in *Caenorhabditis elegans*. *Genetics*, *200*(4), 1327–1339. https://doi.org/10.1534/genetics.115.178491

Gibson, E. M., Purger, D., Mount, C. W., Goldstein, A. K., Lin, G. L., Wood, L. S., Inema, I., Miller, S. E., Bieri, G., Zuchero, J. B., Barres, B. A., Woo, P. J., Vogel, H., & Monje, M. (2014). Neuronal activity promotes oligodendrogenesis and adaptive myelination in the mammalian brain. In *Science* (Vol. 344, Issue 6183, p. 1252304). https://doi.org/10.1126/science.1252304

Gill, K. S. (1963). A mutation causing abnormal courtship and mating behavior in males of Drosophila melanogaster. (Abstract). *American Zoologist*, *3*(4), 507.

Gioanni, Y., Rougeot, C., Clarke, P. B. S., Lepousé, C., Thierry, A. M., & Vidal, C. (1999). Nicotinic receptors in the ratan prefrontal cortex: Increase in glutamate release and facilitation of mediodorsal thalamo-cortical transmission. *European Journal of Neuroscience*, *11*(1), 18–30. https://doi.org/10.1046/j.1460-9568.1999.00403.x

Grazia Turri, M., DeFries, J. C., Henderson, N. D., & Flint, J. (2004). Multivariate analysis of quantitative trait loci influencing variation in anxiety-related behavior in laboratory mice. *Mammalian Genome*, *15*(2), 69–76. https://doi.org/10.1007/s00335-003-3032-y

Gregoriou, G. G., Gotts, S. J., Zhou, H., & Desimone, R. (2009). High-Frequency, Long-Range Coupling Between Prefrontal and Visual Cortex During Attention. *Science*, *324*(5931), 1207–1210. https://doi.org/10.1126/science.1171402

Gulledge, A. T., Bucci, D. J., Zhang, S. S., Matsui, M., & Yeh, H. H. (2009). M1 Receptors Mediate Cholinergic Modulation of Excitability in Neocortical Pyramidal Neurons. *The Journal of Neuroscience*, *29*(31), 9888–9902. https://doi.org/10.1523/JNEUROSCI.1366-09.2009

Hall, J. C. (1978). Courtship among males due to a male-sterile mutation inDrosophila melanogaster. *Behavior Genetics*, *8*(2), 125–141. https://doi.org/10.1007/BF01066870

Hasselmo, M. E., & Sarter, M. (2011). Modes and Models of Forebrain Cholinergic Neuromodulation of Cognition. *Neuropsychopharmacology*, *36*(1), 52–73. https://doi.org/10.1038/npp.2010.104

Hockley, A., & Malmierca, M. (2024). Auditory processing control by the medial prefrontal cortex: A review of the rodent functional organisation. *Hearing Research*, *443*, 108954. https://doi.org/10.1016/j.heares.2024.108954

Hopfinger, J. B., & Mangun, G. R. (1998). Reflexive Attention Modulates Processing of Visual Stimuli in Human Extrastriate Cortex. *Psychological Science*, *9*(6), 441–447. https://doi.org/10.1111/1467-9280.00083

Hopfinger, J. B., & Mangun, G. R. (2001). Tracking the influence of reflexive attention on sensory and cognitive processing. *Cognitive, Affective & Behavioral Neuroscience*, *1*(1), 56–65. https://doi.org/10.3758/cabn.1.1.56

Hsiao, K., Noble, C., Pitman, W., Yadav, N., Kumar, S., Keele, G. R., Terceros, A., Kanke, M., Conniff, T., Cheleuitte-Nieves, C., Tolwani, R., Sethupathy, P., & Rajasethupathy, P. (2020). A Thalamic Orphan Receptor Drives Variability in Short-Term Memory. *Cell*, *183*(2), 522-536.e19. https://doi.org/10.1016/j.cell.2020.09.011

Hu, J.-H., Park, J. M., Park, S., Xiao, B., Dehoff, M. H., Kim, S., Hayashi, T., Schwarz, M. K., Huganir, R. L., Seeburg, P. H., Linden, D. J., & Worley, P. F. (2010). Homeostatic Scaling Requires Group I mGluR Activation Mediated by Homer1a. *Neuron*, *68*(6), 1128–1142. https://doi.org/10.1016/j.neuron.2010.11.008

Hu, S., Xie, Z., Onishi, A., Yu, X., Jiang, L., Lin, J., Rho, H. S., Woodard, C., Wang, H., Jeong, J. S., Long, S., He, X., Wade, H., Blackshaw, S., Qian, J., & Zhu, H. (2009). Profiling the human protein-DNA interactome reveals ERK2 as a transcriptional repressor of

interferon signaling. In *Cell* (Vol. 139, Issue 3, pp. 610–622). https://doi.org/10.1016/j.cell.2009.08.037

Hunter, K. W., & Crawford, N. P. S. (2008). The Future of Mouse QTL Mapping to Diagnose Disease in Mice in the Age of Whole-Genome Association Studies. *Annual Review of Genetics*, *42*(1), 131–141. https://doi.org/10.1146/annurev.genet.42.110807.091659

International Chicken Genome Sequencing Consortium. (2004). Sequence and comparative analysis of the chicken genome provide unique perspectives on vertebrate evolution. *Nature*, *432*(7018), 695–716. https://doi.org/10.1038/nature03154

International Human Genome Sequencing Consortium, Whitehead Institute for Biomedical Research, Center for Genome Research:, Lander, E. S., Linton, L. M., Birren, B., Nusbaum, C., Zody, M. C., Baldwin, J., Devon, K., Dewar, K., Doyle, M., FitzHugh, W., Funke, R., Gage, D., Harris, K., Heaford, A., Howland, J., Kann, L., Lehoczky, J., … Morgan, M. J. (2001). Initial sequencing and analysis of the human genome. *Nature*, *409*(6822), 860–921. https://doi.org/10.1038/35057062

Ito, H., Fujitani, K., Usui, K., Shimizu-Nishikawa, K., Tanaka, S., & Yamamoto, D. (1996). Sexual orientation in Drosophila is altered by the satori mutation in the sex-determination gene fruitless that encodes a zinc finger protein with a BTB domain. *Proceedings of the National Academy of Sciences*, *93*(18), 9687–9692. https://doi.org/10.1073/pnas.93.18.9687

Jacob, S. N., Ott, T., & Nieder, A. (2013). Dopamine Regulates Two Classes of Primate Prefrontal Neurons That Represent Sensory Signals. *The Journal of Neuroscience*, *33*(34), 13724–13734. https://doi.org/10.1523/JNEUROSCI.0210-13.2013

James, W. (1890). *The principles of psychology, Vol I.* Henry Holt and Co. https://doi.org/10.1037/10538-000

Jaubert, P. J., Golub, M. S., Lo, Y. Y., Germann, S. L., Dehoff, M. H., Worley, P. F., Kang, S. H., Schwarz, M. K., Seeburg, P. H., & Berman, R. F. (2006). Complex, multimodal behavioral profile of the Homer1 knockout mouse. In *Genes, Brain and Behavior* (Vol. 6, Issue 2, pp. 141–154). https://doi.org/10.1111/j.1601-183X.2006.00240.x

Jensen, O., & Colgin, L. L. (2007). Cross-frequency coupling between neuronal oscillations. *Trends in Cognitive Sciences*, *11*(7), 267–269. https://doi.org/10.1016/j.tics.2007.05.003

Jin, J., Cheng, J., Lee, K.-W., Amreen, B., McCabe, K. A., Pitcher, C., Liebmann, T., Greengard, P., & Flajolet, M. (2019). Cholinergic Neurons of the Medial Septum Are Crucial for Sensorimotor Gating. In *The Journal of Neuroscience* (Vol. 39, Issue 26, p. 5234). https://doi.org/10.1523/JNEUROSCI.0950-18.2019

Johannsen, W. (1909). *Elemente der exakten erblichkeitslehre. Deutsche wesentlich erweiterte ausgabe in fünfundzwanzig vorlesungen [Elements of an Exact Theory of Heredity.]*. G. Fischer. https://doi.org/10.5962/bhl.title.1060

Johnson, C. D., Duckett, J. G., Culotti, J. G., Herman, R. K., Meneely, P. M., & Russell, R. L. (1981). An Acetylcholinesterase-Deficient Mutant Of The Nematode *Caenorhabditis elegans*. *Genetics*, *97*(2), 261–279. https://doi.org/10.1093/genetics/97.2.261

Johnson, C. D., Rand, J. B., Herman, R. K., Stern, B. D., & Russell, R. L. (1988). The acetylcholinesterase genes of *C. elegans*: Identification of a third gene (ace-3) and mosaic mapping of a synthetic lethal phenotype. *Neuron*, *1*(2), 165–173. https://doi.org/10.1016/0896-6273(88)90201-2

Johnston, W. A., & Heinz, S. P. (1978). Flexibility and capacity demands of attention. *Journal of Experimental Psychology: General*, *107*(4), 420–435. https://doi.org/10.1037/0096-3445.107.4.420

Jones, L., Hills, P., Dick, K., Jones, S., & Bright, P. (2016). Cognitive mechanisms associated with auditory sensory gating. *Brain and Cognition*, *102*, 33–45. PMC. https://doi.org/10.1016/j.bandc.2015.12.005

Joober, R. (2002). Provisional Mapping of Quantitative Trait Loci Modulating the Acoustic Startle Response and Prepulse Inhibition of Acoustic Startle. *Neuropsychopharmacology*, *27*(5), 765–781. https://doi.org/10.1016/S0893-133X(02)00333-0

Judd, L. L., McAdams, L., Budnick, B., & Braff, D. L. (1992). Sensory gating deficits in schizophrenia: New results. *The American Journal of Psychiatry*, *149*(4), 488–493. https://doi.org/10.1176/ajp.149.4.488

Kabanova, A., Pabst, M., Lorkowski, M., Braganza, O., Boehlen, A., Nikbakht, N., Pothmann, L., Vaswani, A. R., Musgrove, R., Di Monte, D. A., Sauvage, M., Beck, H., & Blaess, S. (2015). Function and developmental origin of a mesocortical inhibitory circuit. *Nature Neuroscience*, *18*(6), 872–882. https://doi.org/10.1038/nn.4020

Kahneman, D. (1973). *Attention and effort*. Prentice-Hall.

Kandel, E. R., Koester, J., Mack, S., & Siegelbaum, S. (Eds.). (2021). Chapter 18: The Organization of Cognition. In *Principles of neural science* (Sixth edition). McGraw Hill.

Kang, H. M., Sul, J. H., Service, S. K., Zaitlen, N. A., Kong, S. Y., Freimer, N. B., Sabatti, C., & Eskin, E. (2010). Variance component model to account for sample structure in genome-wide association studies. In *Nat Genet* (Vol. 42, Issue 4, pp. 348–354). https://doi.org/10.1038/ng.548

Kato, A., Ozawa, F., Saitoh, Y., Hirai, K., & Inokuchi, K. (1997). Vesl, a gene encoding VASP/Ena family related protein, is upregulated during seizure, long-term potentiation and synaptogenesis. In *FEBS Lett* (Vol. 412, Issue 1, pp. 183–189). https://doi.org/10.1016/s0014-5793(97)00775-8

Kim, C. K., Yang, S. J., Pichamoorthy, N., Young, N. P., Kauvar, I., Jennings, J. H., Lerner, T. N., Berndt, A., Lee, S. Y., Ramakrishnan, C., Davidson, T. J., Inoue, M., Bito, H., & Deisseroth, K. (2016). Simultaneous fast measurement of circuit dynamics at multiple sites across the mammalian brain. *Nature Methods*, *13*, 325.

Kim, Y., Noh, Y. W., Kim, K., & Kim, E. (2021). Hyperactive ACC-MDT Pathway Suppresses Prepulse Inhibition in Mice. *Schizophrenia Bulletin*, *47*(1), 31–43. https://doi.org/10.1093/schbul/sbaa090

King, D. P., Zhao, Y., Sangoram, A. M., Wilsbacher, L. D., Tanaka, M., Antoch, M. P., Steeves, T. D. L., Vitaterna, M. H., Kornhauser, J. M., Lowrey, P. L., Turek, F. W., & Takahashi, J. S. (1997). Positional Cloning of the Mouse Circadian Gene. *Cell*, *89*(4), 641–653. https://doi.org/10.1016/S0092-8674(00)80245-7

Koch, M., & Schnitzler, H. U. (1997). The acoustic startle response in rats–circuits mediating evocation, inhibition and potentiation. In *Behav Brain Res* (Vol. 89, Issues 1–2, pp. 35–49). https://doi.org/10.1016/s0166-4328(97)02296-1

Konopka, R. J., & Benzer, S. (1971). Clock mutants of Drosophila melanogaster. *Proceedings of the National Academy of Sciences of the United States of America*, *68*(9), 2112–2116. https://doi.org/10.1073/pnas.68.9.2112

Kubicki, M., McCarley, R. W., & Shenton, M. E. (2005). Evidence for white matter abnormalities in schizophrenia: *Current Opinion in*

Psychiatry, *18*(2), 121–134. https://doi.org/10.1097/00001504-200503000-00004

Kuleshov, M. V., Jones, M. R., Rouillard, A. D., Fernandez, N. F., Duan, Q., Wang, Z., Koplev, S., Jenkins, S. L., Jagodnik, K. M., Lachmann, A., McDermott, M. G., Monteiro, C. D., Gundersen, G. W., & Ma'ayan, A. (2016). Enrichr: A comprehensive gene set enrichment analysis web server 2016 update. In *Nucleic Acids Res* (Vol. 44, Issue W1, pp. W90-7). https://doi.org/10.1093/nar/gkw377

Lambe, E. K., Picciotto, M. R., & Aghajanian, G. K. (2003). Nicotine Induces Glutamate Release from Thalamocortical Terminals in Prefrontal Cortex. *Neuropsychopharmacology*, *28*(2), 216–225. https://doi.org/10.1038/sj.npp.1300032

Larson, V. A., Mironova, Y., Vanderpool, K. G., Waisman, A., Rash, J. E., Agarwal, A., & Bergles, D. E. (2018). Oligodendrocytes control potassium accumulation in white matter and seizure susceptibility. *eLife*, *7*, e34829. https://doi.org/10.7554/eLife.34829

Laughlin, R. E., Grant, T. L., Williams, R. W., & Jentsch, J. D. (2011). Genetic Dissection of Behavioral Flexibility: Reversal Learning in Mice. *Biological Psychiatry*, *69*(11), 1109–1116. https://doi.org/10.1016/j.biopsych.2011.01.014

Li, L., Du, Y., Li, N., Wu, X., & Wu, Y. (2009). Top–down modulation of prepulse inhibition of the startle reflex in humans and rats. *Special Section: Neuroscience and Biobehavioral Research: A Chinese Perspective*, *33*(8), 1157–1167. https://doi.org/10.1016/j.neubiorev.2009.02.001

Li, Q., Zhao, Y., Huang, Z., Guo, Y., Long, J., Luo, L., You, W., Sweeney, J. A., Li, F., & Gong, Q. (2021). Microstructural white matter abnormalities in pediatric and adult obsessive-compulsive disorder: A systematic review and meta-analysis. *Brain and Behavior*, *11*(2), e01975. https://doi.org/10.1002/brb3.1975

Li, S., Wang, C., Wang, W., Dong, H., Hou, P., & Tang, Y. (2008). Chronic mild stress impairs cognition in mice: From brain homeostasis to behavior. *Life Sciences*, *82*(17–18), 934–942. https://doi.org/10.1016/j.lfs.2008.02.010

Lia, A., Henriques, V. J., Zonta, M., Chiavegato, A., Carmignoto, G., Gómez-Gonzalo, M., & Losi, G. (2021). Calcium Signals in Astrocyte Microdomains, a Decade of Great Advances. *Frontiers in*

Cellular Neuroscience, *15*, 673433. https://doi.org/10.3389/fncel.2021.673433

Lilue, J., Doran, A. G., Fiddes, I. T., Abrudan, M., Armstrong, J., Bennett, R., Chow, W., Collins, J., Collins, S., Czechanski, A., Danecek, P., Diekhans, M., Dolle, D.-D., Dunn, M., Durbin, R., Earl, D., Ferguson-Smith, A., Flicek, P., Flint, J., … Keane, T. M. (2018). Sixteen diverse laboratory mouse reference genomes define strain-specific haplotypes and novel functional loci. *Nature Genetics*, *50*(11), 1574–1583. https://doi.org/10.1038/s41588-018-0223-8

Lister, R. G. (1987). The use of a plus-maze to measure anxiety in the mouse. In *Psychopharmacology (Berl)* (Vol. 92, Issue 2, pp. 180–185). https://doi.org/10.1007/BF00177912

Liston, C., Miller, M. M., Goldwater, D. S., Radley, J. J., Rocher, A. B., Hof, P. R., Morrison, J. H., & McEwen, B. S. (2006). Stress-Induced Alterations in Prefrontal Cortical Dendritic Morphology Predict Selective Impairments in Perceptual Attentional Set-Shifting. *The Journal of Neuroscience*, *26*(30), 7870–7874. https://doi.org/10.1523/JNEUROSCI.1184-06.2006

Liu, W.-Z., Zhang, W.-H., Zheng, Z.-H., Zou, J.-X., Liu, X.-X., Huang, S.-H., You, W.-J., He, Y., Zhang, J.-Y., Wang, X.-D., & Pan, B.-X. (2020). Identification of a prefrontal cortex-to-amygdala pathway for chronic stress-induced anxiety. *Nature Communications*, *11*(1), 2221. https://doi.org/10.1038/s41467-020-15920-7

Logan, R. W., Robledo, R. F., Recla, J. M., Philip, V. M., Bubier, J. A., Jay, J. J., Harwood, C., Wilcox, T., Gatti, D. M., Bult, C. J., Churchill, G. A., & Chesler, E. J. (2013). High-precision genetic mapping of behavioral traits in the diversity outbred mouse population. *Genes, Brain and Behavior*, *12*(4), 424–437. https://doi.org/10.1111/gbb.12029

Lominac, K. D., Oleson, E. B., Pava, M., Klugmann, M., Schwarz, M. K., Seeburg, P. H., During, M. J., Worley, P. F., Kalivas, P. W., & Szumlinski, K. K. (2005). Distinct Roles for Different Homer1 Isoforms in Behaviors and Associated Prefrontal Cortex Function. In *The Journal of Neuroscience* (Vol. 25, Issue 50, p. 11586). https://doi.org/10.1523/JNEUROSCI.3764-05.2005

Lovett-Barron, M., Andalman, A. S., Allen, W. E., Vesuna, S., Kauvar, I., Burns, V. M., & Deisseroth, K. (2017). Ancestral Circuits for the Coordinated Modulation of Brain State. In *Cell* (Vol. 171, Issue 6, pp. 1411-1423 e17). https://doi.org/10.1016/j.cell.2017.10.021

Maret, S., Dorsaz, S., Gurcel, L., Pradervand, S., Petit, B., Pfister, C., Hagenbuchle, O., O'Hara, B. F., Franken, P., & Tafti, M. (2007). Homer1a is a core brain molecular correlate of sleep loss. *Proceedings of the National Academy of Sciences of the United States of America*, *104*(50), 20090–20095. https://doi.org/10.1073/pnas.0710131104

McCall, J. G., Siuda, E. R., Bhatti, D. L., Lawson, L. A., McElligott, Z. A., Stuber, G. D., & Bruchas, M. R. (2017). Locus coeruleus to basolateral amygdala noradrenergic projections promote anxiety-like behavior. *eLife*, *6*, e18247. https://doi.org/10.7554/eLife.18247

McGrath, P. T., Rockman, M. V., Zimmer, M., Jang, H., Macosko, E. Z., Kruglyak, L., & Bargmann, C. I. (2009). Quantitative mapping of a digenic behavioral trait implicates globin variation in C. elegans sensory behaviors. *Neuron*, *61*(5), 692–699. https://doi.org/10.1016/j.neuron.2009.02.012

Mease, R. A., Krieger, P., & Groh, A. (2014). Cortical control of adaptation and sensory relay mode in the thalamus. *Proceedings of the National Academy of Sciences*, *111*(18), 6798. https://doi.org/10.1073/pnas.1318665111

Mendel, G. (1866). *Versuche über Pflanzen-Hybriden*. Im Verlage des Vereines,. https://doi.org/10.5962/bhl.title.61004

Micoulaud-Franchi, J.-A., Vaillant, F., Lopez, R., Peri, P., Baillif, A., Brandejsky, L., Steffen, M. L., Boyer, L., Richieri, R., Cermolacce, M., Bioulac, S., Aramaki, M., Philip, P., Lancon, C., & Vion-Dury, J. (2015). Sensory gating in adult with attention-deficit/hyperactivity disorder: Event-evoked potential and perceptual experience reports comparisons with schizophrenia. *Biological Psychology*, *107*, 16–23. https://doi.org/10.1016/j.biopsycho.2015.03.002

Moray, N. (1959). Attention in Dichotic Listening: Affective Cues and the Influence of Instructions. *Quarterly Journal of Experimental Psychology*, *11*(1), 56–60. https://doi.org/10.1080/17470215908416289

Morgan, T. H. (1910). Sex Limited Inheritance in *Drosophila*. *Science*, *32*(812), 120–122. https://doi.org/10.1126/science.32.812.120

Morgan, T. H. (1911a). Random Segregation Versus Coupling in Mendelian Inheritance. *Science*, *34*(873), 384–384. https://doi.org/10.1126/science.34.873.384

Morgan, T. H. (1911b). The Origin of Five Mutations in Eye Color in *Drosophila* and Their Modes of Inheritance. *Science*, *33*(849), 534–537. https://doi.org/10.1126/science.33.849.534.b

Mott, R., Talbot, C. J., Turri, M. G., Collins, A. C., & Flint, J. (2000). A method for fine mapping quantitative trait loci in outbred animal stocks. *Proceedings of the National Academy of Sciences*, *97*(23), 12649–12654. https://doi.org/10.1073/pnas.230304397

Mouse Genome Sequencing Consortium. (2002). Initial sequencing and comparative analysis of the mouse genome. *Nature*, *420*(6915), 520–562. https://doi.org/10.1038/nature01262

Mukherjee, A., Lam, N. H., Wimmer, R. D., & Halassa, M. M. (2021). Thalamic circuits for independent control of prefrontal signal and noise. *Nature*, *600*(7887), 100–104. https://doi.org/10.1038/s41586-021-04056-3

Muzzio, I. A., Levita, L., Kulkarni, J., Monaco, J., Kentros, C., Stead, M., Abbott, L. F., & Kandel, E. R. (2009). Attention Enhances the Retrieval and Stability of Visuospatial and Olfactory Representations in the Dorsal Hippocampus. *PLoS Biology*, *7*(6), e1000140. https://doi.org/10.1371/journal.pbio.1000140

Myers, M. P., Wager-Smith, K., Wesley, C. S., Young, M. W., & Sehgal, A. (1995). Positional Cloning and Sequence Analysis of the *Drosophila* Clock Gene, *timeless*. *Science*, *270*(5237), 805–808. https://doi.org/10.1126/science.270.5237.805

Nagai, J., Rajbhandari, A. K., Gangwani, M. R., Hachisuka, A., Coppola, G., Masmanidis, S. C., Fanselow, M. S., & Khakh, B. S. (2019). Hyperactivity with Disrupted Attention by Activation of an Astrocyte Synaptogenic Cue. *Cell*, *177*(5), 1280-1292.e20. https://doi.org/10.1016/j.cell.2019.03.019

Neylan, T. C., Fletcher, D. J., Lenoci, M., McCallin, K., Weiss, D. S., Schoenfeld, F. B., Marmar, C. R., & Fein, G. (1999). Sensory gating in chronic posttraumatic stress disorder: Reduced auditory p50 suppression in combat veterans. *Biological Psychiatry*, *46*(12), 1656–1664. https://doi.org/10.1016/S0006-3223(99)00047-5

Ott, T., & Nieder, A. (2019). Dopamine and Cognitive Control in Prefrontal Cortex. *Trends in Cognitive Sciences*, *23*(3), 213–234. https://doi.org/10.1016/j.tics.2018.12.006

Paolicelli, R. C., Bolasco, G., Pagani, F., Maggi, L., Scianni, M., Panzanelli, P., Giustetto, M., Ferreira, T. A., Guiducci, E., Dumas,

L., Ragozzino, D., & Gross, C. T. (2011). Synaptic Pruning by Microglia Is Necessary for Normal Brain Development. *Science*, *333*(6048), 1456–1458. https://doi.org/10.1126/science.1202529

Papaioannou, V. E., & Behringer, R. R. (2024). Backcrossing to Generate a Congenic Mouse Strain. *Cold Spring Harbor Protocols*, *2024*(1), pdb.prot108039. https://doi.org/10.1101/pdb.prot108039

Parkhurst, C. N., Yang, G., Ninan, I., Savas, J. N., Yates, J. R., Lafaille, J. J., Hempstead, B. L., Littman, D. R., & Gan, W.-B. (2013). Microglia Promote Learning-Dependent Synapse Formation through Brain-Derived Neurotrophic Factor. *Cell*, *155*(7), 1596–1609. https://doi.org/10.1016/j.cell.2013.11.030

Parlatini, V., Itahashi, T., Lee, Y., Liu, S., Nguyen, T. T., Aoki, Y. Y., Forkel, S. J., Catani, M., Rubia, K., Zhou, J. H., Murphy, D. G., & Cortese, S. (2023). White matter alterations in Attention-Deficit/Hyperactivity Disorder (ADHD): A systematic review of 129 diffusion imaging studies with meta-analysis. *Molecular Psychiatry*, *28*(10), 4098–4123. https://doi.org/10.1038/s41380-023-02173-1

Pashler, H., Johnston, J. C., & Ruthruff, E. (2001). Attention and Performance. *Annual Review of Psychology*, *52*(1), 629–651. https://doi.org/10.1146/annurev.psych.52.1.629

Paterson, A. H., Lander, E. S., Hewitt, J. D., Peterson, S., Lincoln, S. E., & Tanksley, S. D. (1988). Resolution of quantitative traits into Mendelian factors by using a complete linkage map of restriction fragment length polymorphisms. *Nature*, *335*(6192), 721–726. https://doi.org/10.1038/335721a0

Perea, G., Navarrete, M., & Araque, A. (2009). Tripartite synapses: Astrocytes process and control synaptic information. *Trends in Neurosciences*, *32*(8), 421–431. https://doi.org/10.1016/j.tins.2009.05.001

Perry, W., Minassian, A., Feifel, D., & Braff, D. L. (2001). Sensorimotor gating deficits in bipolar disorder patients with acute psychotic mania. *Biological Psychiatry*, *50*(6), 418–424. https://doi.org/10.1016/S0006-3223(01)01184-2

Perry, W., Minassian, A., Lopez, B., Maron, L., & Lincoln, A. (2007). Sensorimotor Gating Deficits in Adults with Autism. *Biological Psychiatry*, *61*(4), 482–486. https://doi.org/10.1016/j.biopsych.2005.09.025

Peters, R. W. (1954). *Competing Messages: The Effect of Interfering Messages Upon the Reception of Primary Messages*. Defense Technical Information Center. https://books.google.com/books?id=ulkZOAAACAAJ

Petralia, R. S., Wang, Y. X., Sans, N., Worley, P. F., Hammer, 3rd, J. A., & Wenthold, R. J. (2001). Glutamate receptor targeting in the postsynaptic spine involves mechanisms that are independent of myosin Va. In *Eur J Neurosci* (Vol. 13, Issue 9, pp. 1722–1732). https://doi.org/10.1046/j.0953-816x.2001.01553.x

Petryshen, T. L., Kirby, A., Hammer, R. P., Purcell, S., O'Leary, S. B., Singer, J. B., Hill, A. E., Nadeau, J. H., Daly, M. J., & Sklar, P. (2005). Two Quantitative Trait Loci for Prepulse Inhibition of Startle Identified on Mouse Chromosome 16 Using Chromosome Substitution Strains. *Genetics*, *171*(4), 1895–1904. https://doi.org/10.1534/genetics.105.045658

Posner, M., & Cohen, Y. (1984). Components of Visual Orienting. In *Control of language processes: Proceedings of the 10th International Symposium on Attention and Performance, Venlo, Netherlands* (pp. 531–556). L. Erlbaum.

Posner, M. I. (1980). Orienting of Attention. *Quarterly Journal of Experimental Psychology*, *32*(1), 3–25. https://doi.org/10.1080/00335558008248231

Posner, M. I., Snyder, C. R., & Davidson, B. J. (1980). Attention and the detection of signals. *Journal of Experimental Psychology*, *109*(2), 160–174.

Powell, S. K., Khan, N., Parker, C. L., Samulski, R. J., Matsushima, G., Gray, S. J., & McCown, T. J. (2016). Characterization of a novel adeno-associated viral vector with preferential oligodendrocyte tropism. In *Gene Ther* (Vol. 23, Issue 11, pp. 807–814). https://doi.org/10.1038/gt.2016.62

Quinn, W. G., Harris, W. A., & Benzer, S. (1974). Conditioned Behavior in *Drosophila melanogaster*. *Proceedings of the National Academy of Sciences*, *71*(3), 708–712. https://doi.org/10.1073/pnas.71.3.708

Quinn, W. G., Sziber, P. P., & Booker, R. (1979). The Drosophila memory mutant amnesiac. *Nature*, *277*(5693), 212–214. https://doi.org/10.1038/277212a0

Radulescu, C. I., Doostdar, N., Zabouri, N., Melgosa-Ecenarro, L., Wang, X., Sadeh, S., Pavlidi, P., Airey, J., Kopanitsa, M., Clopath, C., &

Barnes, S. J. (2023). Age-related dysregulation of homeostatic control in neuronal microcircuits. *Nature Neuroscience*, *26*(12), 2158–2170. https://doi.org/10.1038/s41593-023-01451-z

Recla, J. M., Robledo, R. F., Gatti, D. M., Bult, C. J., Churchill, G. A., & Chesler, E. J. (2014). Precise genetic mapping and integrative bioinformatics in Diversity Outbred mice reveals Hydin as a novel pain gene. *Mammalian Genome*, *25*(5–6), 211–222. https://doi.org/10.1007/s00335-014-9508-0

Reddy, P., Zehring, W. A., Wheeler, D. A., Pirrotta, V., Hadfield, C., Hall, J. C., & Rosbash, M. (1984). Molecular analysis of the period locus in Drosophila melanogaster and identification of a transcript involved in biological rhythms. *Cell*, *38*(3), 701–710. https://doi.org/10.1016/0092-8674(84)90265-4

Rikhye, R. V., Gilra, A., & Halassa, M. M. (2018). Thalamic regulation of switching between cortical representations enables cognitive flexibility. *Nature Neuroscience*, *21*(12), 1753–1763. https://doi.org/10.1038/s41593-018-0269-z

Rogers, J. T., Morganti, J. M., Bachstetter, A. D., Hudson, C. E., Peters, M. M., Grimmig, B. A., Weeber, E. J., Bickford, P. C., & Gemma, C. (2011). CX3CR1 Deficiency Leads to Impairment of Hippocampal Cognitive Function and Synaptic Plasticity. *The Journal of Neuroscience*, *31*(45), 16241–16250. https://doi.org/10.1523/JNEUROSCI.3667-11.2011

Rohleder, C., Wiedermann, D., Neumaier, B., Drzezga, A., Timmermann, L., Graf, R., Leweke, F. M., & Endepols, H. (2016). The Functional Networks of Prepulse Inhibition: Neuronal Connectivity Analysis Based on FDG-PET in Awake and Unrestrained Rats. *Frontiers in Behavioral Neuroscience*, *10*. https://doi.org/10.3389/fnbeh.2016.00148

Rutila, J. E., Suri, V., Le, M., So, W. V., Rosbash, M., & Hall, J. C. (1998). CYCLE Is a Second bHLH-PAS Clock Protein Essential for Circadian Rhythmicity and Transcription of Drosophila period and timeless. *Cell*, *93*(5), 805–814. https://doi.org/10.1016/S0092-8674(00)81441-5

Ryner, L. C., Goodwin, S. F., Castrillon, D. H., Anand, A., Villella, A., Baker, B. S., Hall, J. C., Taylor, B. J., & Wasserman, S. A. (1996). Control of Male Sexual Behavior and Sexual Orientation in Drosophila by the fruitless Gene. *Cell*, *87*(6), 1079–1089. https://doi.org/10.1016/S0092-8674(00)81802-4

Saalmann, Y. B., Pigarev, I. N., & Vidyasagar, T. R. (2007). Neural Mechanisms of Visual Attention: How Top-Down Feedback Highlights Relevant Locations. *Science*, *316*(5831), 1612–1615. https://doi.org/10.1126/science.1139140

Samocha, K. E., Lim, J. E., Cheng, R., Sokoloff, G., & Palmer, A. A. (2010). Fine mapping of QTL for prepulse inhibition in LG/J and SM/J mice using F_2 and advanced intercross lines. *Genes, Brain and Behavior*, *9*(7), 759–767. https://doi.org/10.1111/j.1601-183X.2010.00613.x

Santana, N., & Artigas, F. (2017). Laminar and Cellular Distribution of Monoamine Receptors in Rat Medial Prefrontal Cortex. *Frontiers in Neuroanatomy*, *11*, 87. https://doi.org/10.3389/fnana.2017.00087

Sapountzis, P. (2018). Neural signatures of attention insights from decoding population activity patterns. *Frontiers in Bioscience*, *23*(1), 221–246. https://doi.org/10.2741/4588

Sarter, M., Givens, B., & Bruno, J. P. (2001). The cognitive neuroscience of sustained attention: Where top-down meets bottom-up. *Brain Research Reviews*, *35*(2), 146–160. https://doi.org/10.1016/S0165-0173(01)00044-3

Saul, M. C., Philip, V. M., Reinholdt, L. G., & Chesler, E. J. (2019). High-Diversity Mouse Populations for Complex Traits. *Trends in Genetics*, *35*(7), 501–514. https://doi.org/10.1016/j.tig.2019.04.003

Schafer, D. P., Lehrman, E. K., Kautzman, A. G., Koyama, R., Mardinly, A. R., Yamasaki, R., Ransohoff, R. M., Greenberg, M. E., Barres, B. A., & Stevens, B. (2012). Microglia Sculpt Postnatal Neural Circuits in an Activity and Complement-Dependent Manner. *Neuron*, *74*(4), 691–705. https://doi.org/10.1016/j.neuron.2012.03.026

Schmitt, L. I., Wimmer, R. D., Nakajima, M., Happ, M., Mofakham, S., & Halassa, M. M. (2017). Thalamic amplification of cortical connectivity sustains attentional control. *Nature*, *545*(7653), 219–223. https://doi.org/10.1038/nature22073

Schneider, W., Dumais, S. T., & Shiffrin, R. M. (1982). Automatic/Control Processing and Attention. *Human Attention Research Laboratory, Psychology Department, University of ….*

Scholes, K. E., & Martin-Iverson, M. T. (2009). Relationships between prepulse inhibition and cognition are mediated by attentional

processes. In *Behav Brain Res* (Vol. 205, Issue 2, pp. 456–467). https://doi.org/10.1016/j.bbr.2009.07.031

Scholes, K. E., & Martin-Iverson, M. T. (2010). Disturbed prepulse inhibition in patients with schizophrenia is consequential to dysfunction of selective attention. In *Psychophysiology* (Vol. 47, Issue 2, pp. 223–235). https://doi.org/10.1111/j.1469-8986.2009.00927.x

Sehgal, A., Price, J. L., Man, B., & Young, M. W. (1994). Loss of Circadian Behavioral Rhythms and *per* RNA Oscillations in the *Drosophila* Mutant *timeless*. *Science*, *263*(5153), 1603–1606. https://doi.org/10.1126/science.8128246

Shiraishi-Yamaguchi, Y., & Furuichi, T. (2007). The Homer family proteins. In *Genome Biology* (Vol. 8, Issue 2, p. 206). https://doi.org/10.1186/gb-2007-8-2-206

Shirley, R. L., Walter, N. A. R., Reilly, M. T., Fehr, C., & Buck, K. J. (2004). Mpdz is a quantitative trait gene for drug withdrawal seizures. *Nature Neuroscience*, *7*(7), 699–700. https://doi.org/10.1038/nn1271

Shorter, J., Couch, C., Huang, W., Carbone, M. A., Peiffer, J., Anholt, R. R. H., & Mackay, T. F. C. (2015). Genetic architecture of natural variation in *Drosophila melanogaster* aggressive behavior. *Proceedings of the National Academy of Sciences*, *112*(27). https://doi.org/10.1073/pnas.1510104112

Sjöstedt, E., Zhong, W., Fagerberg, L., Karlsson, M., Mitsios, N., Adori, C., Oksvold, P., Edfors, F., Limiszewska, A., Hikmet, F., Huang, J., Du, Y., Lin, L., Dong, Z., Yang, L., Liu, X., Jiang, H., Xu, X., Wang, J., … Mulder, J. (2020). An atlas of the protein-coding genes in the human, pig, and mouse brain. *Science*, *367*(6482), eaay5947. https://doi.org/10.1126/science.aay5947

Slatkin, M. (2008). Linkage disequilibrium—Understanding the evolutionary past and mapping the medical future. *Nature Reviews Genetics*, *9*(6), 477–485. https://doi.org/10.1038/nrg2361

Smallwood, T. L., Gatti, D. M., Quizon, P., Weinstock, G. M., Jung, K.-C., Zhao, L., Hua, K., Pomp, D., & Bennett, B. J. (2014). High-Resolution Genetic Mapping in the Diversity Outbred Mouse Population Identifies *Apobec1* as a Candidate Gene for Atherosclerosis. *G3 Genes|Genomes|Genetics*, *4*(12), 2353–2363. https://doi.org/10.1534/g3.114.014704

Sokolov, A., Pavlova, M., Lutzenberger, W., & Birbaumer, N. (2004). Reciprocal modulation of neuromagnetic induced gamma activity by attention in the human visual and auditory cortex. *NeuroImage*, *22*(2), 521–529. https://doi.org/10.1016/j.neuroimage.2004.01.045

Solberg Woods, L. C. (2013). QTL mapping in outbred populations: Successes and challenges. *Physiological Genomics*, *46*(3), 81–90. https://doi.org/10.1152/physiolgenomics.00127.2013

Solberg Woods, L. C. (2014). QTL mapping in outbred populations: Successes and challenges. *Physiological Genomics*, *46*(3), 81–90. https://doi.org/10.1152/physiolgenomics.00127.2013

Soltani, A., Noudoost, B., & Moore, T. (2013). Dissociable dopaminergic control of saccadic target selection and its implications for reward modulation. *Proceedings of the National Academy of Sciences*, *110*(9), 3579–3584. https://doi.org/10.1073/pnas.1221236110

Stanewsky, R., Kaneko, M., Emery, P., Beretta, B., Wager-Smith, K., Kay, S. A., Rosbash, M., & Hall, J. C. (1998). The cryb Mutation Identifies Cryptochrome as a Circadian Photoreceptor in Drosophila. *Cell*, *95*(5), 681–692. https://doi.org/10.1016/S0092-8674(00)81638-4

Steinberger, D., Reynolds, D. S., Ferris, P., Lincoln, R., Datta, S., Stanley, J., Paterson, A., Dawson, G. R., & Flint, J. (2003). Genetic Mapping of Variation in Spatial Learning in the Mouse. *The Journal of Neuroscience*, *23*(6), 2426–2433. https://doi.org/10.1523/JNEUROSCI.23-06-02426.2003

Stobart, J. L., Ferrari, K. D., Barrett, M. J. P., Glück, C., Stobart, M. J., Zuend, M., & Weber, B. (2018). Cortical Circuit Activity Evokes Rapid Astrocyte Calcium Signals on a Similar Timescale to Neurons. *Neuron*, *98*(4), 726-735.e4. https://doi.org/10.1016/j.neuron.2018.03.050

Stobart, J. L., Ferrari, K. D., Barrett, M. J. P., Stobart, M. J., Looser, Z. J., Saab, A. S., & Weber, B. (2018). Long-term In Vivo Calcium Imaging of Astrocytes Reveals Distinct Cellular Compartment Responses to Sensory Stimulation. *Cerebral Cortex*, *28*(1), 184–198. https://doi.org/10.1093/cercor/bhw366

Sturtevant, A. H. (1913). The linear arrangement of six sex-linked factors in Drosophila, as shown by their mode of association. *Journal of Experimental Zoology*, *14*(1), 43–59. https://doi.org/10.1002/jez.1400140104

Suzuki, T., Hattori, S., Mizukami, H., Nakajima, R., Hibi, Y., Kato, S., Matsuzaki, M., Ikebe, R., Miyakawa, T., & Yamakawa, K. (2024). Inversed Effects of Nav1.2 Deficiency at Medial Prefrontal Cortex and Ventral Tegmental Area for Prepulse Inhibition in Acoustic Startle Response. *Molecular Neurobiology*, *61*(2), 622–634. https://doi.org/10.1007/s12035-023-03610-6

Svenson, K. L., Gatti, D. M., Valdar, W., Welsh, C. E., Cheng, R., Chesler, E. J., Palmer, A. A., McMillan, L., & Churchill, G. A. (2012). High-Resolution Genetic Mapping Using the Mouse Diversity Outbred Population. *Genetics*, *190*(2), 437–447. https://doi.org/10.1534/genetics.111.132597

Swerdlow, N. R., Benbow, C. H., Zisook, S., Geyer, M. A., & Braff, D. L. (1993). A preliminary assessment of sensorimotor gating in patients with obsessive compulsive disorder. In *Biological Psychiatry* (Vol. 33, Issue 4, pp. 298–301). https://doi.org/10.1016/0006-3223(93)90300-3

Szumlinski, K. K., Lominac, K. D., Kleschen, M. J., Oleson, E. B., Dehoff, M. H., Schwarz, M. K., Seeburg, P. H., Worley, P. F., & Kalivas, P. W. (2005). Behavioral and neurochemical phenotyping of Homer1 mutant mice: Possible relevance to schizophrenia. In *Genes Brain Behav* (Vol. 4, Issue 5, pp. 273–288). https://doi.org/10.1111/j.1601-183X.2005.00120.x

Takahashi, A., Kato, K., Makino, J., Shiroishi, T., & Koide, T. (2006). Multivariate Analysis of Temporal Descriptions of Open-field Behavior in Wild-derived Mouse Strains. *Behavior Genetics*, *36*(5), 763–774. https://doi.org/10.1007/s10519-005-9038-3

Tanksley, S. D. (1993). Mapping Polygenes. *Annual Review of Genetics*, *27*(1), 205–233. https://doi.org/10.1146/annurev.ge.27.120193.001225

The C. elegans Sequencing Consortium*. (1998). Genome Sequence of the Nematode *C. elegans*: A Platform for Investigating Biology. *Science*, *282*(5396), 2012–2018. https://doi.org/10.1126/science.282.5396.2012

The Collaborative Cross Consortium. (2012). The Genome Architecture of the Collaborative Cross Mouse Genetic Reference Population. *Genetics*, *190*(2), 389. https://doi.org/10.1534/genetics.111.132639

Thiele, A., & Bellgrove, M. A. (2018). Neuromodulation of Attention. *Neuron*, *97*(4), 769–785. https://doi.org/10.1016/j.neuron.2018.01.008

Thoday, J. M. (1961). Location of Polygenes. *Nature*, *191*(4786), 368–370. https://doi.org/10.1038/191368a0

Thul, P. J., Åkesson, L., Wiking, M., Mahdessian, D., Geladaki, A., Ait Blal, H., Alm, T., Asplund, A., Björk, L., Breckels, L. M., Bäckström, A., Danielsson, F., Fagerberg, L., Fall, J., Gatto, L., Gnann, C., Hober, S., Hjelmare, M., Johansson, F., … Lundberg, E. (2017). A subcellular map of the human proteome. *Science*, *356*(6340), eaal3321. https://doi.org/10.1126/science.aal3321

Treisman, A., & Geffen, G. (1967). Selective Attention: Perception or Response? *Quarterly Journal of Experimental Psychology*, *19*(1), 1–17. https://doi.org/10.1080/14640746708400062

Treisman, A. M. (1960). Contextual Cues in Selective Listening. *Quarterly Journal of Experimental Psychology*, *12*(4), 242–248. https://doi.org/10.1080/17470216008416732

Treisman, A. M. (1964). Verbal Cues, Language, and Meaning in Selective Attention. *The American Journal of Psychology*, *77*(2), 206. https://doi.org/10.2307/1420127

Treisman, A. M. (1969). Strategies and models of selective attention. *Psychological Review*, *76*(3), 282–299. https://doi.org/10.1037/h0027242

Tschermak, E. (1900). Ueber künstliche Kreuzung bei *Pisum sativum* . *Berichte Der Deutschen Botanischen Gesellschaft*, *18*(6), 232–239. https://doi.org/10.1111/j.1438-8677.1900.tb04903.x

Tu, J. C., Xiao, B., Yuan, J. P., Lanahan, A. A., Leoffert, K., Li, M., Linden, D. J., & Worley, P. F. (1998). Homer Binds a Novel Proline-Rich Motif and Links Group 1 Metabotropic Glutamate Receptors with IP3 Receptors. *Neuron*, *21*(4), 717–726. https://doi.org/10.1016/S0896-6273(00)80589-9

Turner, K. M., Peak, J., & Burne, T. H. J. (2016). Measuring Attention in Rodents: Comparison of a Modified Signal Detection Task and the 5-Choice Serial Reaction Time Task. In *Frontiers in Behavioral Neuroscience* (Vol. 9, p. 370). https://doi.org/10.3389/fnbeh.2015.00370

Turrigiano, G. (2012). Homeostatic Synaptic Plasticity: Local and Global Mechanisms for Stabilizing Neuronal Function. *Cold Spring Harbor Perspectives in Biology*, *4*(1), a005736–a005736. https://doi.org/10.1101/cshperspect.a005736

Valentino, R. J., & Van Bockstaele, E. (2008). Convergent regulation of locus coeruleus activity as an adaptive response to stress. *European Journal of Pharmacology*, *583*(2–3), 194–203. https://doi.org/10.1016/j.ejphar.2007.11.062

Van Bockstaele, E. J., Colago, E. E. O., & Valentino, R. J. (1998). Amygdaloid Corticotropin-Releasing Factor Targets Locus Coeruleus Dendrites: Substrate for the Co-ordination of Emotional and Cognitive Limbs of the Stress Response. *Journal of Neuroendocrinology*, *10*(10), 743–758. https://doi.org/10.1046/j.1365-2826.1998.00254.x

Venter, J. C., Adams, M. D., Myers, E. W., Li, P. W., Mural, R. J., Sutton, G. G., Smith, H. O., Yandell, M., Evans, C. A., Holt, R. A., Gocayne, J. D., Amanatides, P., Ballew, R. M., Huson, D. H., Wortman, J. R., Zhang, Q., Kodira, C. D., Zheng, X. H., Chen, L., … Zhu, X. (2001). The Sequence of the Human Genome. *Science*, *291*(5507), 1304–1351. https://doi.org/10.1126/science.1058040

Viggiano, D., Ruocco, L. A., Arcieri, S., & Sadile, A. G. (2004). Involvement of Norepinephrine in the Control of Activity and Attentive Processes in Animal Models of Attention Deficit Hyperactivity Disorder. *Neural Plasticity*, *11*(1–2), 133–149. https://doi.org/10.1155/NP.2004.133

Vitaterna, M. H., King, D. P., Chang, A.-M., Kornhauser, J. M., Lowrey, P. L., McDonald, J. D., Dove, W. F., Pinto, L. H., Turek, F. W., & Takahashi, J. S. (1994). Mutagenesis and Mapping of a Mouse Gene, *Clock* , Essential for Circadian Behavior. *Science*, *264*(5159), 719–725. https://doi.org/10.1126/science.8171325

Von Bartheld, C. S., Bahney, J., & Herculano-Houzel, S. (2016). The search for true numbers of neurons and glial cells in the human brain: A review of 150 years of cell counting. *Journal of Comparative Neurology*, *524*(18), 3865–3895. https://doi.org/10.1002/cne.24040

von Jonquieres, G., Frohlich, D., Klugmann, C. B., Wen, X., Harasta, A. E., Ramkumar, R., Spencer, Z. H., Housley, G. D., & Klugmann, M. (2016). Recombinant Human Myelin-Associated Glycoprotein Promoter Drives Selective AAV-Mediated Transgene Expression in

Oligodendrocytes. In *Front Mol Neurosci* (Vol. 9, p. 13). https://doi.org/10.3389/fnmol.2016.00013

Wang, M., Ramos, B. P., Paspalas, C. D., Shu, Y., Simen, A., Duque, A., Vijayraghavan, S., Brennan, A., Dudley, A., Nou, E., Mazer, J. A., McCormick, D. A., & Arnsten, A. F. T. (2007). α2A-Adrenoceptors Strengthen Working Memory Networks by Inhibiting cAMP-HCN Channel Signaling in Prefrontal Cortex. *Cell*, *129*(2), 397–410. https://doi.org/10.1016/j.cell.2007.03.015

Wang, Y., & Goldman-Rakic, P. S. (2004). D2 receptor regulation of synaptic burst firing in prefrontal cortical pyramidal neurons. *Proceedings of the National Academy of Sciences*, *101*(14), 5093–5098. https://doi.org/10.1073/pnas.0400954101

White, J. G., Southgate, E., Thomson, J. N., & Brenner, S. (1986). The structure of the nervous system of the nematode *Caenorhabditis elegans*. *Philosophical Transactions of the Royal Society of London. B, Biological Sciences*, *314*(1165), 1–340. https://doi.org/10.1098/rstb.1986.0056

Willott, J. F., Tanner, L., O'Steen, J., Johnson, K. R., Bogue, M. A., & Gagnon, L. (2003). Acoustic startle and prepulse inhibition in 40 inbred strains of mice. *Behavioral Neuroscience, 117*(4), 716–727. https://doi.org/10.1037/0735-7044.117.4.716

Wolock, S. L., Lopez, R., & Klein, A. M. (2019). Scrublet: Computational Identification of Cell Doublets in Single-Cell Transcriptomic Data. In *Cell Syst* (Vol. 8, Issue 4, pp. 281-291 e9). https://doi.org/10.1016/j.cels.2018.11.005

Xiao, B., Tu, J. C., Petralia, R. S., Yuan, J. P., Doan, A., Breder, C. D., Ruggiero, A., Lanahan, A. A., Wenthold, R. J., & Worley, P. F. (1998). Homer Regulates the Association of Group 1 Metabotropic Glutamate Receptors with Multivalent Complexes of Homer-Related, Synaptic Proteins. In *Neuron* (Vol. 21, Issue 4, pp. 707–716). https://doi.org/10.1016/S0896-6273(00)80588-7

Xie, Z., Bailey, A., Kuleshov, M. V., Clarke, D. J. B., Evangelista, J. E., Jenkins, S. L., Lachmann, A., Wojciechowicz, M. L., Kropiwnicki, E., Jagodnik, K. M., Jeon, M., & Ma'ayan, A. (2021). Gene Set Knowledge Discovery with Enrichr. In *Current Protocols* (Vol. 1, Issue 3, p. e90). https://doi.org/10.1002/cpz1.90

Yerkes, R. M., & Dodson, J. D. (1908). The relation of strength of stimulus to rapidity of habit-formation. *Journal of Comparative*

Neurology and Psychology, *18*(5), 459–482. https://doi.org/10.1002/cne.920180503

Yuen, E. Y., Liu, W., Karatsoreos, I. N., Feng, J., McEwen, B. S., & Yan, Z. (2009). Acute stress enhances glutamatergic transmission in prefrontal cortex and facilitates working memory. *Proceedings of the National Academy of Sciences*, *106*(33), 14075–14079. https://doi.org/10.1073/pnas.0906791106

Zehring, W. A., Wheeler, D. A., Reddy, P., Konopka, R. J., Kyriacou, C. P., Rosbash, M., & Hall, J. C. (1984). P-element transformation with period locus DNA restores rhythmicity to mutant, arrhythmic Drosophila melanogaster. *Cell*, *39*(2 Pt 1), 369–376. https://doi.org/10.1016/0092-8674(84)90015-1

Zeisel, A., Hochgerner, H., Lönnerberg, P., Johnsson, A., Memic, F., van der Zwan, J., Häring, M., Braun, E., Borm, L. E., La Manno, G., Codeluppi, S., Furlan, A., Lee, K., Skene, N., Harris, K. D., Hjerling-Leffler, J., Arenas, E., Ernfors, P., Marklund, U., & Linnarsson, S. (2018). Molecular Architecture of the Mouse Nervous System. In *Cell* (Vol. 174, Issue 4, pp. 999-1014.e22). https://doi.org/10.1016/j.cell.2018.06.021

Zhang, Y., Proenca, R., Maffei, M., Barone, M., Leopold, L., & Friedman, J. M. (1994). Positional cloning of the mouse obese gene and its human homologue. *Nature*, *372*(6505), 425–432. https://doi.org/10.1038/372425a0